Doctoral Dissertation (Censored)

博士論文（要約）

Cross-scale Interaction in the Realization Processes of the Madden–Julian Oscillation

(マッデン・ジュリアン振動の顕在化過程における
スケール間相互作用に関する研究)

A Dissertation Submitted for the Degree of Doctor of Philosophy
December 2019

令和元年 12 月博士（理学）申請

Department of Earth and Planetary Science,
Graduate School of Science, The University of Tokyo

東京大学大学院理学系研究科地球惑星科学専攻

Daisuke Takasuka

髙須賀 大輔

Abstract

The Madden–Julian oscillation (MJO) is characterized by slow eastward propagation of organized convective envelopes coupled with a planetary-scale zonal overturning circulation over the Indo-Pacific warm pool. Since the MJO is the most dominant intraseasonal variability in the tropics and globally affects various meteorological and climatological phenomena, there have been dedicated efforts to reveal physical processes of the MJO and improve its predictability. While previous studies have primarily focused on MJO-scale dynamical and thermodynamical variations to propose the mechanisms of MJO initiation and propagation, there are also some evidences which implicate the importance of synoptic-scale and interannual variabilities to MJO dynamics. However, our knowledge of such cross-scale processes in MJO realization is piecemeal compared to MJO-scale process-oriented understanding. The aim of this study is to clarify the detailed mechanisms which explain MJO convective initiation and subsequent propagation based on the multi-scale framework involving active roles of synoptic-scale equatorial waves and the mutual relationship between the intraseasonal and interannual variability.

In Chapter 2, mainly from observational data analyses of an MJO event initiated in December 2017 during the field campaign of the Years of the Maritime Continent Project, it is found that dynamical variations associated with mixed Rossby–gravity waves (MRGs) are directly responsible for MJO convective initiation and propagation in the Indian Ocean (IO). The in-situ intensive observation and reanalysis data have captured westward-propagating MRG-related meridional wind signals in the mid-troposphere over the IO during the MJO-suppressed phase. Before MJO convection is activated, tight MRG–convection coupling is enhanced in accordance with zonal wave contraction due to weak mid-tropospheric conver-

gence in the western IO. Basin-scale midlevel moisture resurgence caused by MRG shallow circulations is also observed. These processes stimulate the MRG wave packet formation in the lower-troposphere and successive triggering of MJO convection via MRG dynamics, with the eastward MRG group velocity corresponding to MJO propagation. This MRG-driving mechanism is also confirmed to a certain degree in other two MJO events initiated in October and November 2011, although it is not so evident in the October event.

In Chapter 3, the robustness and inevitability of the MJO–MRG relationship is explored by statistical analyses of 47 MJO events realized in the IO during December–March in 1982–2012. On average, MJO convection is initiated in the southwestern IO (SWIO), where strong MRG–convection coupling is statistically found. Further classification suggests that initiation of 26 of 47 MJO cases is related to more enhanced MRG activities than any other convectively coupled equatorial waves. MJO initiation for MRG-enhanced cases is characterized as convective triggering by low-level MRG circulations which develop via active downward energy dispersion related to upper-tropospheric baroclinic conversion, consistent with Chapter 2. This is supported by the modulation of MRG structure associated with upper-level background zonal convergence, and plentiful moisture advected into the western IO. In addition to this MRG-induced convection in the SWIO, mid-tropospheric pre-moistening in the IO due to MRG shallow circulations and MJO convective propagation driven by low-level MRG winds are also recognized as in Chapter 2. The comparison between the MRG-enhanced events and all others suggests that intraseasonal cross-equatorial circulations during the MJO-suppressed phase in the IO, which is possibly originated from the equatorial asymmetry of background convective activities, may be the source of MRGs. Whether the MRG-related processes are effective or not may depend on the strength in this asymmetry modulated by the low-frequency variability and seasonal march.

Chapter 4 focuses on the diversity of MJO initiation regions associated with the intraseasonal and interannual variability to understand favorable environments for MJO initiation comprehensively. MJOs initiated in the IO (IO-MJO), Maritime Continent (MC-MJO), and western Pacific (WP-MJO) are targeted. Both observations and a series of 15-yr perpetual-

boreal-winter experiments using an atmospheric GCM reveal the following two points: (i) horizontal moisture advection mainly by equatorial intraseasonal circulations is commonly important before MJO initiation in every region, and (ii) the variety of MJO source basins is partly generated by the change of where advective moistening is more likely to work due to the modulation of background circulations forced by interannual SST variability. For IO-MJO cases as the canonical MJO, because climatological ascent in the MC–WP can support intraseasonal convective organization there, resultant convective suppression around the western MC can lead to moisture advection to the IO via intraseasonal low-level easterly anomalies. MC-MJO cases are more favored under the eastern-Pacific (EP) El Niño-like condition, because SST-induced background suppressed convection in the eastern MC can cause the eastward shift of the intraseasonal circulation and convective pattern seen in IO-MJO cases and result in efficient moistening and subsequent development of convection around the western MC. WP-MJO cases tend to occur under the central-Pacific (CP) Niño-like state and dipole SST structure in the southern IO. This is owing to selective moistening in the WP associated with westward intrusion of enhanced disturbances as a result of background convective enhancement in the WP–CP and suppression in the southeastern IO and EP.

Taken together, my results suggest that potential roles of interannual, intraseasonal, and synoptic-scale variations in the mechanics of the MJO are to affect the existence of equatorial intraseasonal zonal circulations related to the MJO, to provide a necessary environment for MJO realization through allowance of sufficient moistening, and to directly trigger MJO convection and assist moisture transport in a favorable environment for the MJO, respectively. This study has emphasized that considering the hierarchical relationship ranging from synoptic-scale variations to interannual variabilities is important to the precise and comprehensive understanding of MJO realization.

Acknowledgments

I am deeply indebted to my principal supervisor, Prof. Masaki Satoh, for his patient guidance and thoughtful encouragements in the master's and doctoral course at the Atmosphere and Ocean Research Institute (AORI), The University of Tokyo. He allowed me to pursue completely freely what I am interested in, provided me with constructive comments and discussions in a timely fashion, and gave me many opportunities to appeal my works to other research communities and public. I would also like to express my gratitude to the members of my dissertation committee, Profs. Yukari Takayabu, Keita Iga, Hiroaki Miura, and Tomoki Tozuka for their time and helpful comments.

I would particularly like to thank to Prof. Hiroaki Miura for his critical but hearty comments and continuous encouragements. His stimulative and interesting advices at the MJO workshops and seminars which he organized and other free discussions helped this study. I have also benefited from discussions and comments given by Profs. Atsushi Hamada, Masaru Inatsu, Hirohiko Masunaga, Tomoki Miyakawa, Takashi Mochizuki, Noriyuki Nishi, and Kazuaki Yasunaga, and Drs. Yuiko Ichikawa, Tsubasa Kohyama, Tamaki Suematsu, and Satoru Yokoi, and Ms. Ching-Shu Hung and Mr. Tomoro Yanase at the above workshops and/or seminars.

The work in Chapter 2 arose from my participation in the field campaign of YMC-Sumatra 2017 led by Japan Agency for Marine-Earth Science and Technology (JAMSTEC). I am grateful to Dr. Kunio Yoneyama, the director of Dynamic Coupling of Ocean-Atmosphere-Land Research Program (DCOP) in JAMSTEC, for giving me an opportunity to take part in the in-situ observation at R/V *Mirai* (MR17-08 cruise) as a research student in DCOP. I also appreciate the members of DCOP and all those who were engaged in YMC-Sumatra 2017.

I would like to offer my special thanks to Dr. Satoru Yokoi, who was the chief scientist in MR17-08 and provided helpful comments and discussions for Chapter 2.

I am grateful to the members and ex-members of the Division of Climate System Research in AORI, especially, Profs. Yukari Takayabu, Masahiro Watanabe, and Tomoki Miyakawa, and Drs. Minoru Chikira and Sam Sherriff-Tadano for giving me valuable questions and suggestions about this study at the seminar. Thanks are also extended to Dr. Tomoki Ohno for fruitful discussions, Drs. Takanori Kodama, Hiroyasu Kubokawa, and Takashi Obase for helpful conversations and encouragements about this study, Drs. Yasuhiro Hoshiba, Takao Kawasaki, Akira Yamauchi, and Mr. Taro Higuchi for encouraging me, and Ms. Midori Kubota for her administrative support. I also acknowledge the members and ex-members of Department of Physical Oceanography in AORI. Prof. Emer. Hiroshi Niino, Prof. Keita Iga, Drs. Junshi Ito, Kaya Kanemaru, Woosub Roh, and Eigo Tochimoto gave me constructive questions and suggestions at the regular seminar. I greatly appreciate Dr. Tamaki Suematsu for her kind comments, discussions, and encouragements. My colleague Mr. Shuhei Matsugishi have entertained and stimulated me through chatting and scientific discussions. I am grateful to Ms. Hidemi Hibino, Ms. Hisae Tamura, Dr. Masatoshi Miyamoto, Mr. Shin-ichi Kodama, Mr. Hiroshi Morii, and Mr. Kanta Nakae for their encouragements.

I have benefited from discussing my research with Drs. Kazuyoshi Kikuchi and Tomoe Nasuno. I am also grateful to Drs. Chihiro Kodama and Hisashi Yashiro for giving me some advices about configurations in numerical experiments in Chapter 4. A script of tracking of MJO precipitation in Chapter 4 is kindly provided by Dr. Jian Ling and Mr. Guiwan Chen.

All the numerical experiments in Chapter 4 were conducted using the Fujitsu PRIMERGY CX600M1/CX1640M1 (Oakforest-PACS) in the Information Technology Center, The University of Tokyo. This work and my graduate school life was financially supported by JSPS KAKENHI grant 17J00713 and JSPS Research Fellowships for Young Scientists, respectively.

Finally, I would like to my sincere gratitude to my parents, sister, grandmother, and late grandfather, who have deeply understood all my pursuits and supported me with warm encouragements. This dissertation is dedicated to them.

Contents

Abstract **i**

Acknowledgments **iv**

Chapter 1 General Introduction **1**

1.1 Mystery of the Madden-Julian oscillation 2

1.2 Understanding of MJO initiation and propagation based on its large-scale intraseasonal feature 5

1.3 Implications of the importance of cross-scale processes in MJO realization 14

1.4 Purpose of this study 22

Chapter 2 Observational Evidence of Mixed Rossby–Gravity Waves as a Driving Force for the MJO Convective Initiation and Propagation **24**

2.1 Introduction 25

2.2 Data 28

2.3 Overview of the MJO and synoptic-scale wave activities 29

2.4 Impacts of MRGs on the MJO initiation and propagation 31

2.5 Discussion 40

2.6 Summary and concluding remarks 46

Chapter 3 Dynamical Roles of Mixed Rossby–Gravity Waves in Driving Convective Initiation and Propagation of the MJO: General Views **49**

Chapter 4 Diversity of Initiation Regions of the MJO Associated with the

Mutual Relationship Between the Intraseasonal and Low-frequency Variability **50**

Chapter 5 General Discussion and Conclusion **51**

5.1 Summary 52

5.2 Concluding discussion 55

References **63**

Chapter 1

General Introduction

1.1 Mystery of the Madden-Julian oscillation

The Madden-Julian oscillation (MJO) (Madden and Julian, 1971, 1972) is known to be the most prominent convective variability in the tropics with a quasi-periodicity on the 20–100-day time scale. The MJO is characterized by slow eastward propagation ($\sim$ 3–8 m s^{-1}) of convective envelopes with $O(10^3$ km) spatial scale over the Indo-Pacific warm pool sector, and is coupled with a planetary-scale zonal overturning circulation (e.g., Hendon and Salby, 1994; Kiladis et al., 2005). As an example of these features, Figs. 1.1a and 1.1b display the time–longitude diagrams of equatorial convection and 850- and 200-hPa zonal wind anomalies for an MJO event realized on December 1996, respectively. Large-scale organized convection in phase with low-level zonal convergence accompanied by strong westerlies and upper-level divergence propagates eastward at about 4 m s $^{-1}$ from the Indian Ocean through the western Pacific, and then dissipates. Furthermore, in Fig. 1.1c, MJO convective areas are in good agreement with anomalously moist regions, which is another notable characteristics that MJO convective variations are tightly related to the evolution of moisture fields (e.g., Kiladis et al., 2005; Benedict and Randall, 2007; Adames and Wallace, 2015).

Since MJO convection modulates large-scale circulations on the intraseasonal time scale, the MJO has extensive impacts on not only local rainfall systems but also global weather and climatological patterns as reviewed by Zhang (2013). For instance, we observe the change of diurnal cycles in precipitation in accordance with phase progression of the MJO (e.g., Ichikawa and Yasunari, 2007; Peatman et al., 2014), the activation of Indian and Australian summer monsoons related to MJO onset (e.g., Yasunari, 1979; Hendon and Liebmann, 1990), and more frequent genesis of tropical cyclones under MJO low-level westerly phases (e.g., Maloney and Hartmann, 2000; Frank and Roundy, 2006). In addition to these impacts on the tropical atmosphere, we also recognize tropics–mid-latitude teleconnection induced by upper-level divergence related to the MJO (e.g., Matthews et al., 2004; Seo and Son, 2012) and the phase shift of the El Niño-Southern Oscillation (ENSO) through the interaction between MJO-associated surface winds and ocean dynamics (e.g., McPhaden, 1999; Takayabu et al., 1999;

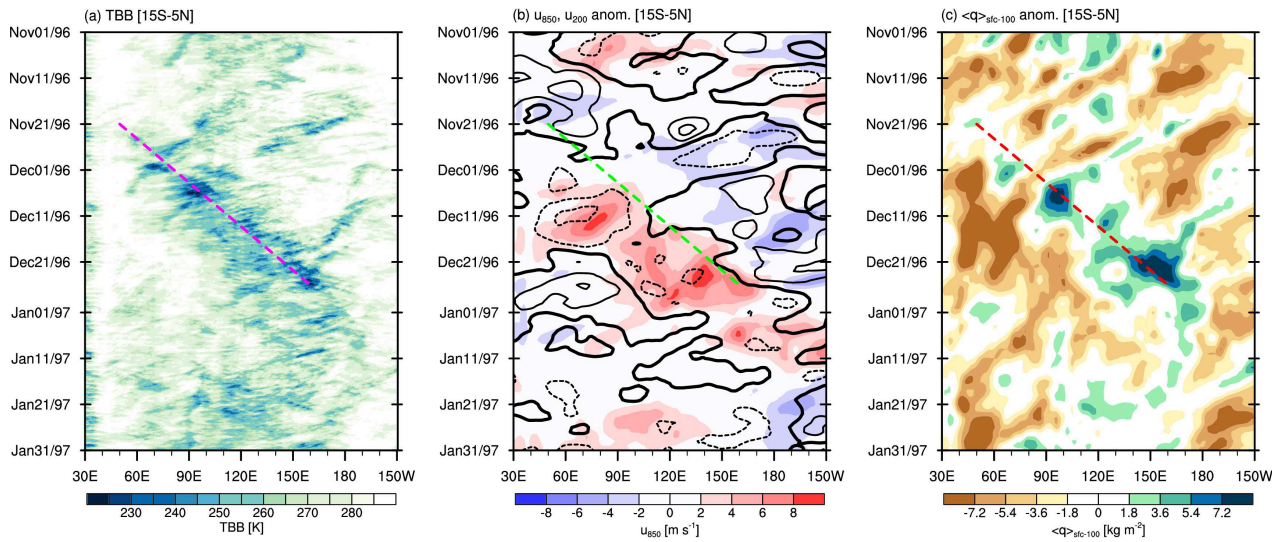

Figure 1.1: Time–longitude diagrams of (a) infrared channel brightness temperature (TBB), (b) 850-hPa (shading) and 200-hPa zonal wind anomalies (contours), and (c) column-integrated water vapor (CWV) anomalies averaged over 15°S–5°N from 1 November 1996 to 31 January 1997. Contour interval in (b) is 7 m s^{-1}, with negative (zero) values dashed (bolded). The colored broken line in each plot indicates the convective center of an MJO event.

Hendon et al., 2007). Understanding the physics of the MJO and improving its predictability are therefore major issues in tropical meteorology.

The comparisons among tropical convective activities over a wide range of spatio-temporal scale suggest the necessity of a special care for the MJO. Following Takayabu (1994) and Wheeler and Kiladis (1999), Figs. 1.2a and 1.2b show the normalized power spectra of the equatorially symmetric and asymmetric components of outgoing longwave radiation (OLR) in the tropics (15°S–15°N) on the wavenumber-frequency domain. Dispersion curves of the equatorial waves with various meridional modes and equivalent depths, which are derived from the linear theory in dry shallow water systems (Matsuno, 1966), are also superimposed on Fig. 1.2. Most of significant spectral peaks exist along the dispersion relations of Kelvin, $n = 1$ equatorial Rossby (ERs), and $n = 1$ westward inertia–gravity waves (WIGs) for symmetric components and mixed Rossby–gravity (MRGs) and $n = 0$ eastward inertia–gravity waves (EIGs) for asymmetric ones. Meanwhile, there is another dominant signal for eastward wavenumbers 1–4 and periods of 20–100 days corresponding to the MJO, which is distinct from the classical equatorial wave modes. This uniqueness of the MJO which cannot

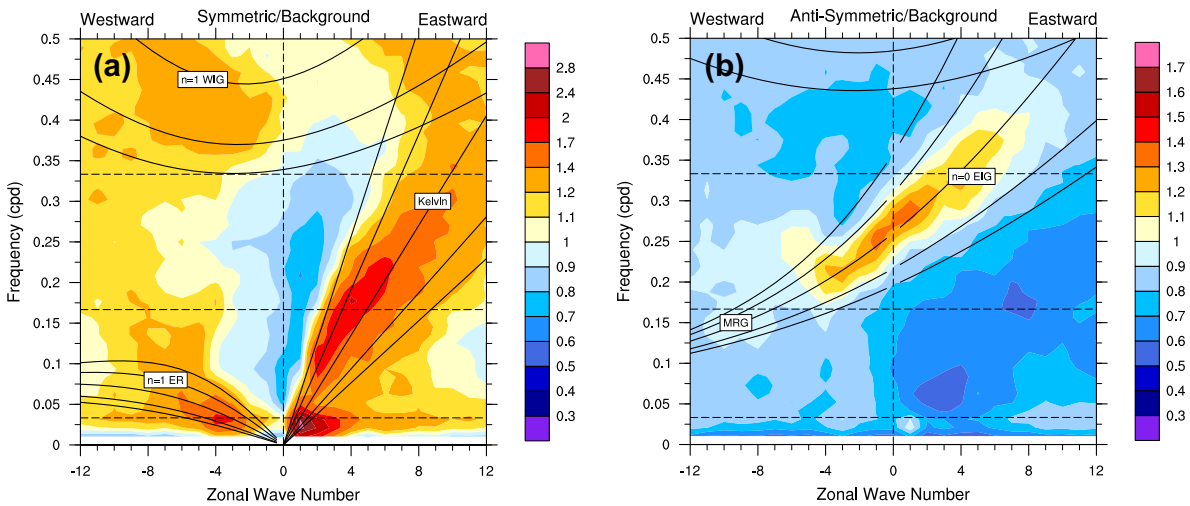

Figure 1.2: Wavenumber–frequency power spectra for (a) equatorially symmetric and (b) antisymmetric daily OLR in 1979–2013 summed over 15°S–15°N and normalized by their backgrounds. Dispersion curves for the equatorial waves are superimposed for equivalent depths of 8, 12, 25, 50, and 90 m.

be explained only based on dry dynamics makes its straightforward understanding difficult.

In fact, although extensive works through observational data analyses, modeling, and theoretical approaches over the past several decades have improved our knowledge of the MJO since its discovery (Zhang, 2005; Lau and Waliser, 2012), the comprehensive framework about MJO dynamics remains elusive. Specifically, we have yet to reach a consensus about the conditions and processes which more universally lead to MJO convective initiation, the driving mechanisms of the subsequent propagation and maintenance of the MJO, the reason why MJO convective systems are organized on the typical horizontal scale of about 5000 km, and the cause of the intraseasonal quasi-periodicity. This situation is reflected in the fact that many general circulation models (GCMs) still struggle with simulating MJO convection with realistic amplitude, propagation characteristics, and occurrence (Hung et al., 2013; Jiang et al., 2015; Ahn et al., 2017; Ling et al., 2019), even though the importance of appropriate representation of the moisture–convection–dynamical feedback has been implicated by successful MJO simulations and/or improved MJO prediction skills with a global cloud/cloud-system resolving model (GCRM) (Miura et al., 2007; Miyakawa et al., 2014) and GCMs whose convective parameterization is improved to be sensitive to environmental moisture (e.g., Bechtold et al., 2008; Hannah and Maloney, 2011; Vitart and Robertson, 2018)

or replaced with a 2-D cloud resolving model (e.g., Benedict and Randall, 2009).

In this dissertation, I especially focus on the realization processes of the MJO, that is, how, when, and where MJO convection is initiated and starts to propagate eastward slowly. The detailed understanding of them can be expected to provide not only some essences in both MJO initiation and propagation as a set of processes but also more precise indicators for the prediction. The remaining mystery, a fundamental origin about the spatio-temoporal scale peculiar to the MJO, is also an interesting and challenging topic as examined with an idealized framework such as radiative-convective equilibrium experiments (e.g., Grabowski and Moncrieff, 2004; Arnold and Randall, 2015; Pritchard and Yang, 2016; Wing and Cronin, 2016; Beucler et al., 2018; Yang, 2018; Khairoutdinov and Emanuel, 2018) or aqua-planet experiments with sea surface temperature (SST) gradient (e.g., Arnold et al., 2013; Takasuka et al., 2018; Shi et al., 2018). This important theme should be revisited in the future.

1.2 Understanding of MJO initiation and propagation based on its large-scale intraseasonal feature

1.2.1 Observed primary structure of the MJO

The dynamical and thermodynamical structure associated with the MJO is primarily characterized by large-scale wind, pressure, and moisture patterns related to its organized convection (e.g., Kiladis et al., 2005). Figures 1.3a and 1.3b display horizontal maps of time-averaged meteorological fields at 850 and 200 hPa along the convective center for the MJO event shown in Fig. 1.1, respectively. At 850 hPa, the twin cyclonic gyres exist across the equator to the west of MJO convection and the equatorial anomalous easterlies are prominent to the east (Fig. 1.3a), which is generally interpreted as a Matsuno-Gill response to MJO convective heating (Matsuno, 1966; Gill, 1980). The wind fields at 200 hPa have the significantly divergent circulations in concert with MJO active convection (Fig. 1.3b). It is also reconfirmed that large-scale tropospheric moisture fields well correspond to MJO convective envelopes (Figs. 1.3a, b) as pointed out in Fig. 1.1c. Figure 1.3c presents these

circulation and moisture structures in the zonal–vertical cross section. The first baroclinic mode composed of low-level convergence and upper-level divergence is dominant around the MJO convective center, and the overall dynamical and moisture fields have the westward-tilted structure associated with the shallow convergence and moistened region to the east (Kiladis et al., 2005; Benedict and Randall, 2007; Adames and Wallace, 2015).

It has been, therefore, a main stream in understanding the MJO initiation and propagation mechanisms to focus on the evolution of large-scale intraseasonal fields related to the primary structure of the MJO mentioned above. The literature review about this perspective is provided in the next two subsections.

1.2.2 Initiation mechanisms

The pre-existing mechanisms of MJO initiation based on large-scale processes stress the importance of dynamical and thermodynamical variations inside the tropics. The following three elements are considered to be key recipes for MJO initiation: 1) equatorial circumnavigation of large-scale Kelvin waves, 2) "discharge-recharge" hypothesis, and 3) MJO-scale moisture advection. Now I introduce the details and related caveats for each proposed mechanism.

Equatorial circumnavigation of large-scale Kelvin waves

Many observational studies have highlighted the role of equatorial circumnavigation of large-scale Kelvin waves decoupled from MJO convection dissipating around the central Pacific region (e.g., Matthews, 2000; Kikuchi and Takayabu, 2003; Seo and Kim, 2003; Matthews, 2008; Haertel et al., 2015; Powell and Houze, 2015a), ever since Knutson and Weickmann (1987) found the correspondence between the arrival of equatorially circumnavigating upper-tropospheric negative velocity potential anomalies at the Indian Ocean and MJO initiation. While how Kelvin-wave signals in the upper-troposphere can trigger a next MJO cycle has been the matter of speculation (Matthews, 2008; Haertel et al., 2015), Powell and Houze (2015a) showed that the approach of Kelvin-wave-induced anomalous ascending

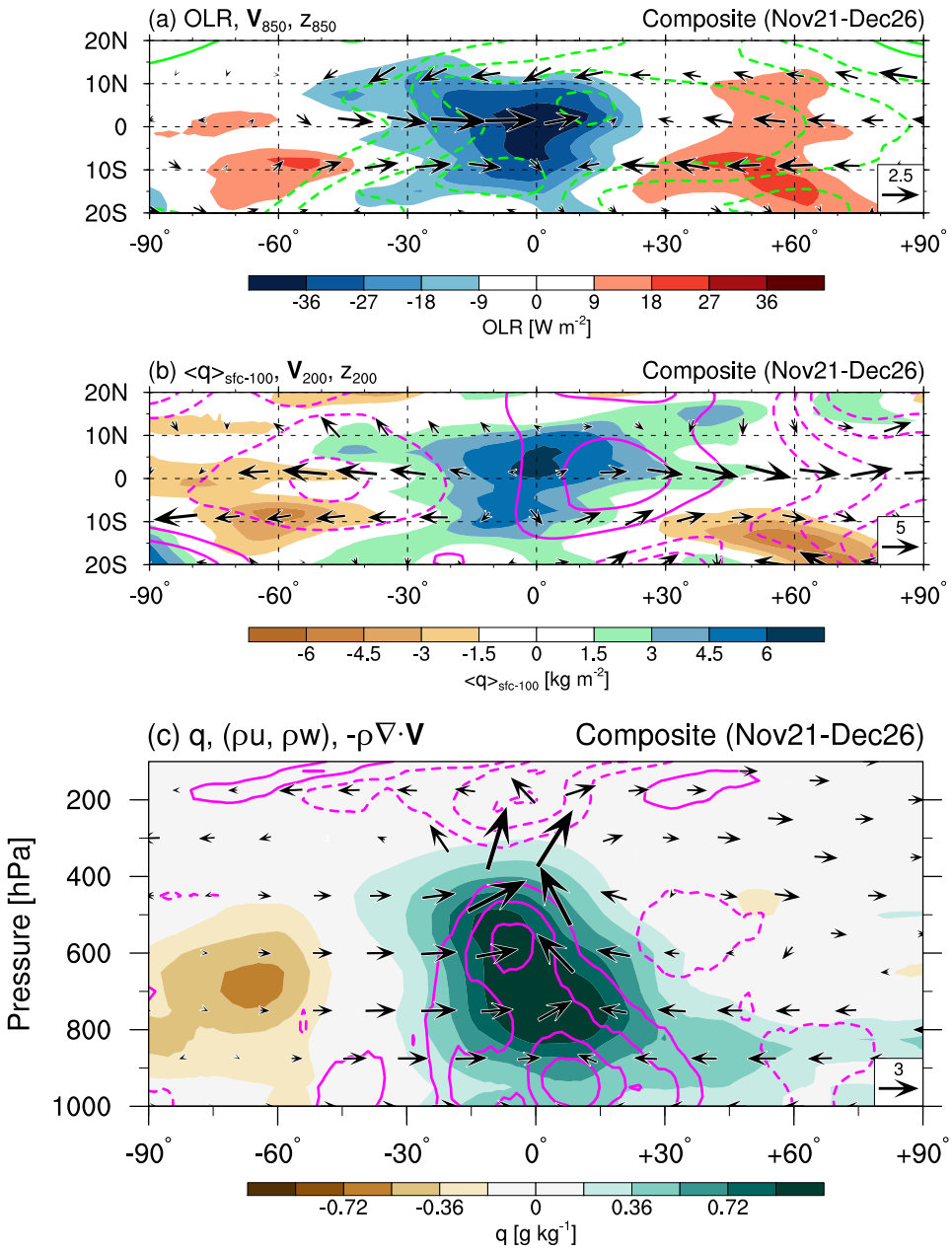

Figure 1.3: (a) Horizontal structure of OLR (shading), 850-hPa horizontal wind (vectors; m s^{-1}), and geopotential height anomalies (contours) averaged along the convective center (0°) of the MJO shown in Fig. 1.1. Contour interval is 3 m, with negative (zero) values dashed (omitted). (b) As in (a), but for CWV (shading), 200-hPa horizontal wind (vectors), and geopotential anomalies (contours). Contour interval is 6 m. (c) Zonal–vertical structure of 10°S–10°N averaged specific humidity (shading), mass flux (vectors; kg m^{-2} s^{-1}), and horizontal mass convergence anomalies (contours). Contour interval is 3.0×10^{-7} kg m^{-3} s^{-1}, with negative (zero) values dashed (omitted). The vertical component of vectors is multiplied by 1000.

motions at 500–300 hPa supports deep convective onset in the Indian Ocean through the weakening of large-scale subsidence and the resultant steepening of the lower-tropospheric lapse rate. As first speculated by Matthews (2000), the intrusion of lower-tropospheric dynamical signals rather than upper-tropospheric ones may also directly trigger MJO convection. In fact, Kikuchi and Takayabu (2003) and Seo and Kim (2003) have suggested the importance of moisture convergence associated with low-level easterlies of circumnavigating Kelvin waves in excitation of enhanced convection, which is validated at least for a single MJO event in a regional modeling study of Chen and Zhang (2019). Recent mechanism-denial studies with long-term GCM simulations, however, have claimed that a global circuit of large-scale Kelvin waves is not a necessary condition for MJO initiation (Zhao et al., 2013; Maloney and Wolding, 2015; Ma and Kuang, 2016; Takasuka et al., 2018). This implicates that there are other possible pathways to MJO convective triggering.

Discharge-recharge hypothesis

With a theoretical approach, Bladé and Hartmann (1993) have first hypothesized that a local buildup and release of instability over the warm water can be responsible for the periodic MJO initiation. In observation, this "discharge-recharge" hypothesis is interpreted in terms of basin-scale but local variations in sea surface temperature (SST), surface fluxes, and radiative cooling (e.g., Kemball-Cook and Weare, 2001; Benedict and Randall, 2007). Specifically, Benedict and Randall (2007) presented the statistical view that MJO initiation is a result of gradual column moistening and heating caused by vertical convective transport of moisture and heat in accordance with the development of convection from shallow to deep under warm SSTs. Indeed, this shallow-to-deep cloud transition associated with the MJO evolution is confirmed in the satellite observations (e.g., Riley et al., 2011; Del Genio et al., 2012). In some MJO cases, however, the time scale on which MJO deep convection develops is shorter than the discharge-recharge hypothesis predicts (Powell and Houze, 2013, 2015a,b; Xu and Rutledge, 2016), which suggests that gradual destabilization from the lower troposphere is not always a suitable explanation for MJO initiation. In addition, in the context

of more general situations in tropical convection, the correlation between the convective development and column destabilization may not necessarily imply direct contributions of shallow cloud processes to the preconditioning. For example, based on a statistical analysis using satellite data, Masunaga (2013) suggested that free-tropospheric moistening before deep convection may result from the large-scale updraft forcing rather than convective eddy transport. Hohenegger and Stevens (2013) also presented the similar perspective with large-eddy simulations. Hence, it is still worth targeting at larger-scale dynamics such as equatorial waves compared to convective cloud scales in MJO initiation processes (Hagos et al., 2014; Chen and Zhang, 2019).

MJO-scale moisture advection

Motivated by the evident moisture–convection relationship in the MJO (Figs. 1.3b, c), some researchers have recently had a special focus on the evolutions of the moisture budget in initiation processes of the MJO. They suggested that anomalous horizontal advection of climatological moisture by intraseasonal wind anomalies associated with the Rossby wave response to the MJO-suppressed phase (i.e., the opposite pattern to Fig. 1.3a) is responsible for free-tropospheric pre-moistening (e.g., Zhao et al., 2013; Li et al., 2015; Maloney and Wolding, 2015; Nasuno et al., 2015; Takasuka et al., 2018; Hung and Sui, 2018). Note that this process is completely reversed to one which one of MJO theories emphasizes in explaining the eastward propagation of MJO convection as described later (see "moisture mode" in Section 1.2.3). Meanwhile, there is also a report of contributions of high-frequency circulations to the moistening in some cases (Nasuno et al., 2015; Takasuka et al., 2018). In addition, although the community does not care, it may be inappropriate to apply temporal filtering to moisture signals in the moisture budget analysis because moisture itself is a tracer with local and instant phase change and does not actively have temporal information. The decomposition of moisture fields that is adopted in most of the above studies might lead to misleading interpretation of the results.

Although every proposed mechanism sometimes appears to work in initiation processes of the MJO, there are also the criticisms that some mechanisms are not always required and that the contributions from synoptic-scale high-frequency variations can be actually important. Furthermore, all the above mechanisms are derived on the assumption that the MJO is initiated in the Indian Ocean. Thus, they alone cannot completely predict where MJO initiation should be observed.

1.2.3 Propagation mechanisms

Understanding of MJO propagation has been advanced by both construction of theoretical models and their validation through modeling and/or observational studies (e.g., Lau and Waliser, 2012). Although early works tried to interpret the MJO as the wave-CISK (CISK: conditional instability of the second kind) for Kelvin waves (e.g., Lau and Peng, 1987) and an unstable mode via the wind-induced surface heat exchange (WISHE; Emanuel, 1987; Neelin et al., 1987), both are inconsistent with observation in that the former and latter require too bottom-heavy heating for a slow propagation and mean easterlies, respectively (Zhang, 2005). At present, there are three proposed theories focused on large-scale intraseasonal variations: 1) atmosphere–ocean coupled processes, 2) Kelvin–Rossby wave dynamics interacted with planetary boundary layer (PBL) frictional moisture convergence, and 3) moisture mode. Although all the theories make much of the Matsuno-Gill-type structure and moisture-convection relationship seen in Fig. 1.3c, they are distinguished from each other depending on what processes they put more emphasis on. Their details and unsatisfactory points are now described.

Importance of atmosphere–ocean coupled processes

Some past theoretical works have pointed out the importance of atmosphere–ocean coupled processes (e.g., Flatau et al., 1997; Wang and Xie, 1998; Liu and Wang, 2013, see also a comprehensive review by Demott et al. (2015)). Overall, this theory postulates that the SST–convection–evaporation/radiation feedback prompts the slow eastward propagation

of the MJO in a following manner. To the east of the MJO convective center (i.e., suppressed phase), SST warming is caused by enhanced solar insolation and less surface evaporation and shallower ocean mixed layer depth (MLD) due to weak easterlies associated with the Kelvin wave response, whereas SST drops to the west because of shutdown of incoming shortwave radiation, deeper MLD, and enhanced evaporation under increased cloud cover and strong westerlies as a result of both mean and anomalous westerlies. This resultant zonal SST gradient can induce the enhancement of low-level convergence and increases in moisture on the eastern side, which destabilizes eastward-propagating MJO convection.

In fact, the relationship between SST and surface and radiative flux variations on the intraseasonal time scale is confirmed by observations (e.g., Shinoda et al., 1998; Demott et al., 2015), and modeling studies have suggested that air–sea coupling can improve the skill in MJO simulations (e.g., Inness and Slingo, 2003; Benedict and Randall, 2011; DeMott et al., 2014; Klingaman and Woolnough, 2014; Tseng et al., 2015; Miyakawa et al., 2017; Zhu et al., 2017). However, some theoretical models (e.g., Wang and Xie, 1998; Liu and Wang, 2013) may overemphasize the impacts of SST on atmospheric heat and moisture because of the simplified formulation in the SST–wind–evaporation relationship (Demott et al., 2015). Furthermore, intraseasonal SST-induced atmospheric processes such as enhanced PBL convergence can be observed as secondary effects, if any (e.g., Hsu and Li, 2012), consistent with the fact that some atmospheric-only GCMs prescribed by climatological SST can reproduce the realistic MJO (e.g., Kemball-Cook et al., 2002; Maloney and Sobel, 2004; Klingaman and Woolnough, 2014) and that some MJO cases are well simulated even without the air–sea interaction (e.g., Fu et al., 2015). This suggests that we have room for scrutinizing atmosphere-driving processes as a basis of MJO dynamics.

Kelvin–Rossby wave dynamics with PBL frictional moisture convergence

Based on the large-scale dynamical structure in the MJO, one considers that the equatorial wave dynamics associated with the Kelvin–Rossby couplet which interacts with PBL frictional moisture convergence is the essence in slow propagation of the MJO (e.g., Wang and Rui,

1990; Wang and Li, 1994; Kang et al., 2013; Wang et al., 2016; Wang and Chen, 2017). This framework was first developed by Wang and Rui (1990) based on the 2.5-layer (i.e., two free-tropospheric layers with PBL) equatorial β-plane model with the long-wave approximation and a diagnostic convective heating parameterization related to PBL convergence (i.e., simplified CISK-type parameterization). They found that convective heating via PBL convergence can lead to the continuous coupling between equatorial Kelvin and Rossby waves and that, for sufficiently high SST, the resultant Kelvin–Rossby couplet has a planetary-scale slowly eastward-propagating unstable mode similar to the MJO. This Kelvin–Rossby coupled model has been lately updated to a simpler version that implements moisture feedback processes by Wang et al. (2016) and Wang and Chen (2017). They claim that slow propagation of the MJO can result from both decreased phase speeds in Kelvin waves due to reduced static stability via sufficient convective heating and Rossby-wave hinderance enhanced by the moisture feedback to eastward-propagating Kelvin waves destabilized by PBL frictional moisture convergence.

Large-scale PBL frictional moisture convergence, a key element in this theory, is actually observed especially to the east of the MJO convective center (e.g., Maloney and Hartmann, 1998; Sperber, 2003; Hsu and Li, 2012; Adames and Wallace, 2015; Chen and Wang, 2018b, Fig. 1.3c). Good representation of this dynamical characteristics in GCMs also appears to be related to good simulation skill of MJO propagation (e.g., Wang et al., 2016; Wang and Chen, 2017; Wang et al., 2018a). However, it is non-trivial whether the theoretical model parameters such as the PBL Ekman number and Newtonian damping coefficients are appropriate compared to observation. This uncertainty can shake the validity of this theory through overemphasis of the strength in PBL convergence. In addition, there is no physical justification for considering only long-wave approximated Kelvin and Rossby waves.

Moisture mode

Different from the mechanism in terms of the equatorial Kelvin–Rossby wave *dynamics*, a theory called a "moisture mode" puts importance on the atmospheric *thermodynamical* relationship between large-scale moisture and convective variations (Figs. 1.1c and 1.3b,c)

(e.g., Neelin and Yu, 1994; Sobel et al., 2001; Raymond and Fuchs, 2007, 2009; Sugiyama, 2009; Sobel and Maloney, 2012, 2013; Adames and Kim, 2016). This theory explains eastward propagation of MJO convection in terms of the intraseasonal spatio-temporal evolution of moisture as a prognostic variable, which relies on the observational fact that there is a positive correlation between precipitation and column-integrated water vapor in the tropics (e.g., Bretherton et al., 2004; Holloway and Neelin, 2009). More practically, since the horizontal temperature gradient in the tropics is very weak because of rapid and broad adjustment of buoyancy perturbations via gravity waves (Sobel et al., 2001), this view has been reduced to discussing the variations of column-integrated moist static energy (MSE) (Sugiyama, 2009; Sobel and Maloney, 2012, 2013; Adames and Kim, 2016) or moist entropy (Raymond and Fuchs, 2007, 2009) approximately conserved in moist adiabatic processes. This enables us to interpret the evolution of MJO convection based on the interaction among moisture, circulations and radiative and surface heat fluxes as sources or sinks of MSE, which can incorporate the previously proposed (and presently examined) framework that the MJO can be maintained by the cloud–radiation interaction (Raymond, 2001; Bony and Emanuel, 2005; Crueger and Stevens, 2015; Andersen and Kuang, 2012; Zhang et al., 2019) and the wind–evaporation feedback (Neelin and Yu, 1994; Sobel et al., 2008, 2010).

Recently, by expanding the 1-D linear model of Sobel and Maloney (2012) and Sobel and Maloney (2013), Adames and Kim (2016) have developed the 2-D equatorial β-plane moisture-mode model which adopts the long-wave approximation and has only a prognostic equation of column-integrated MSE on the assumption that MJO-related dynamical fields are just diagnosed as a Matsuno-Gill response to column-integrated heating. With this model, Adames and Kim (2016) have suggested that the MJO may be regarded as a linear dispersive eastward-propagating moisture wave with a westward group velocity. In essence, MJO convective propagation can be mainly driven by both moistening to the east due to Kelvin wave-response-induced PBL moisture convergence and drying to the west via horizontal advection of subtropical dry air by equatorward winds associated with the Rossby wave response, although the effects of synoptic-scale eddy activities on the moisture evolution are

empirically and implicitly considered.

While the moisture-mode view seems to be consistent with past observational studies (e.g., Kiranmayi and Maloney, 2011; Adames and Wallace, 2015; Adames and Kim, 2016; Kim et al., 2017) and modeling studies (e.g., Maloney, 2009; Arnold et al., 2013; Pritchard and Bretherton, 2014; Jiang, 2017; Jiang et al., 2018), there are several unclear points and criticisms. One is that, as pointed out in the second theory, the additive parameters to represent the effects of PBL moisture convergence and eddy moisture transport and scaling of the governing equations are highly empirically determined in the model. Another stems from the results in Pritchard and Yang (2016), who questioned the validity of considering moisture variations alone explicitly as a driver of the MJO by conducting several idealized numerical experiments. They have shown that the MJO propagates eastward even when the mean meridional moisture gradient is reversed to the real world and speculated the importance of high-frequency tropical waves rather than large-scale horizontal moisture advection. This means that it may be required to scrutinize the interactive processes between dynamics and moisture to understand the MJO more precisely.

As reviewed above, it is true that each theory of MJO propagation has been constructed based on the qualitative observational characteristics in SST and/or atmospheric variations associated with the MJO. As suggested by some previous studies, however, there is the possibility that the theories may overemphasize their corresponding specific processes beyond observation by imposing the non-trivial assumptions in spatio-temporal scaling and physical parameterizations, Thus, it is worthwhile to pursue a different view from the pre-existing mechanisms focused on MJO-scale processes.

1.3 Implications of the importance of cross-scale processes in MJO realization

The previous section describes that MJO behavior has primarily been understood by emphasis on large-scale intraseasonal variations in dynamics and thermodynamics, whereas

the resultant proposed mechanisms alone may not be enough to capture the precise picture of how and where MJO convection is initiated and starts its propagation. Considering this situation, it is natural to look for influences from the spatio-temporal scale outside the MJO, that is, synoptic-scale and interannual variabilities. In the following subsections, I will briefly review previous studies which discuss the impacts of synoptic-scale variations and interannual variabilities on MJO initiation and propagation, and will introduce the importance of cross-scale processes in MJO realization along with related unsolved issues.

1.3.1 Relationship with equatorial synoptic-scale variations

One of observational evidences for the involvement of equatorial synoptic-scale variations in MJO realization is the hierarchical structure in the MJO-related fields. Beginning with the pioneering work by Nakazawa (1988), who found that large-scale convective envelopes associated with the MJO are composed of high-frequency eastward- and westward-propagating cloud clusters, many observational studies have suggested that various kinds of convectively coupled equatorial waves (Fig. 1.2) are embedded within MJO convection (e.g., Hendon and Liebmann, 1994; Dunkerton and Crum, 1995; Chen et al., 1996; Takayabu et al., 1996; Straub and Kiladis, 2003; Masunaga et al., 2006; Kikuchi and Wang, 2010; Yang and Ingersoll, 2011; Yasunaga, 2011; Dias et al., 2013, 2017). This characteristic in the MJO event shown in Fig. 1.1 is presented in Fig. 1.4. We find that WIGs are mainly observed during the entire MJO active period (Hendon and Liebmann, 1994; Takayabu et al., 1996; Chen et al., 1996; Kikuchi and Wang, 2010). The enhancement of other specific waves such as MRGs (Straub and Kiladis, 2003; Yang and Ingersoll, 2011), Kelvin waves (Dunkerton and Crum, 1995; Masunaga et al., 2006), and Rossby waves (Masunaga et al., 2006) has also been recognized, while several works point out that it appears not to be uniquely determined what kinds of waves are prominent in the MJO convective structure (Yasunaga, 2011; Dias et al., 2013, 2017). At any rate, these studies suggest that the contributions from synoptic-scale disturbances can be transferred to the components at the MJO scale. Note that this view is consistent with the results of the MJO model intercomparison by Guo et al. (2015), who have found that models

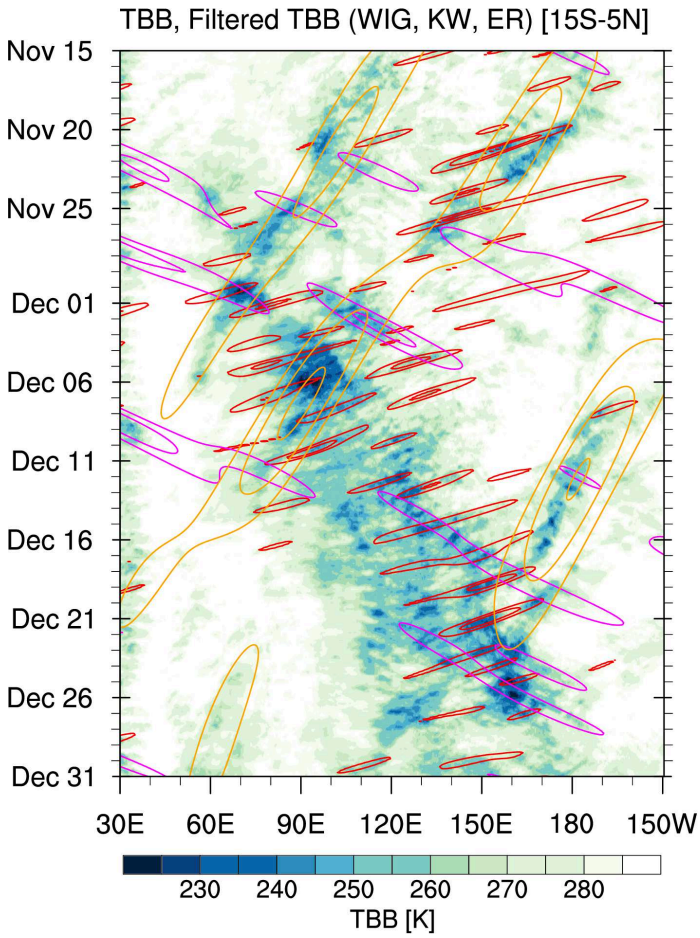

Figure 1.4: As in Fig. 1.1a, but negative TBB anomalies filtered for WIGs (red), Kelvin waves (magenta), and Rossby waves (orange) are also plotted. Contour interval is 4 K, with zero values omitted.

with good MJO simulation skill can reproduce strong precipitation variances of the equatorial waves in association with MJO precipitation anomalies.

In some theoretical studies, one of possible processes about the MJO–synoptic-scale interaction is considered as upscale convective momentum transport associated with the vertically-tilted structure of convectively coupled equatorial waves (e.g., Kiladis et al., 2009) embedded within MJO convective envelopes (e.g., Majda and Biello, 2004; Biello and Majda, 2005; Majda and Stechmann, 2009a; Wang and Liu, 2011). This process actually appears to be important to the realistic wind structure of the MJO (e.g., Biello and Majda, 2005; Wang and Liu, 2011) and its slow propagation (e.g., Wang and Liu, 2011). In contrast, Majda and Stechmann (2009b) and Majda and Stechmann (2011) have proposed the MJO

"skeleton" model without its "muscle" such as convective momentum transport. They explain the eastward propagation of MJO convection by parameterizing the collective heating effects of synoptic-scale wave activities related to moisture fields on the MJO-scale dynamics. From another standpoint, Yang and Ingersoll (2013) have focused on convective triggering via high-frequency equatorial wave dynamics, and interpreted MJO convection as the interference pattern of EIGs and WIGs by using a 2-D shallow water model which implements the effects of triggered convective heating. This situation in the theoretical approaches implicates that some of fundamental properties in MJO realization may come from the interactive processes between moisture and synoptic-scale wave dynamics rather than convective momentum transport, although the validity of this implication should be clarified in observation.

Fortunately, there are some evidences that dynamical and moisture variations associated with synoptic-scale equatorial waves actually play a direct role in MJO initiation and propagation processes based on observational data analyses (e.g., Straub and Kiladis, 2003; Masunaga et al., 2006; Yasunaga et al., 2010; Yang and Ingersoll, 2011; Kerns and Chen, 2014; Chen et al., 2015; Kubota et al., 2015; Muraleedharan et al., 2015; Nasuno et al., 2015; Kikuchi et al., 2018) and modeling studies (e.g., Miura et al., 2007, 2009; Nasuno et al., 2009; Yang and Ingersoll, 2011; Pritchard and Yang, 2016; Takasuka et al., 2018). In particular, the knowledge of the interaction between the MJO initiation and synoptic-scale variations has been greatly accumulated in the two intensive observational field campaigns in the Indian Ocean — the Mirai Indian Ocean cruise for the Study of the MJO-convection Onset (MISMO; Yoneyama et al., 2008) and the Dynamics of the MJO (DYNAMO; Yoneyama et al., 2013) field campaign. For example, Yasunaga et al. (2010) have reported pre-moistening by MRGs with 3–4-day-period dynamical and moisture variations before the onset of MJO convection during MISMO. Similarly, several analyses for the DYNAMO campaign have suggested that moisture resurgence leading to the MJO initiation around the Indian Ocean is prompted by MRGs (Chen et al., 2015; Muraleedharan et al., 2015) and/or WIGs (Kubota et al., 2015). These observational facts are complemented by an idealized modeling study to examine the intrinsic mechanism of the MJO; Takasuka et al. (2018) have provided an insight that MRGs

might be essentially important to MJO initiation through free-tropospheric moisture accumulation by analyzing a set of initiation processes of many MJO-like disturbances reproduced in an aqua-planet experiment. Meanwhile, since the above studies are based on the analyses of each single case or the idealized framework, it is still unclear how robust pre-moistening involving such equatorial waves are for other observed MJO cases. In addition, as another aspect other than moistening processes, the possibility that MJO initiation is characterized as convective triggering by synoptic-scale wave disturbances, which is inferred from a theoretical context (Yang and Ingersoll, 2013), has not been verified in details for observation.

With respect to the MJO propagation, several insights which challenge the candidate mechanisms focused on large-scale processes (see Section 1.2.3) have been provided. Straub and Kiladis (2003) has statistically found that enhanced MRG convective activities are in phase with MJO convection and speculated that the eastward energy dispersion ofconvectively-coupled MRG wave packets at the group velocity of ~ 5 m s^{-1} (Wheeler and Kiladis, 1999) can be sometimes recognized as the eastward-moving convective clusters of the MJO. Yang and Ingersoll (2011) have also further tested this hypothesis with both idealized numerical experiments and observational data and have shown that the MJO–MRG relationship is one of allowed solutions but that it cannot be always detected in observed convective fields. Nonetheless, the analysis of an MJO event which Miura et al. (2007) have successfully simulated using a GCRM with a 7-km horizontal grid intervals has revealed that westward-propagating cloud clusters related to cross-equatorial meridional winds are enhanced at the leading edge of the eastward-propagating MJO (Nasuno et al., 2009), which implicates the importance of MRG-type dynamics in MJO propagation. In addition, Kikuchi et al. (2018) recently proposed a hypothesis that slow Kelvin waves appear to drive MJO propagation as main building blocks of the MJO by analyzing all five MJO events observed in the DYNAMO campaign. In terms of moisture variations, Miura et al. (2007) have pointed out that westward intrusion of equatorial Rossby waves into the western Pacific can contribute to sufficient moistening responsible for eastward migration of the whole MJO convection, consistent with Masunaga et al. (2006)'s satellite data analysis. These findings and hypotheses are not covered

by the Kelvin–Rossby couplet mechanism and the moisture-mode theory, which supports the speculation that synoptic-scale waves may drive MJO convective propagation (Pritchard and Yang, 2016). However, the detailed interactive mechanism, necessity, and robustness of those MJO–synoptic-scale variations still remain elusive because they have had little recognition compared to large-scale dynamical and thermodynamical processes.

1.3.2 Impacts of the interannual variability

The interannual variability, as the other time scale outside the MJO, is also important for comprehensive understanding of MJO realization because it modulates the background environment favorable for MJO convection. One of the examples is recognized as the spatial change in mean MJO convective activities in accordance with the ENSO. For instance, the comparison of 20–100-day-filtered OLR variance during boreal winter (December–March) between all years in 1982–2012 and only the typical eastern-Pacific (EP) El Niño years (1982/1983, 1986/1987, 1991/1992, and 1997/1998) suggests that the EP El Niño condition tends to enhance MJO activities to the east of date line (Fig. 1.5), as reported by previous studies (e.g., Fink and Speth, 1997; Vincent et al., 1998; Hendon et al., 1999; Kessler, 2001; Tam and Lau, 2005; Chen et al., 2016). Different from this condition, under the central-Pacific (CP) El Niño (Kao and Yu, 2009) or El Niño Modoki (Ashok et al., 2007), which is another type of El Niño characterized as SST warming around the equatorial CP rather than the EP, MJO convective perturbations become more significant around the western Pacific (e.g., Feng et al., 2015; Chen et al., 2016; Wang et al., 2018b). These studies indicate that where MJO convection is favored on average is very sensitive to the spatial pattern of the interannual SST variability.

While the above observational fact itself is for the modulation of the *mean* characteristics of MJO convective activities, it has been recently shown that interannual variations of SSTs and associated atmospheric circulations also have an impact on whether MJO initiation as a *transient* phenomenon is realized or not (Suematsu and Miura, 2018; Suematsu, 2018). By comparing MJO events and large-scale convective events confined in the Indian Ocean

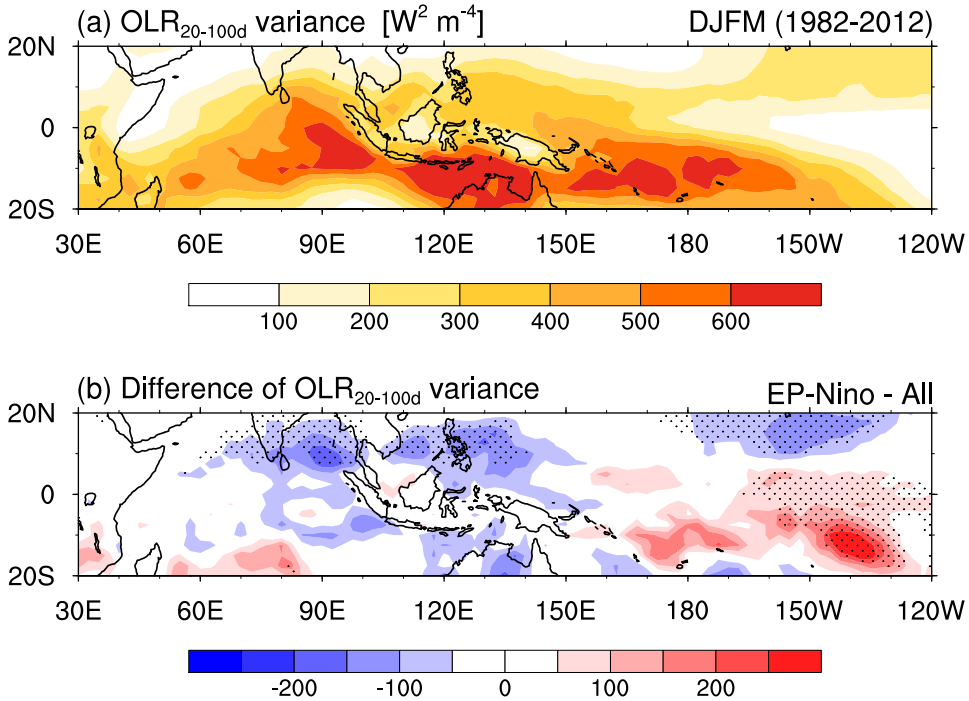

Figure 1.5: (a) Map of 20–100-day-filtered OLR variance during December–March in 1982–2012, and (b) its difference from all the years for typical EP El Niño years (1982/1983, 1986/1987, 1991/1992, and 1997/1998). Stippled areas indicate the statistical significance at the 90% level assessed by the F-test.

statistically, Suematsu and Miura (2018) have found that MJO initiation in the Indian Ocean is more favored when there is a more positive zonal gradient of background SSTs for the MJO scale from the Indian Ocean to the western Pacific (e.g., under CP El Niño conditions). This perspective has been reduced to the relationship between MJO initiation and the strength in the mean equatorial zonal circulation (i.e., the Walker circulation); that is, the enhanced background Walker circulation can lead to the situation that MJO convection is more favorably initiated in the Indian Ocean (Suematsu, 2018).

Our present perception that the interannual variability modulates the spatial distributions of mean MJO activities and the probability of MJO initiation in the Indian Ocean may provide a clue to understanding where MJO should be realized. At present, any pre-existing mechanisms for MJO initiation cannot explain an observational fact that MJO convection can be initiated even around the Maritime Continent and western Pacific (Matthews, 2008, Fig. 1.6). Looking into such a non-canonical MJO, which is initiated outside the Indian Ocean, is expected to be

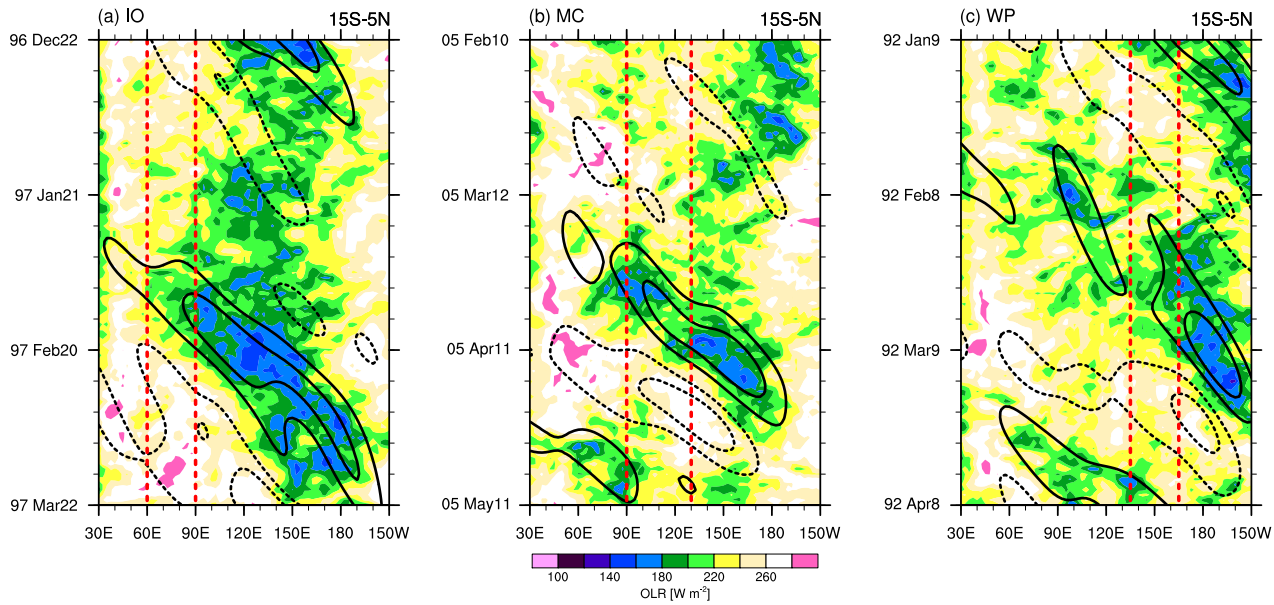

Figure 1.6: Time–longitude diagrams of OLR (shading) and its anomalies filtered for the MJO (contours) for an MJO event initiated in the (a) Indian Ocean, (b) Maritime Continent, and (c) western Pacific. Contour interval is 15 W m^{-2}, with positive (zero) values dashed (omitted).

helpful for comprehensive understanding of favorable conditions for MJO initiation. To the best of my knowledge, however, there are very few previous works to tackle this topic in terms of the relationship between intraseasonal and interannual variations (Bellenger and Duvel, 2012; Hirata et al., 2013). Bellenger and Duvel (2012) have focused on the event-to-event variability of the amplitude distribution in the boreal winter MJO in relation to the diversity of MJO initiation, and suggested that the MJO initiated in the western Pacific is more likely to be observed in El Niño conditions. However, they have not clarified the specific processes leading to such a modulation of MJO initiation regions. Although Hirata et al. (2013) have compared atmospheric and SST fields before MJO initiation around the Indian Ocean and the Maritime Continent, the mechanism which makes the difference between the two cases has not been revealed at least in their analysis. Hence, the detailed processes of MJO realization in the hierarchical structure involving lower-frequency variabilities than the MJO are not well understood.

1.4 Purpose of this study

Since the discovery of the MJO around 50 years ago, there have been many dedicated efforts to understand the mechanisms of MJO initiation and propagation. Although most of previous studies have attempted to clarify the intrinsic processes of the MJO with a main focus on dynamical and thermodynamical variations on the MJO spatial scale and intraseasonal time scale, they fail to explain all aspects of the MJO characteristics which are recognized in the observational and modeling studies. In fact, there are some evidences that synoptic-scale wave disturbances can be responsible for moistening and convective development in initiation and/or propagation processes of MJO convection. In addition, interannual variabilities can also affect MJO initiation by modulating the background conditions, which is not explicitly considered in the preexisted initiation mechanisms. As described in Section 1.3, however, our knowledge of the cross-scale interaction in MJO realization is piecemeal compared to large-scale process-oriented understandings.

Based on this present research status, the objective of this study is to reveal the detailed processes and mechanisms which realize MJO convective initiation and subsequent propagation in terms of the multi-scale framework ranging from synoptic-scale disturbances to interannual variabilities. In particular, I clarify the following topics by means of observational data analyses and numerical model experiments:

- Do synoptic-scale equatorial waves have a central role in determining the initiation and the start of eastward propagation of MJO convection in the Indian Ocean through moistening and/or convective triggering processes? If so, how robust and necessary is the observed wave–MJO interaction?
- How is the modulation of MJO initiation regions understood from a standpoint of the mutual relationship between the intraseaonal and interannual variability? Is there a common environment and process which is favorable for MJO initiation even among different regions?

This dissertation is organized as follows. In the next chapter, mainly through an observational case study of an MJO event which was realized in the Indian Ocean during a field campaign in December 2017, I propose a new perspective that MRG dynamics is responsible for MJO convective initiation and propagation in the Indian Ocean. To examine the robustness of the mechanism proposed in Chapter 2, I conduct statistical analyses of MJO events initiated in the Indian Ocean during boreal winter in 1982–2012 using various kinds of observational daily data in Chapter 3. I also discuss the necessity of the MRG-related mechanism and the difference between when it works and when it does not. In Chapter 4, to advance comprehensive understanding of MJO initiation, I investigate a potential source of the diversity of MJO initiation regions and common initiation processes of the MJO among that diversity in terms of the influences of interannual variabilities of SSTs and associated atmospheric circulations on intraseasonal processes by utilizing both observational data and an atmospheric GCM. The last chapter summarizes the main results of this study and discusses the relationship among Chapters 2, 3 and 4, implications for the previous studies, and future perspectives.

Chapter 2

Observational Evidence of Mixed Rossby–Gravity Waves as a Driving Force for the MJO Convective Initiation and Propagation

The contents of this chapter have already been published as follows:

Takasuka, D., M. Satoh, and S. Yokoi (2019), Observational evidence of mixed Rossby-gravity waves as a driving force for the MJO convective initiation and propagation, *Geophys. Res. Lett.*, **46**, 5546-5555, doi:10.1029/2019GL083108.

2.1 Introduction

As reviewed in Chapter 1, the mechanism of MJO convective initiation and propagation is of great interest in tropical meteorology because the MJO has large impacts on global weather patterns as well as local rainfall systems (Zhang, 2013, and references therein). Most of previous works about the mechanics of the MJO emphasize the influence of atmospheric large-scale low-frequency physics. In terms of large-scale dynamical variations, it has been pointed out that intrusion of equatorially circumnavigating planetary-scale Kelvin waves (Knutson and Weickmann, 1987) can trigger MJO initiation through moisture accumulation associated with lower-tropospheric easterlies (Kikuchi and Takayabu, 2003; Seo and Kim, 2003) and/or the weakening of subsidence (Powell and Houze, 2015a) and that equatorial Kelvin–Rossby long-wave couplet dynamics with frictional convergence can drive MJO propagation (e.g., Wang and Rui, 1990; Wang and Chen, 2017). The importance of intraseasonal moisture variations to MJO realization is also recognized, as represented by the "discharge-recharge" mechanism related to gradual shallow-to-deep moistening (e.g., Bladé and Hartmann, 1993; Kemball-Cook and Weare, 2001; Benedict and Randall, 2007) and the moisture-mode theory (e.g., Raymond and Fuchs, 2009; Sobel and Maloney, 2012, 2013; Adames and Kim, 2016). In particular, the latter is nowadays featured because it appears to well describe preconditioning via horizontal moisture advection by MJO flows (e.g., Zhao et al., 2013; Maloney and Wolding, 2015; Hung and Sui, 2018) and qualitative characteristics of MJO propagation (e.g., Adames and Wallace, 2015; Maloney and Hartmann, 1998; Yokoi and Sobel, 2015).

Meanwhile, the moisture-mode views, in which horizontal moisture advection by MJO flows mainly acts on propagation (e.g., Adames and Wallace, 2015), are questioned by Pritchard and Yang (2016) with their analysis of the idealized simulations using a superparameterized Community Atmospheric Model (SP-CAM). In their numerical results, MJO-like disturbances propagated eastward through vertical processes, regardless of the direction of the mean meridional moisture gradient. From this evidence, they speculate on the relevance of high-frequency equatorial wave dynamics. There also exists an "MJO skeleton" theory,

which parameterizes the effects of synoptic-scale waves within MJO convective envelopes on MJO-scale dynamics (Majda and Stechmann, 2009b). These studies implicate that there is still room to reconsider the MJO in terms of scale interactions with synoptic-scale high-frequency equatorial waves.

Of various kinds of local high-frequency equatorial waves, my focus in this chapter is MRGs. MRGs theoretically have westward phase speed and eastward group velocity relative to the background wind (Matsuno, 1966). Beginning with Yanai and Maruyama (1966), who discovered westward-propagating wind variations at around the 5-day cycle in the tropical stratosphere using sounding data, subsequent observational studies showed that cross-equatorial circulations associated with MRGs with zonal wavenumbers 4–5 and periods of 4–5 days are evident in the upper troposphere over the equatorial central Pacific (e.g., Yanai et al., 1968; Yanai and Hayashi, 1969; Yanai and Murakami, 1970; Wallace, 1971). In addition, lower-tropospheric MRGs characterized by equatorial meridional wind fluctuations with a 4–5-day cycle also exist in the Pacific and that their phase line is tilted eastward with height (e.g., Yanai et al., 1968; Nitta, 1970; Liebmann and Hendon, 1990). These MRG-related dynamical variations are often coupled to convection around the date line (e.g., Takayabu and Nitta, 1993; Dunkerton and Baldwin, 1995; Wheeler and Kiladis, 1999; Kiladis et al., 2009). Some works have further revealed that MRGs tend to transition into tropical depression (TD)-type disturbances with shorter wavelength, more upright vertical structure, and stronger dynamics–convection coupling over the western Pacific as they propagate westward in a large-scale environmental convergence zone (e.g., Takayabu and Nitta, 1993; Sobel and Bretherton, 1999; Zhou and Wang, 2007). Thus, observational characteristics of MRGs have been greatly accumulated by detailed analyses in the Pacific region.

While tropospheric MRGs propagating over the Indian Ocean (IO) have had much less attention compared to the Pacific, several observational and numerical modeling studies have suggested that MRGs are prominent in initiation processes of the MJO in the IO. Using the in-situ observations from the MISMO field campaign (Yoneyama et al., 2008), Yasunaga et al. (2010) have found meridional wind variations associated with MRGs especially trapped in

the mid-troposphere and related moisture resurgence before an MJO convective outbreak. During the DYNAMO campaign (Yoneyama et al., 2013), the contributions of MRGs to MJO initiation have also been confirmed in the modulation of moisture fields through dry air intrusion (Kerns and Chen, 2014) and in vertical and horizontal moisture transport (Chen et al., 2015; Muraleedharan et al., 2015). Moreover, to understand the intrinsic initiation mechanism of the MJO, Takasuka et al. (2018) conducted long-term aqua-planet experiments using the Nonhydrostatic Icosahedral Atmospheric Model (NICAM) and suggested the importance of mid-tropospheric moistening by cross-equatorial shallow circulations for triggering MJO convection. This result implies that MRGs may have an essential role in MJO initiation, although only limited observational case studies have demonstrated the relationship between the MJO and MRGs.

It has also been pointed out that MRGs act on MJO propagation. Straub and Kiladis (2003) and Yang and Ingersoll (2011) have proposed that MJO convection can be the packet of convectively coupled MRGs with eastward group velocity of ~ 5 m s^{-1} which is almost equal to the MJO propagation speed (Wheeler and Kiladis, 1999), a hypothesis that is consistent with the MJO's multi-scale structure (e.g., Nakazawa, 1988). Combining this hypothesis with the aforementioned insight about the impacts of MRGs on MJO initiation, I come up with an idea that MRGs may be key to unified interpretation of the initiation and the start of eastward propagation of MJO convection.

In this chapter, the above idea is validated mainly by the detailed analysis of an MJO event initiated in late December 2017 during the intensive observation campaign, the Years of the Maritime Continent (YMC)-Sumatra 2017. Specifically, I show that MRGs actually contribute to MJO initiation and propagation through wave–convection coupling, mid-tropospheric moistening, and associated successive lower-tropospheric wave packet formation. This chapter is organized as follows. In Section 2.2, the observational data used in this study are described. Section 2.3 provides an overview of the MJO and synoptic-scale wave activities observed in YMC-Sumatra 2017. The specific processes of the MJO initiation and propagation driven by MRGs are clarified in Section 2.4. Section 2.5 discusses potential for

robustness of the revealed MRG-related mechanism and comparison with another process, and the summary is given in Section 2.6

2.2 Data

YMC-Sumatra 2017 was conducted from 16 November 2017 to 15 January 2018. I utilize 3-hourly radiosonde observations from the research vessel (R/V) *Mirai* stationed at 4.24°S, 101.52°E from 0700 LT 5 December to 1300 LT 1 January (LT; local time). I use 6-hourly atmospheric data from ERA-Interim (Dee et al., 2011) for the entire observation period of YMC-Sumatra 2017. The dataset has a horizontal resolution of 0.5°× 0.5°, with 27 vertical layers spanning 1000–100 hPa. Convective signals are captured by 6-hourly precipitation of the Global Satellite Mapping of Precipitation (GSMaP; Okamoto et al. (2005)) product and the infrared channel brightness temperature (TBB) of the Gridded Satellite (GridSat-B1; Knapp et al. (2011)) data with a 0.1°× 0.1° and about 0.07°× 0.07° horizontal resolution, respectively. Anomaly fields are defined as deviations from the 27-day mean from 5 to 31 December, which effectively removes the December climatology and the interannual variability. To monitor MJO activity, I use two independent MJO indices: Real-time Multivariate MJO (RMM) index (Wheeler and Hendon, 2004) and the bimodal tropical intraseasonal oscillation (BISO) index (Kikuchi et al., 2012). Note that the latter is derived from only equatorial (30°S–30°N) OLR anomalies.

To discuss my target processes in other MJO events in Section 2.5, I also use another in-situ observational data and the above products from 1 October to 30 November 2011 during the DYNAMO campaign (Yoneyama et al., 2013). For the former, 3-hourly radiosonde observations at Gan Island (0.7°S, 73.2°E) from 0000 UTC 1 October to 2100 UTC 30 November are utilized. Anomalies for this period are calculated by subtracting the corresponding 62-day mean.

2.3 Overview of the MJO and synoptic-scale wave activities

The slow eastward propagation of two large-scale precipitation systems is evident in a time–longitude diagram of 10°S–10°N precipitation from November 2017 to January 2018 (Fig. 2.1a). These systems can be regarded as active MJO events, denoted with MJO1 and MJO2, as inferred from the two MJO indices (Fig. 2.1b). Although the amplitude of the BISO index is not so strong until around 10 December, both the RMM and BISO indices show smooth phase progression to phase 8 with amplitudes more than unity around 20 December, indicating that MJO1 is active. The BISO index passes into phase 1 on 24 December and evolves the subsequent phases with significant amplitudes to mid-January. In fact, around 21–25 December, the convection develops roughly over 40°–60°E and starts to propagate eastward in association with MJO2 (Fig. 2.1a). The RMM index has similar characteristics, but tends to be predated by the BISO index.

The intensive observations from R/V *Mirai* captured the MJO-suppressed phase leading to the MJO2 realization. Therefore, I can examine characteristics of synoptic-scale disturbances in the MJO2 initiation processes using the radiosonde-derived data at R/V *Mirai*. Meridional winds have clear spectral peaks at 5–6 days over 600–450 hPa, where zonal winds also have large power spectra (Fig. 2.1c). There is another spectral peak around 4–5 days in both 1000–800-hPa zonal and meridional winds. Hence, wind variations with rotational components were observed in the 4–6-day cycle in the mid- to lower troposphere around R/V *Mirai*.

The vertical and horizontal structure of these fluctuations are further examined. Figure 2.2a shows the time–height section of radiosonde-derived meridional (shading) and zonal wind anomalies (contours) filtered for 3.5–7-day periods using a Lanczos filter (Duchon, 1979) with a filter length of 25 days. Mid-tropospheric meridional wind signals are evident especially after 10 December, and they are almost in quadrature with zonal wind signals. This corresponds to very clear cross-equatorial circulations as shown in the time–latitude section of mid-tropospheric wind fields at 101.5°E (Fig. 2.2b), which is consistent with the MRG

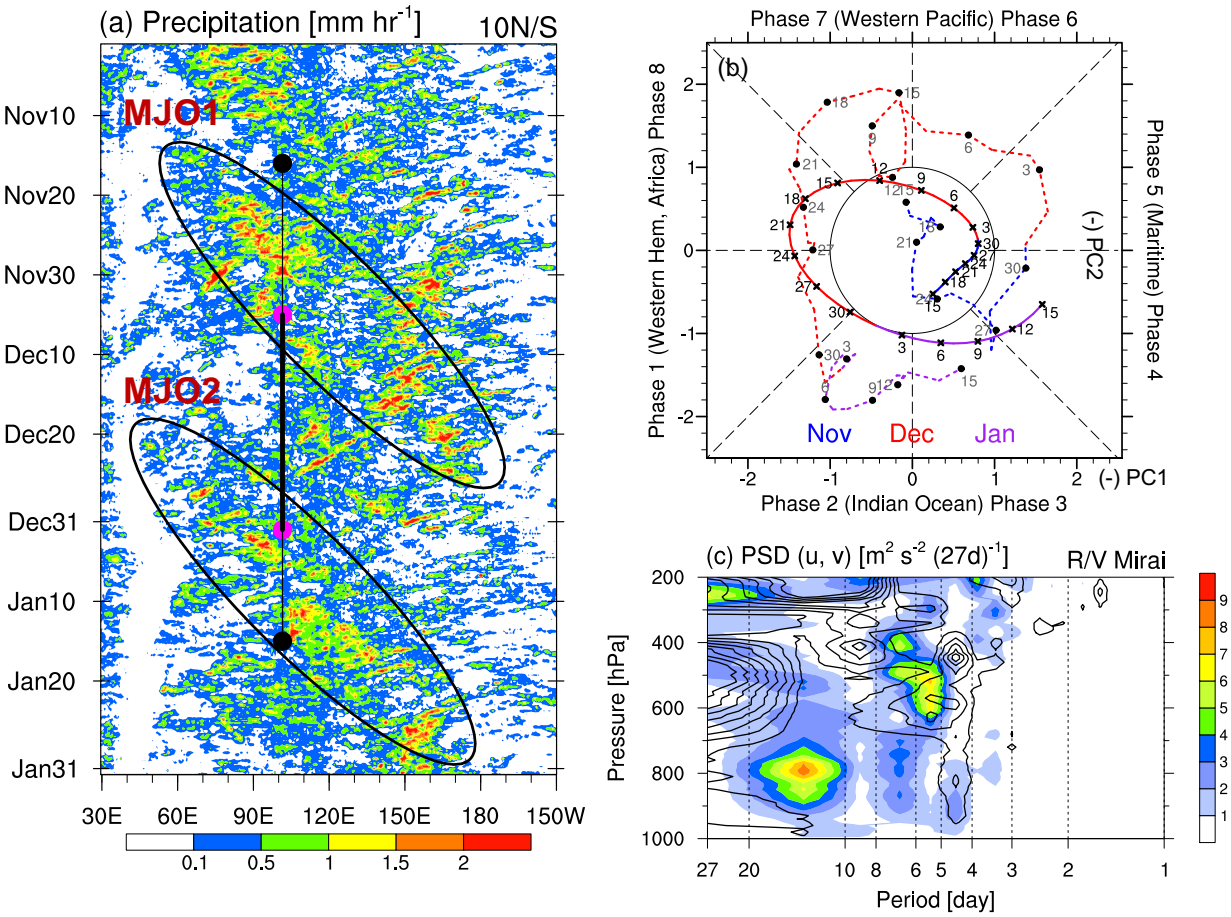

Figure 2.1: (a) Time–longitude diagram of 10°S–10°N averaged precipitation. Ellipses indicate two MJO events. The vertical line connecting black (magenta) circles denotes the longitude and period of the intensive observation (at R/V *Mirai*). (b) Phase diagram of RMM (broken) and BISO (solid) indices from 15 November 2017 to 15 January 2018, with every 3 days plotted as black circles and cross marks, respectively. (c) Power spectral density of radiosonde-derived meridional (shading) and zonal (contours) winds at R/V *Mirai*. Contour interval is 1.5 $m^2\ s^{-2}\ (27d)^{-1}$.

horizontal structure in dry shallow water systems (Matsuno, 1966). It is also found that lower-tropospheric meridional winds have an equatorially symmetric feature until 10 December and after 15 December. As for the wind fluctuations after 15 December, I can say that MRGs are active in mid- to lower-troposphere, and their vertical structure is largely inclined eastward to the mid-troposphere. Note that this is similar to the structure of the fast-propagating MRG shown later (see Fig. 2.5b).

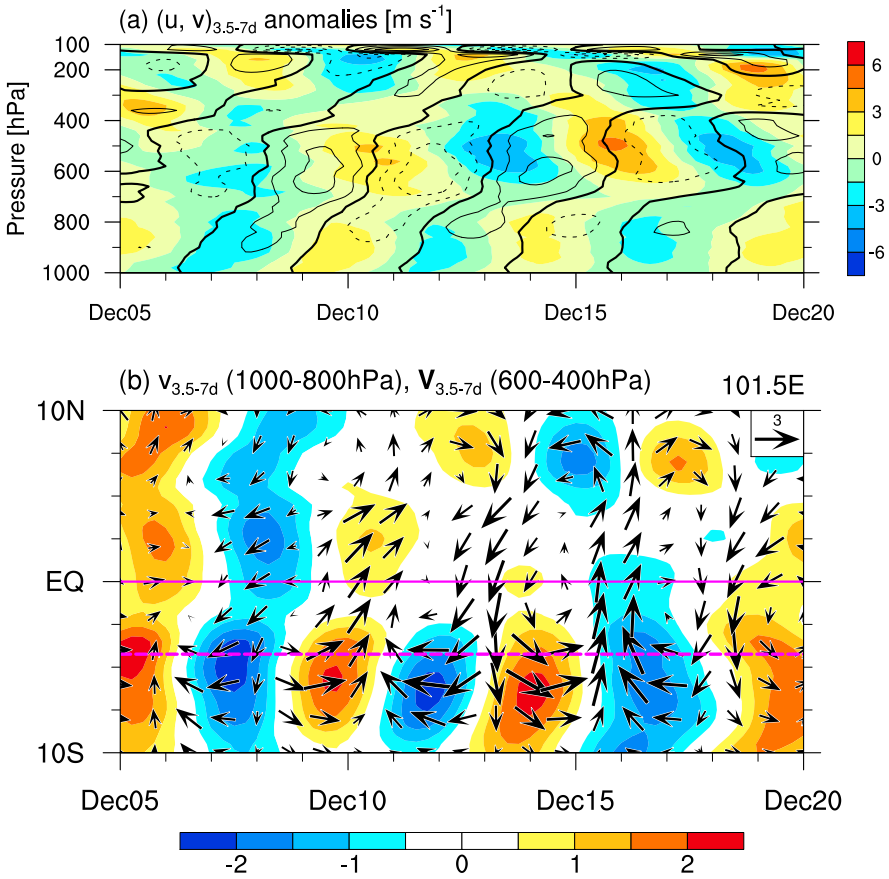

Figure 2.2: (a) Time–height section of radiosonde-derived meridional (shading) and zonal wind anomalies (contours) filtered for 3.5–7-day periods at R/V *Mirai*. Contour interval is 2 m s^{-1}, with negative (zero) values dashed (bolded). (b) Time-latitude section of 3.5–7-day filtered meridional wind anomalies over 1000–800 hPa (shading) and horizontal wind anomalies over 600–400 hPa (vectors; m s^{-1}) at 101.5°E. The magenta broken line denote the latitudinal location of R/V *Mirai*.

2.4 Impacts of MRGs on the MJO initiation and propagation

2.4.1 Processes leading to MJO realization

Figure 2.3a displays the time–longitude diagram of 3.5–7-day-filtered equatorial meridional wind anomalies averaged over the 600–400-hPa layer; the non-filtered precipitation field is also plotted. Meridional wind signals associated with MRGs propagate westward from the active convective areas around 120°E, which are related to MJO1 over the Maritime Conti-

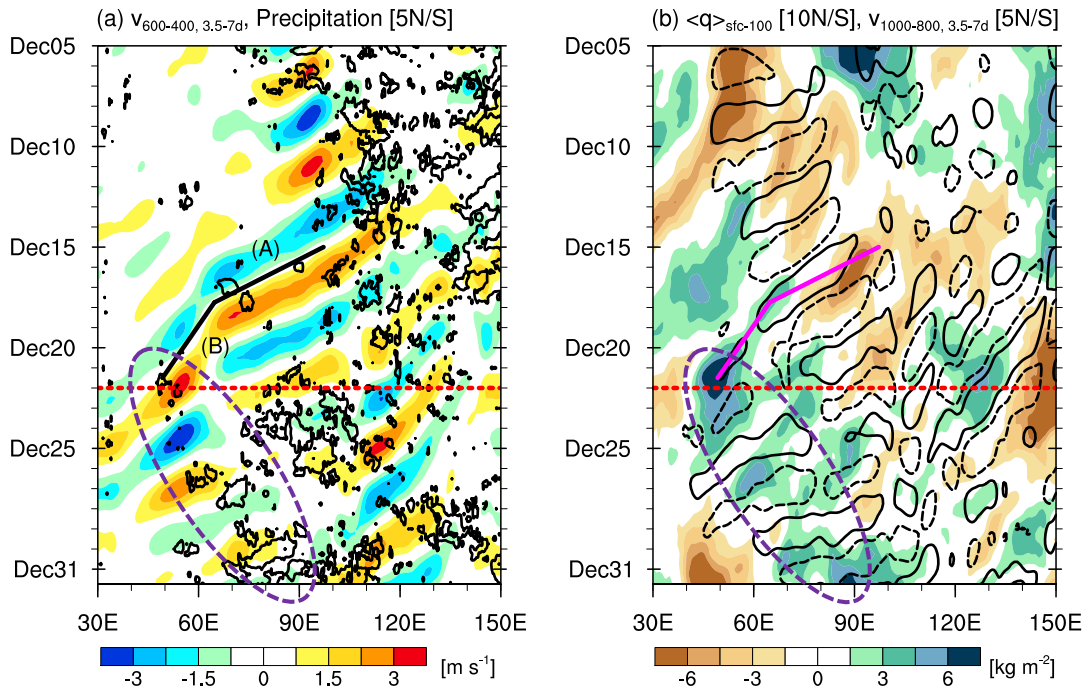

Figure 2.3: (a, b) Time–longitude diagram of filtered 600–400-hPa meridional wind (24-h running mean CWV) anomalies (shading) and precipitation with 0.8 mm hr^{-1} (filtered 1000–800-hPa meridional wind anomalies with ±0.75 m s^{-1}) (contours). CWV and all other values are averaged over 10°S–10°N and 5°S–5°N, respectively. Purple ellipses enclose the MJO2 event and red dashed lines denote its initiation.

nent, and they are more active over the IO after 15 December. Notably, the MJO2 initiation on 22 December, defined as the enhancement of precipitation, occurs around the time when mid-tropospheric meridional wind anomalies amplify after a slowdown of their westward phase speed in 60°–70°E. As will be shown in the following subsection, this slowdown is caused by zonal wavelength shortening. In Fig. 2.3b, which shows 24-hour running mean equatorial CWV and filtered 1000–800-hPa meridional wind anomalies, moisture signals are enhanced in conjunction with westward propagation of southerlies in 50°–60°E during 20–22 December, and northerlies are newly formed around 60°E on 22 December. Subsequently, this wave packet development continuously precedes the center of convection or moist anomalies associated with MJO2, which strongly suggests that the MRG group velocity can drive MJO2 propagation over the IO.

To explore the horizontal distributions of convection and moisture before MJO2 initiation, snapshots of TBB, precipitation, and CWV anomalies during 16–22 December are plotted in

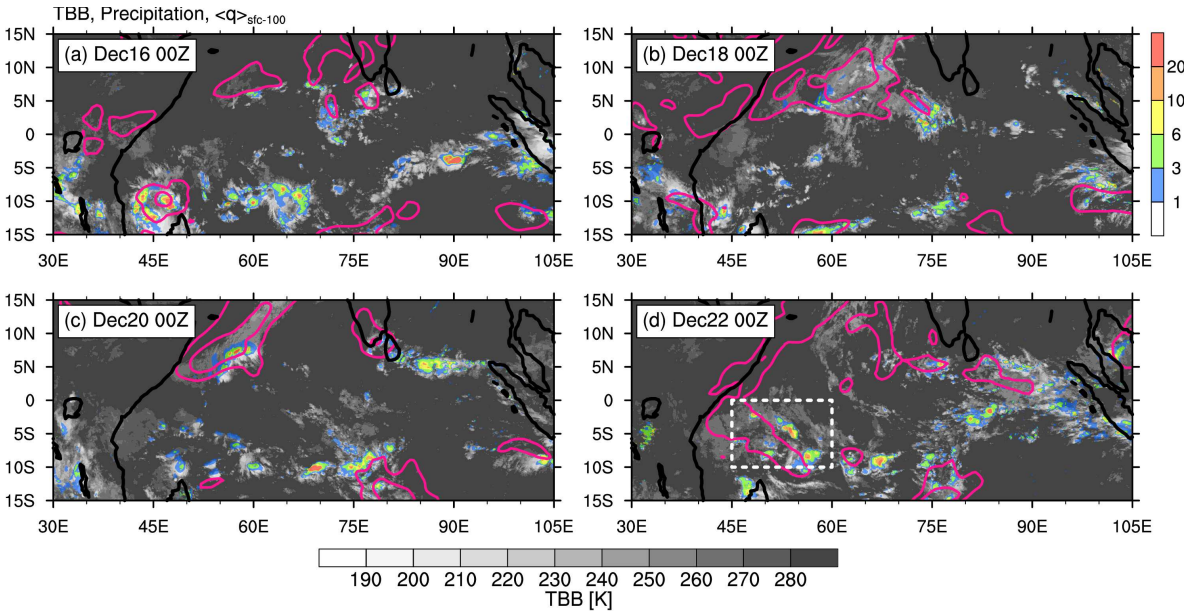

Figure 2.4: Snapshots of TBB (gray), precipitation (color), and positive CWV anomalies (contours) at 00Z (a) 16, (b) 18, (c) 20, and (d) 22 December. Contour interval is 7 kg m^{-2}.

Fig. 2.4. On 16 December, convective activities over the IO have equatorially antisymmetric features around 60°E, 10°S and 75°E, 5°N (Fig. 2.4a). In particular, active convection with moisture around 75°E, 5°N propagates westward and is further enhanced in 50°–60°E on 20 December (Figs. 2.4a,c). This suggests a strong coupling between the convection and the MRG. Considering its timing, this behavior is reminiscent of the relationship with the phase speed change of mid-tropospheric MRGs (Fig. 2.3a). Subsequently, MJO2 is realized as the convective development over 10°S–0°, 45°–60°E (Fig. 2.4d). Note that active convection around this region can be found in the boreal winter MJO composite in phase 1 by Wheeler and Hendon (2004) and Kikuchi et al. (2012).

In summary, the modulation of wave–convection coupling associated with the phase speed change, along with the subsequent wave packet formation, can lead to MJO2 initiation and propagation. I next examine these elements, focusing on the wave structure change, eddy kinetic energy (EKE) and moisture variations, and MRG-induced convective triggering.

2.4.2 Tight coupling between MRGs and convection

I compare dynamical and moisture fields between fast- and slow-propagating MRGs in Figs. 2.5a and 2.5b. The horizontal structure (Fig. 2.5a) of filtered 600–400-hPa winds and 1000–800-hPa meridional winds shows that the wavelength is shorter for the slow mode than the fast mode, especially in the mid-troposphere. This is also confirmed in Fig. 2.6a, which shows a time evolution of the mid-tropospheric MRG characteristics such as the mean-flow (i.e., 11-day running mean 600–400-hPa zonal winds averaged over 10°S–10°N, hereafter $\overline{u}$) relative westward phase speed along a node near lines A and B (Fig. 2.6b) and the zonal wavenumber estimated from the wavelength defined as twice the distance between the maximum and minimum meridional wind phase lines (Fig. 2.6b). I recognize that a decrease in the phase speed begins at almost the same time as an increase in the wavenumber. This indicates a causal relationship between phase speed change and wavelength shortening. Another structure change in Fig. 2.5a is that the location of the low-level meridional wind maximum is closer to that of the mid-level maximum, and moist anomalies to the north are more enhanced in the slow mode. These characteristics are clearer in the vertical structure (Fig. 2.5b): the dynamical structure is more upright (but with eastward tilting maintained) and the more upper troposphere up to 400 hPa becomes moistened with stronger ascent during the slow propagation. As expected, the dynamics in the slow mode is tightly coupled to moisture and convection.

As introduced in Section 2.1, similar phase speed change and strong wave–convection coupling due to the wave contraction, known as the MRG–TD transition, have been observed to the west of the dateline (e.g., Takayabu and Nitta, 1993; Sobel and Bretherton, 1999; Zhou and Wang, 2007). Because they have not yet been reported for the western IO, I speculate as to what triggers wavelength shortening. One candidate that I found is the basic zonal convergence for zonally propagating waves. Figures 2.6a and 2.6b show the time–longitude diagram of $d\overline{u}/dx$ and time series of $d\overline{u}/dx$ at nodes of the mid-tropospheric MRG, respectively. MRG westward phase speeds (zonal wavenumbers) begin to decrease (increase) in the weak zonal

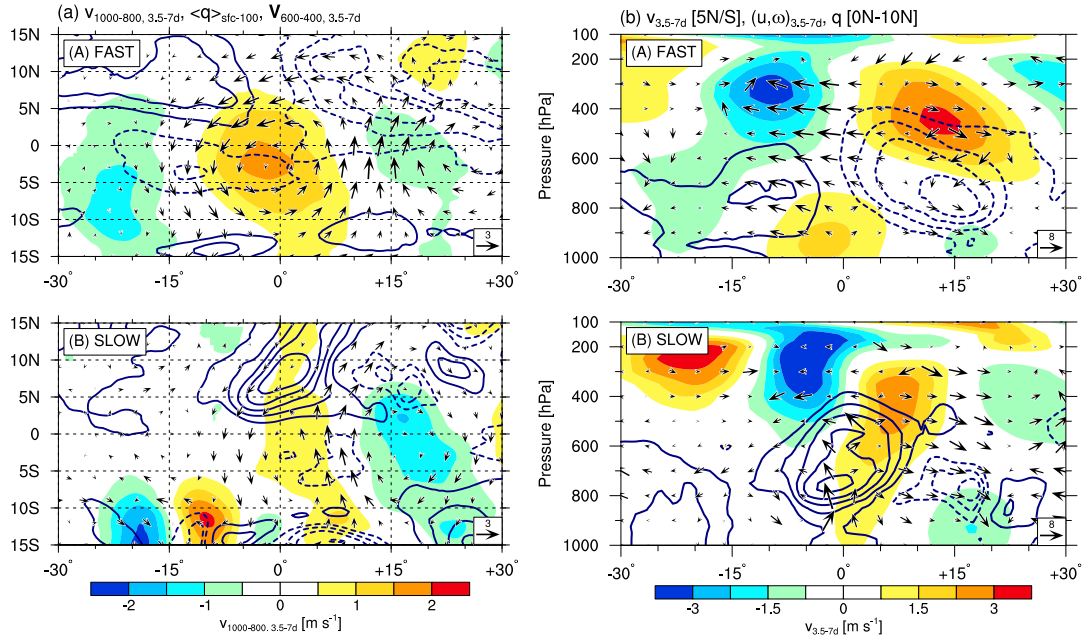

Figure 2.5: (a) Horizontal structure of filtered 1000–800-hPa meridional wind (shading) and 600–400-hPa horizontal wind (vectors; m s^{-1}) anomalies, and CWV anomalies (contours), averaged along the solid lines A (top) and B (bottom) in Fig. 2.3a. Contour interval is 3 kg m^{-2}, with negative (zero) contours dashed (omitted). (b) Similar to (a), but longitude–height section of filtered meridional (shading) and zonal-vertical (vectors; m s^{-1} and Pa s^{-1} for horizontal and vertical components, respectively) winds, and specific humidity (contours). Meridional winds and all other values are averaged over 5°S–5°N and 0°–10°N, respectively. Contour interval is 0.5 g kg^{-1}. The vertical *p*-velocity in vectors is multiplied by 500.

convergence region of 50°E–70°E. This behavior is qualitatively consistent with the linear wave theory (Lighthill, 1978), although a WKB assumption is not rigorously satisfied.

To grasp a source of the mid-level convergence around the western IO, I check 11-day running mean equatorial dynamical and moisture fields associated with the Walker circulations. Figure 2.7 shows 11-day running mean Walker circulation components of zonal and vertical winds and specific humidity averaged over 10°S–10°N. The Walker circulation components are defined as the deviations from the zonal mean of each field. Convective activities are suppressed over the IO during the period of 10–15 December, paired with the top-heavy upward motions around 100°–120°E associated with MJO1 (Fig. 2.7a). Meanwhile, by 20 December, large-scale ascent and moist signals develop to the mid-troposphere (600–400 hPa) in the IO, and the related easterly outflows can be seen in 70°–80°E (Fig. 2.7b). In addition,

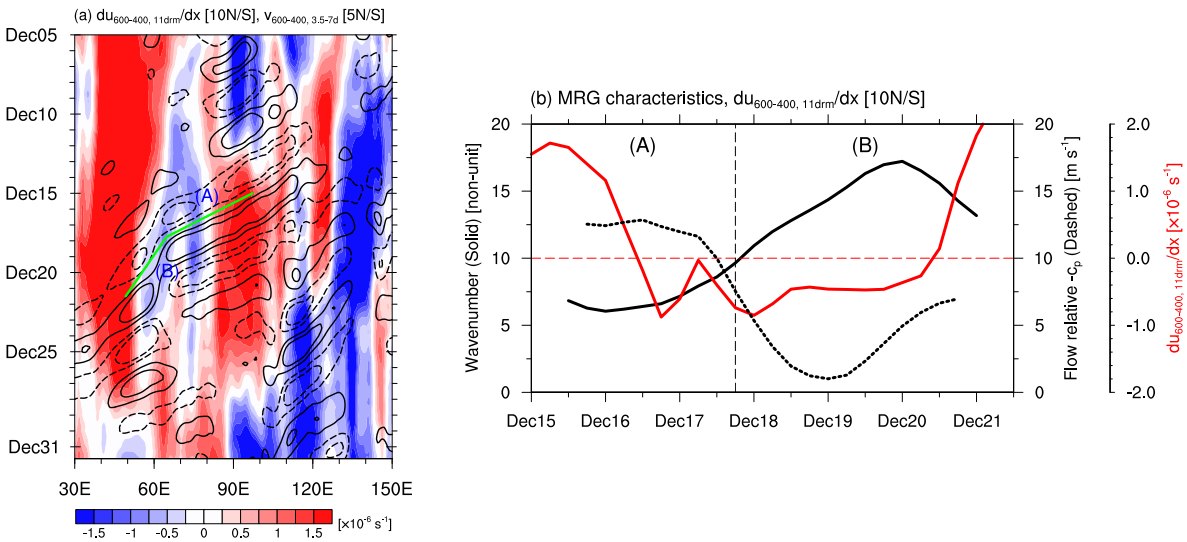

Figure 2.6: (a) Time–longitude diagram of $d\overline{u}/dx$ (shading) and 5°S–5°N averaged and filtered 600–400-hPa meridional wind anomalies with ±1 and ±2 m s^{-1} (contours). (b) Time series of 24-hour running mean zonal wavenumber (black solid) and flow relative westward phase speeds (dashed), and $d\overline{u}/dx$ at nodes of the mid-tropospheric MRG (red solid).

600–400-hPa easterlies in 50°E–60°E are weaker relative to the central IO. Hence, the weak zonal convergence zone is formed in the mid-troposphere of 50°E–70°E (Fig. 2.5c), leading to the modulation of MRGs.

2.4.3 MRG wave packet formation and the start of MJO propagation

The convective development associated with MJO2 initiation occurs almost at the same time as the formation of equatorial northerlies of an MRG wave packet around 60°E (Figs. 2.3b and 2.4d). In fact, I confirm the enhancement of the filtered low-level cyclonic circulation in 10°S–0°S, 45°–60°E on 22 December (Fig. 2.8a), which suggests dynamics-convection coupling. To evaluate why MRG-related northerlies are newly formed, I conduct the EKE budget analysis (e.g., Seiki and Takayabu, 2007) as follows:

$$\frac{\partial K'}{\partial t} = -\underbrace{\overline{\mathbf{V}'_h(\mathbf{V}'\cdot\nabla)\overline{\mathbf{V}}_h}}_{K_mK_e} - \underbrace{\overline{\mathbf{V}}\cdot\nabla K'}_{A_mK_e} - \underbrace{\overline{\mathbf{V}'\cdot\nabla K'}}_{A_eK_e} - \overbrace{\frac{R}{p}\overline{\omega' T'}}^{P_eK_e} - \underbrace{\overline{\nabla\cdot(\mathbf{V}'\Phi')}}_{GK_e} + (Resid.) \tag{2.1}$$

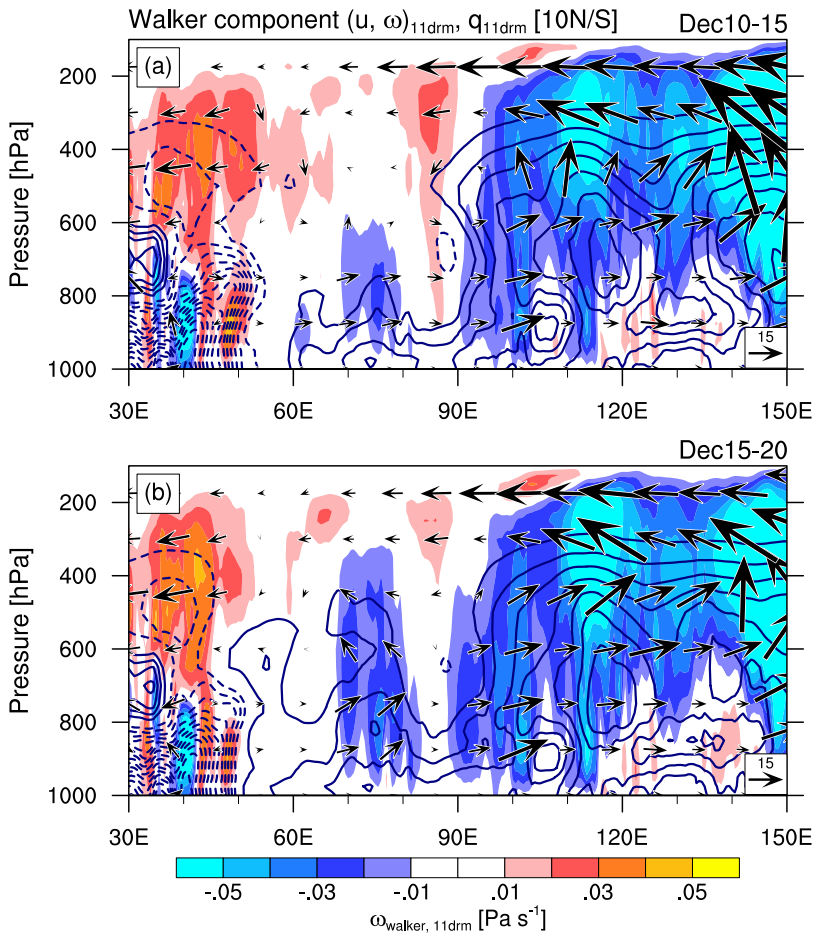

Figure 2.7: Longitude–height sections of 11-day running mean p-velocity (shading), specific humidity (contours), and zonal-vertical winds (vectors; m s^{-1} and Pa s^{-1} for horizontal and vertical components, respectively) associated with Walker circulation components defined as the deviations from zonal mean. All values are averaged over 10°S–10°N (a) from 00Z 10 to 15 December and (b) from 00Z 15 to 20 December. Contour interval is 0.3 g kg^{-1}, with negative (zero) contours dashed (omitted). The vertical p-velocity in vectors is multiplied by 500.

where $K' = (\overline{u'^2} + \overline{v'^2})/2$ is the EKE associated with MRG waves; $\mathbf{V}$ and $\mathbf{V}_h$ are three-dimensional and horizontal wind vector, respectively; ω is vertical p-velocity; T is temperature; Φ is geopotential; and R is gas constant. Overbars and primes denote 11-day running mean and 3.5–7-day-filtered values, respectively. The physical meanings of each term on the right-hand side in Eq. (2.1) are briefly described; $K_m K_e$ is barotropic conversion from the background to EKE; $A_m K_e$ and $A_e K_e$ are EKE advection by background and eddy flows, respectively; $P_e K_e$ is baroclinic conversion from eddy available potential energy (EAPE);

GK_e is EKE redistribution associated with the work done by the pressure gradient force; and the last term (*Resid.*) is a residual including sub-grid scale diffusive processes. The EKE source and sink terms are K_mK_e, P_eK_e, and the residual, and all the other terms contribute to redistributing EKE.

The anomalous 1000–800-hPa EKE tendency during 20–22 December is positive in 5°S–5°N, 60°–65°E (red square in Fig. 2.8a), consistent with the development of low-level northerlies. EKE budget terms averaged over that period and region suggest the dominance of geopotential eddy flux convergence (GK_e) (Fig. 2.8b). However, the GK_e process is only a redistribution of EKE, not its source. Here, it is thought that EKE is generated in the mid-troposphere and redistributed to lower-level fields. The 600–400-hPa EKE tendency anomalies are significantly positive in 5°S–5°N, 45°–60°E (blue square in Fig. 2.8a). This comes from the conversion from EAPE (P_eK_e) due to strong wave–convection coupling as well as GK_e (Fig. 2.8b), which overcomes large negative residual anomalies due to unresolved strong dissipation partly associated with cumulus friction. In addition, the mid-level EKE positive tendency maximum is to the west of the low-level one (Fig. 2.8a). This confirms that the slow MRG, which is vertically tilted eastward to the mid-troposphere, has downward and eastward energy dispersion (Fig. 2.8b); the lower-tropospheric wave packet formation is the result of efficient production of mid-level EKE.

Another essential feature for MJO2 realization is a basin-scale moistening and atmospheric overturning. Figure 2.8c shows the time–height section of 5-day running mean moisture tendency and vertical p-velocity anomalies averaged over 10°S–10°N, 60°–90°E. There are large positive tendency anomalies over 600–400 hPa on 15–17 December prior to bottom-to-middle moistening and ascent. Hence, the mid-tropospheric moisture resurgence helps make conditions favorable for the convective development over the IO in late December. According to the moisture budget analysis for this region and period (Fig. 2.9a), this mid-tropospheric moistening comes primarily from meridional advection and secondarily from column processes as the sum of vertical advection and residual terms. Figures 2.8d and 2.9b show that the mid-tropospheric equatorial IO has positive horizontal advective tendencies

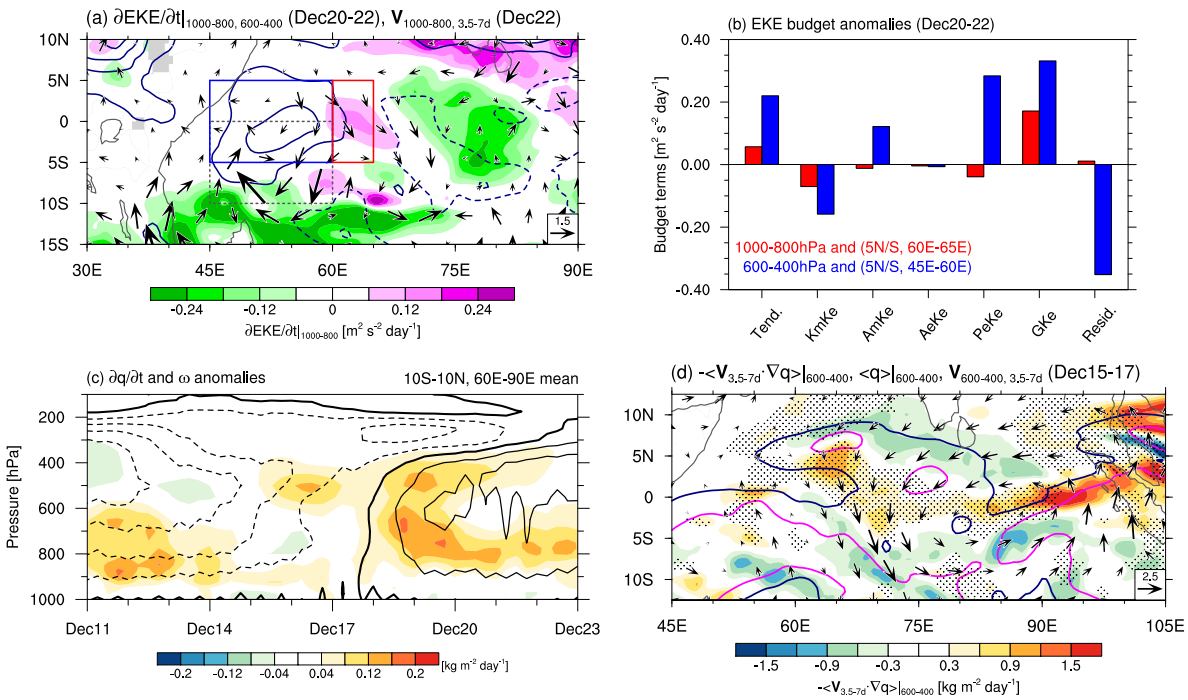

Figure 2.8: (a) 1000–800-hPa (shading) and 600–400-hPa (contours) EKE tendency anomalies averaged from 00Z 20 to 22 December, and filtered 1000–800-hPa horizontal wind anomalies on 00Z 22 December (vectors; m s^{-1}). Contour interval is 0.15 m^{-2} s^{-2} d^{-1}, with negative (zero) contours dashed (omitted). (b) (red) 1000–800- (blue: 600–400-) hPa anomalous EKE budget terms averaged over 5°S–5°N, 60°–65°E (45°–60°E) from 00Z 20 to 22 December. (c) Time–height sections of 5-day running mean moisture tendency (shading) and vertical *p*-velocity anomalies (contours) averaged over 10°S–10°N, 60°–90°E. Contour interval is 0.006 Pa s^{-1}, with positive (zero) contours dashed (bolded). (d) Horizontal moisture advection anomalies by filtered winds (vectors; m s^{-1}) and non-filtered winds (shading and hatched), and raw values of water vapor with 3.0 and 4.5 kg m^{-2} (navy and magenta contours), averaged over 600–400 hPa from 00Z 15 to 17 December. Hatched ares have more than 0.3 kg m^{-2} d^{-1}.

mainly by cross-equatorial flows from off-equatorial humid regions (e.g., 0°–10°N, 60°–80°E) associated with MRG shallow circulations, or broadening of moistened areas around the IO. This is consistent with a preconditioning process in the aqua-planet MJO study by Takasuka et al. (2018).

The relationship between MJO2 propagation and the continuous MRG wave packet formation is seen clearly in horizontal maps. Figure 2.10 displays snapshots of TBB, CWV, and filtered low-level winds and convergence with certain strength every 2 days from 00Z 24 December. Southerlies associated with an anticlockwise circulation around 60°–70°E on 24

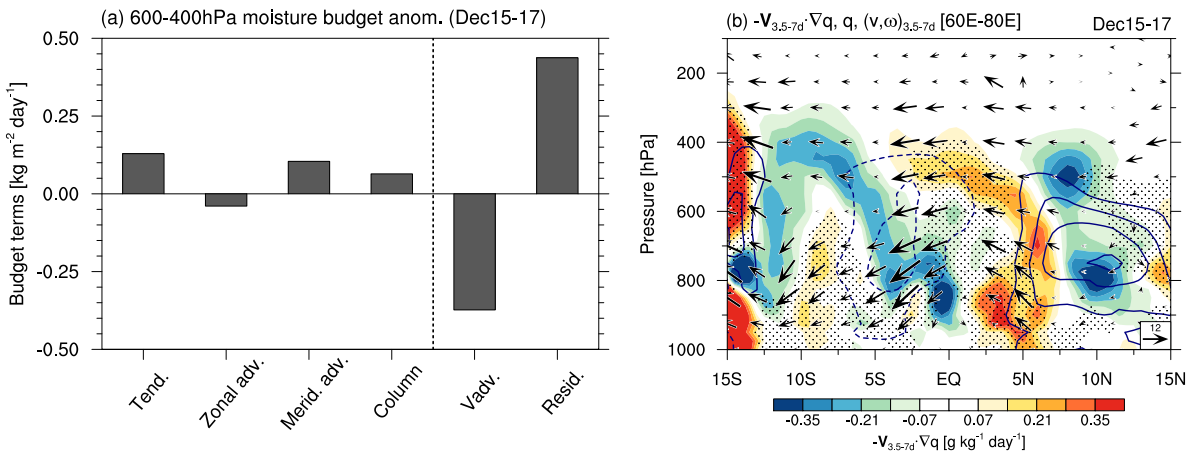

Figure 2.9: (a) 5-day running mean 600–400-hPa anomalous moisture budget terms averaged over 10°S–10°N, 60°–90°E from 00Z 15 to 17 December. "Column" means the column process, the sum of vertical advection and residual terms. (b) Latitude–height section of horizontal moisture advection anomalies by 3.5–7-day-filtered winds (vectors; m s^{-1} and Pa s^{-1} for horizontal and vertical components, respectively) and non-filtered winds (shading and hatched), and specific humidity anomalies (contours) averaged over 60°–80°E from 00Z 15 to 17 December. Hatched are the areas with more than 0.14 g kg^{-1} d^{-1}. Contour interval is 0.5 g kg^{-1}, with negative (zero) contours dashed (omitted). The vertical *p*-velocity in vectors is multiplied by 700.

December induce convergence A* (Conv-A*) and convective system A (CS-A) is developed by 26 December. At the same time, northerlies of a newly formed clockwise circulation enhance Conv-B* to the east (Fig. 2.10b), which leads to organized CS-B on 28 December (Fig. 2.10c). Similarly, Conv-C* is realized with cross-equatorial southerlies in 80°–90°E and leads to developed CS-C on 30 December, and Conv-D* is also induced by northerlies (Fig. 2.10d): the eastward amplification of low-level flows related to the MRG group velocity effectively triggers convective systems to the east, one after another, and the group of subsequent triggered and organized systems propagates eastward slowly at MJO spatial scales.

2.5 Discussion

2.5.1 Potential for robustness of the MRG-related processes

In previous sections, the roles of MRGs in MJO convective initiation and propagation over the IO are highlighted for only one case. To discuss potential for robustness of this

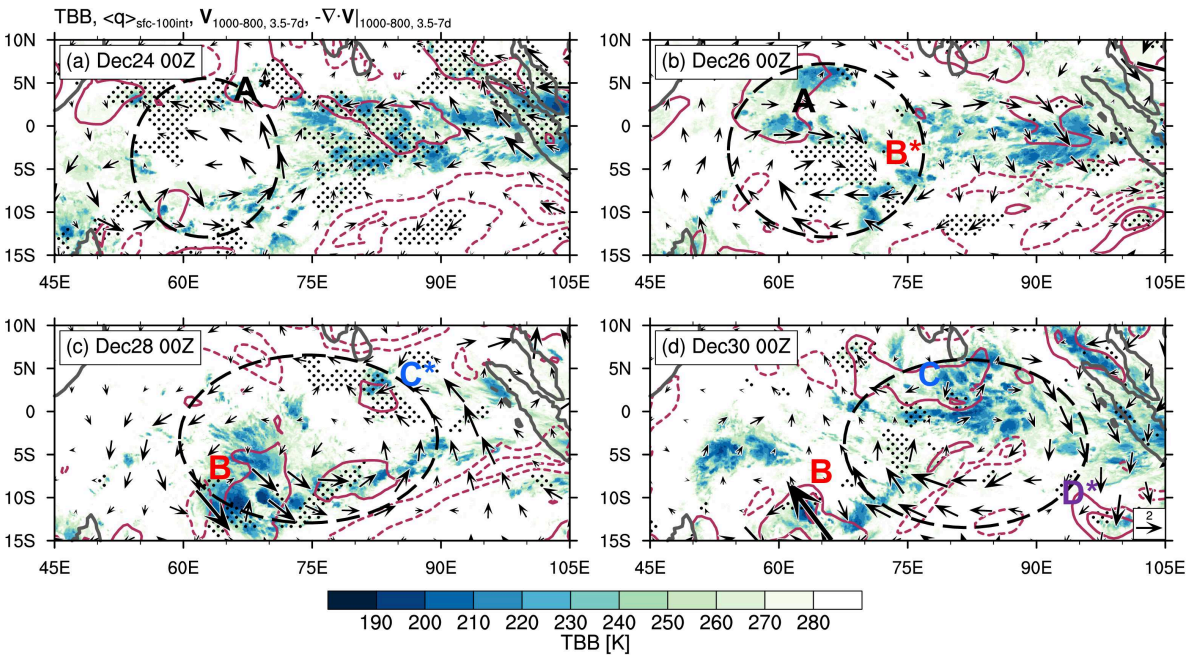

Figure 2.10: Snapshots of TBB (shading), anomalous CWV (contours), and filtered 1000–800-hPa horizontal wind (vectors; m s^{-1}) and convergence anomalies (hatched) from 00Z 24 to 30 December. Contour interval is 7 kg m^{-2}, with negative (zero) contours dashed (omitted). Hatched are the areas with less than -1.0×10^{-6} s^{-1}. Letters A–C and A*–D* denote developed CSs building MJO2 convective envelopes and convergence leading to developed CSs, respectively.

perspective, I compare MJO2 with two additional MJO events in October–November 2011 (Oct-MJO and Nov-MJO) during the DYNAMO campaign. The reason for selecting these cases is that they are obviously initiated in the western IO as with MJO2 during YMC-Sumatra 2017 and I can use in-situ observational data. Figure 2.11a displays a time–longitude diagram of 10°S–10°N averaged precipitation from October to December 2011. I find two dominant MJO convective envelopes from the western IO to the Maritime Continent. In Oct-MJO, MJO convection is initially triggered around 17 October (blue dashed line) but actually starts eastward propagation several days later (22 October; first red dashed line). Nov-MJO convection smoothly propagates eastward after it is triggered around 50°E on 17 November (second red one).

To examine whether dynamical variations associated with MRGs are observed, Figs. 2.11b and 2.11c show power spectral density of 3-hourly radiosonde-derived meridional wind at Gan Island in October and November, respectively. Meridional wind variations with about

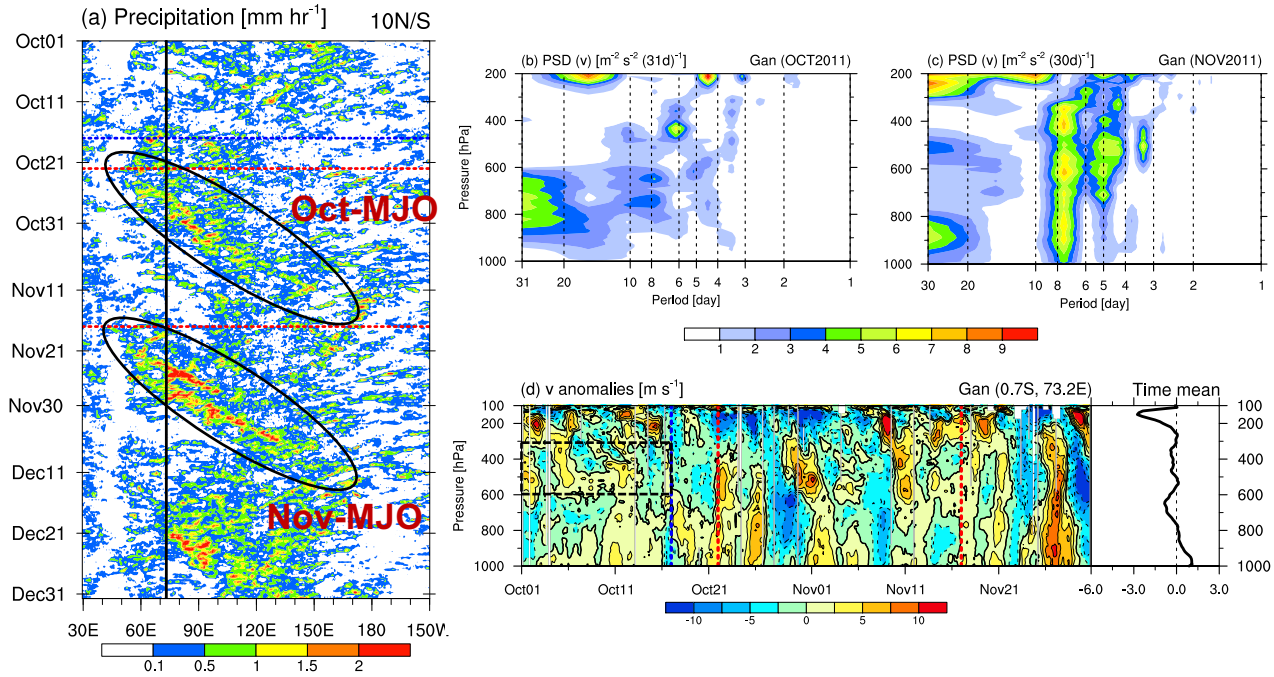

Figure 2.11: (a) Time–longitude diagram of 10°S–10°N averaged precipitation from October to December 2011. Ellipses indicate two MJO events. The vertical line denotes the longitude of Gan Island. Oct-MJO convection is initially triggered on 17 October (blue dashed line) and starts eastward propagation on 22 October (first red dashed line), and Nov-MJO convection is initiated on 17 November (second red dashed line). (b, c) Power spectral density of radiosonde-derived meridional wind at Gan Island in October (November). (d) Time-height section of 24-hour running mean meridional wind anomalies at Gan. Anomalies are defined as deviations from (right) a mean profile for the October–November period.

a 6-day cycle are prominent over 500–400 hPa in October, although it is difficult to detect robust peaks in other domains (Fig. 2.11b). Meanwhile in November, strong peaks at 4–8 days in the troposphere are clearly detected, and upper-tropospheric (less than 400 hPa) wind variations are more obvious than the YMC-Sumatra 2017 case (Figs. 2.11c and 2.1c). These characteristics are also recognized in a time–height section of non-filtered meridional wind anomalies at Gan (Fig. 2.11d); wind variations with a specific cycle are especially seen in the mid- to upper troposphere before Oct-MJO initiation (black square in Fig. 2.11d), and they are clearer in the whole troposphere around Nov-MJO event. Hence, I expect that MRG activities can affect both MJO initiation more or less.

Based on the above observations, I display similar figures to Fig. 2.3 for Oct-MJO (Figs. 2.12a,b) and Nov-MJO (Figs. 2.12c,d), except for using 24-hour running mean values

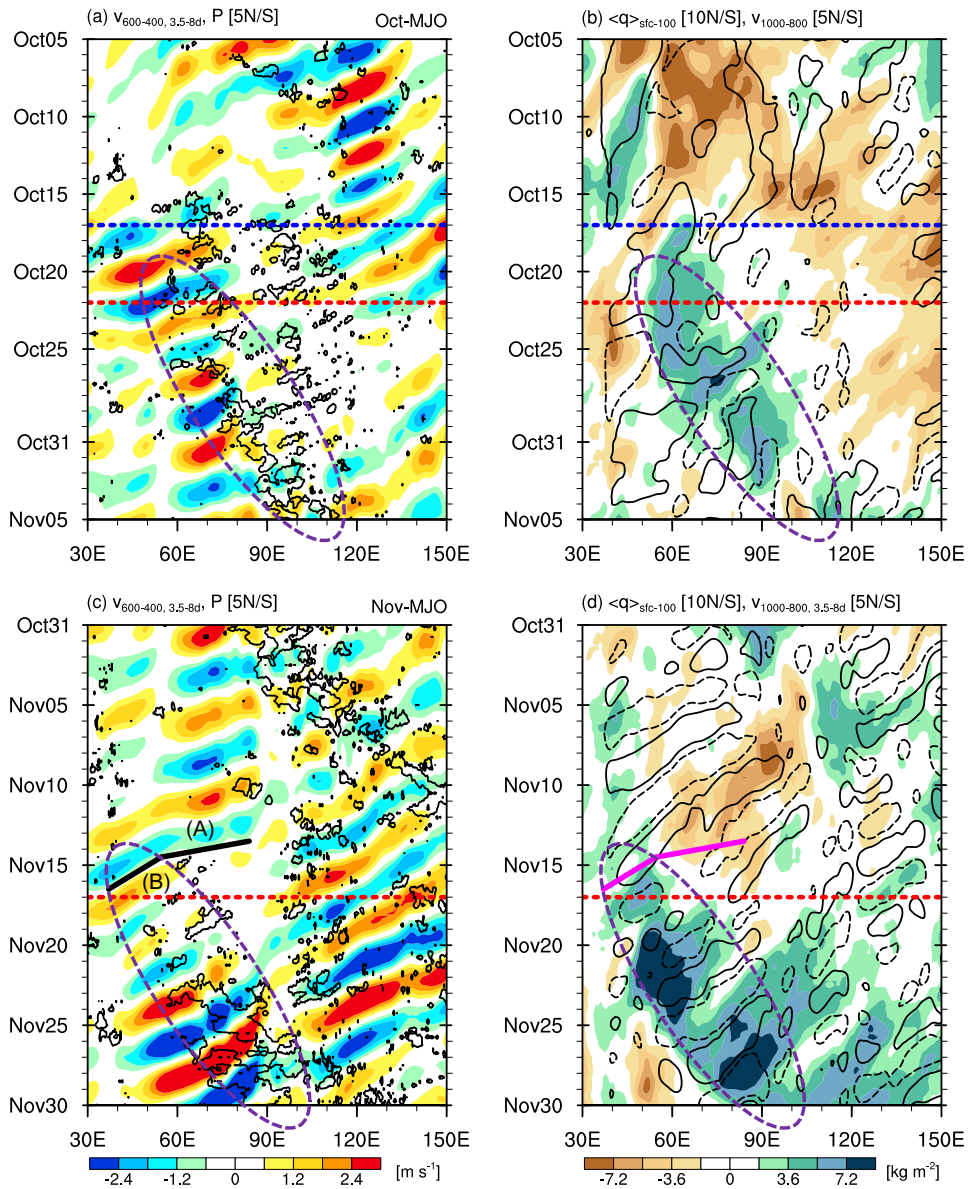

Figure 2.12: As in Fig. 2.3, but for (a, c) 3.5–8-day-filtered 600–400-hPa meridional wind anomalies (shading) and (b, d) 24-hour running mean (3.5-8-day-filtered) 1000–800-hPa meridional wind anomalies (contours). Contours in (a) and (c) are precipitation with 1.2 and 0.8 mm hr^{-1}, respectively. Contours in (b) and (d) are denoted with ±1.5 and ±0.75 m s^{-1}, respectively.

in 1000–800-hPa meridional winds in October (Fig. 2.12b) because of little evidence for specific periodicity, and 3.5–8-day filtered ones in all other meridional wind fields. In both events, lower-tropospheric westward-propagating meridional wind signals appear to trigger MJO convection on 17 October and November (Figs. 2.12b,d) after slowdown of westward

propagation of mid-tropospheric MRGs over the western IO around 10 October and 15 November (Figs. 2.12a,c), although the case in October is not as evident as in November. As for the MJO propagation, the lower-tropospheric MRG wave packet formation precedes the center of moist anomalies over the IO especially in Nov-MJO and faintly even in Oct-MJO (Figs. 2.12b,d). Note that the wave packet of westward-propagating signals in the lower-troposphere around 17 October continuously develops to the east, but that moist anomalies associated with Oct-MJO start to propagate eastward several days after this initial convective triggering (Fig. 2.12b). The above results suggest that the MJO–MRG relationship is observed to some extent in other MJO events and not limited during YMC-Sumatra 2017.

I now focus on Nov-MJO because that event has highly similar characteristics to MJO2. In Figs. 2.13a–c, which are the same as Fig. 2.4 but for the processes to Nov-MJO initiation, convective triggering via low-level southerlies in cross-equatorial circulations is confirmed. The modulation in the vertical structure associated with the westward phase speed change of MRGs shown in Fig. 2.12c is displayed in Fig. 2.13d in the same way as Fig. 2.5b. While the lower-tropospheric signals seem to be independent from upper-tropospheric ones in the fast-propagating mode, the slow-propagating mode shows more upright (but eastward tilted) structure, stronger ascent in the mid- to upper troposphere around the composite center, and enhanced lower-tropospheric northerlies to the east. The wave contraction is more evident in the higher layer (e.g., 400–300 hPa), which corresponds to the fact that background zonal convergence is in that layer of the western IO (Fig. 2.13e). These processes are basically consistent with a view in YMC-Sumatra 2017, except for the difference in the altitude where MRG modulation is obvious.

2.5.2 Comparison with the roles of equatorially circumnavigating Kelvin waves

Since MJO2, Oct-MJO, and Nov-MJO follow previous events (Fig. 2.1a and Yoneyama et al., 2013), I especially look into the roles of equatorially circumnavigating Kelvin waves in MJO initiation in comparison with my proposed mechanism. Figures 2.14 and 2.15

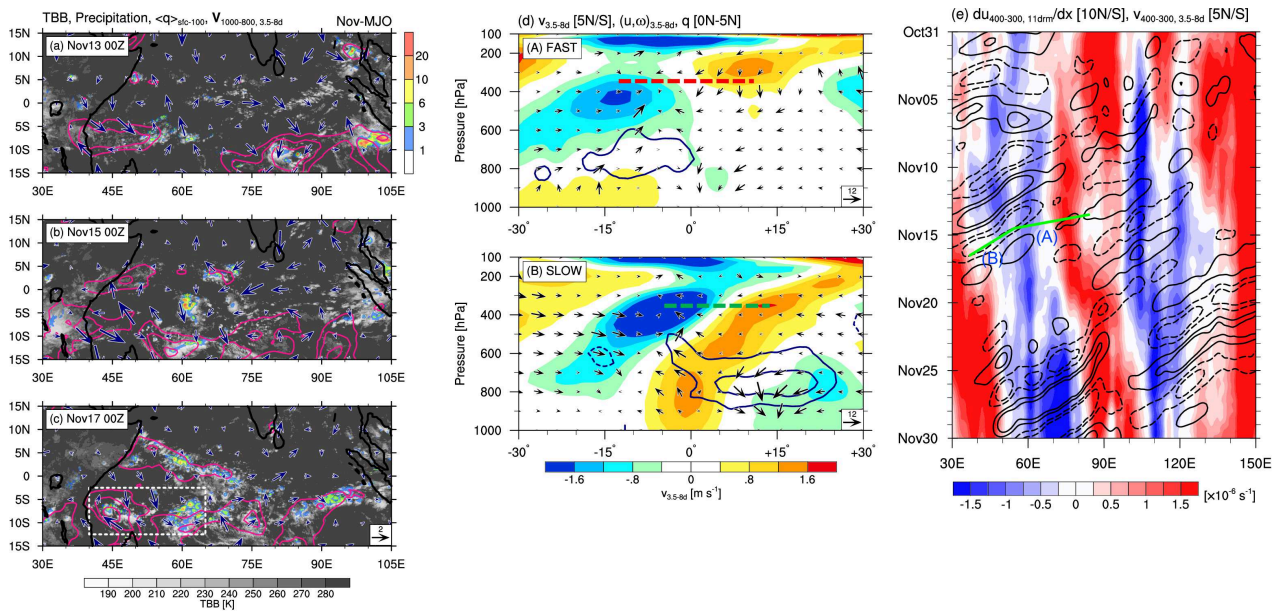

Figure 2.13: (a–c) Similar to Fig. 2.4, but 3.5–8-day-filtered 1000–800-hPa horizontal wind anomalies are also displayed with vectors (m s^{-1}) at 00Z (a) 13, (b) 15, and (c) 17 November. Contour interval is 6 kg m^{-2}. (d) As in Fig. 2.5b, but all fields are averaged along the solid lines A (top) and B (bottom) in Fig. 2.12c. Specific humidity anomalies (contours) are averaged over 0°–5°N. Contour interval is 0.8 kg m^{-2}. The horizontal red and green dashed lines denote the estimated MRG half-wavelengths. (e) As in Fig. 2.5c, but for 400–300 hPa. Contours are denoted with ±0.9 and ±1.8 m s^{-1}.

show time–longitude diagrams of 850- and 200-hPa zonal wind and sea level pressure (SLP) anomalies averaged over 10°S–10°N during DYNAMO and YMC-Sumatra 2017 campaign, respectively. Because 850-hPa zonal convergence and negative SLP anomalies associated with Kelvin waves are not in phase with initial convective triggering in all MJO cases (blue and second red lines in Fig. 2.14 and red one in Fig. 2.15), low-level MRGs dominantly contribute to dynamical triggering of MJO convection as mentioned before. However, the Kelvin-wave-induced modulation of large-scale circulations can make favorable condition for deep organized convection, as suggested by the fact that Oct-MJO starts eastward propagation as upper-level convergence is gradually relaxed in accordance with Kelvin-wave propagation (Fig. 2.14b). The importance of circumnavigating Kelvin waves in starting eastward propagation of Oct-MJO convection after convective triggering has already been reported by Zhang et al. (2017). Powell and Houze (2015a) also suggest that reduction in subsidence due to large-scale Kelvin waves helps shallow-to-deep convective development leading to MJO realization.

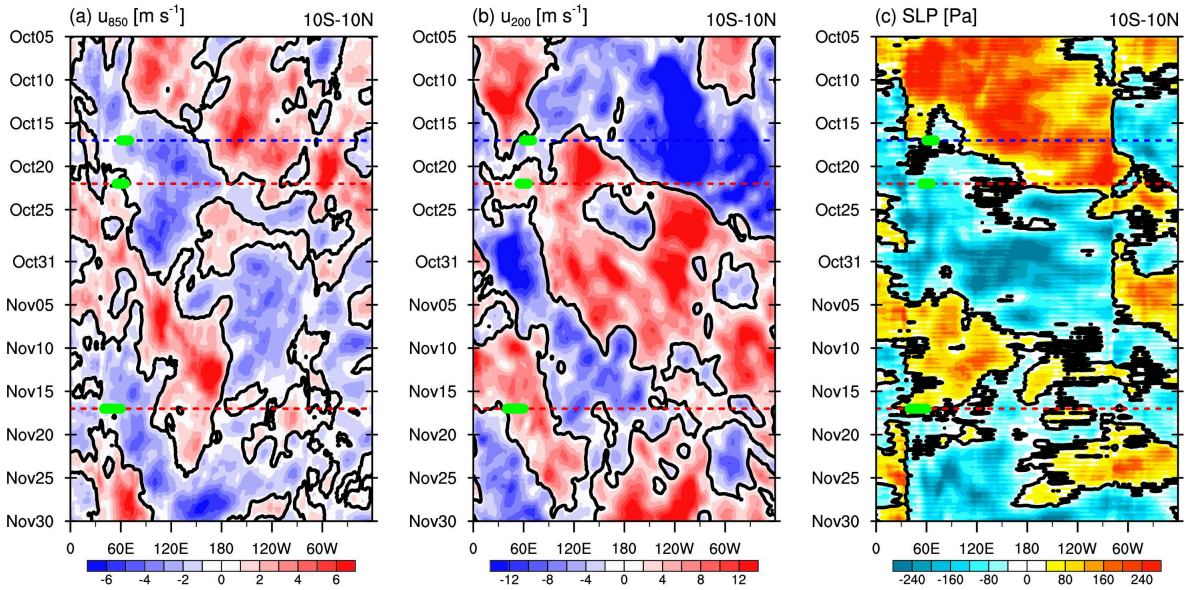

Figure 2.14: (a) 850-hPa and (b) 200-hPa zonal wind anomalies, and (c) mean sea level pressure anomalies averaged over 10°S–10°N. Thick solid contours denote zero contours, and thick green lines represent the MJO onset region and date.

2.6 Summary and concluding remarks

Using the radiosonde observation and reanalysis data obtained during YMC-Sumatra 2017, I have discovered an MJO convective initiation and propagation mechanism in which MRGs have a key role. One feature of this mechanism is the lower-tropospheric MRG wave packet formation that leads to the convective enhancement in the southwestern IO. This wave packet formation is due to a tight wave–convection coupling triggered by zonal wavelength shortening for an MRG propagating over the central IO. The wave contraction is associated with the mid-tropospheric weak convergence of a large-scale zonal circulation, and the contracted MRG efficiently generates EKE in the mid-troposphere and disperses it downward and eastward around the western IO. Another notable feature is basin-scale mid-tropospheric moistening due to MRG shallow circulations in the MJO-suppressed phase, which makes conditions favorable for MJO convective development. Consequently, MJO convection starts to propagate at the MRG group velocity via MRG-induced successive convective triggering to the east.

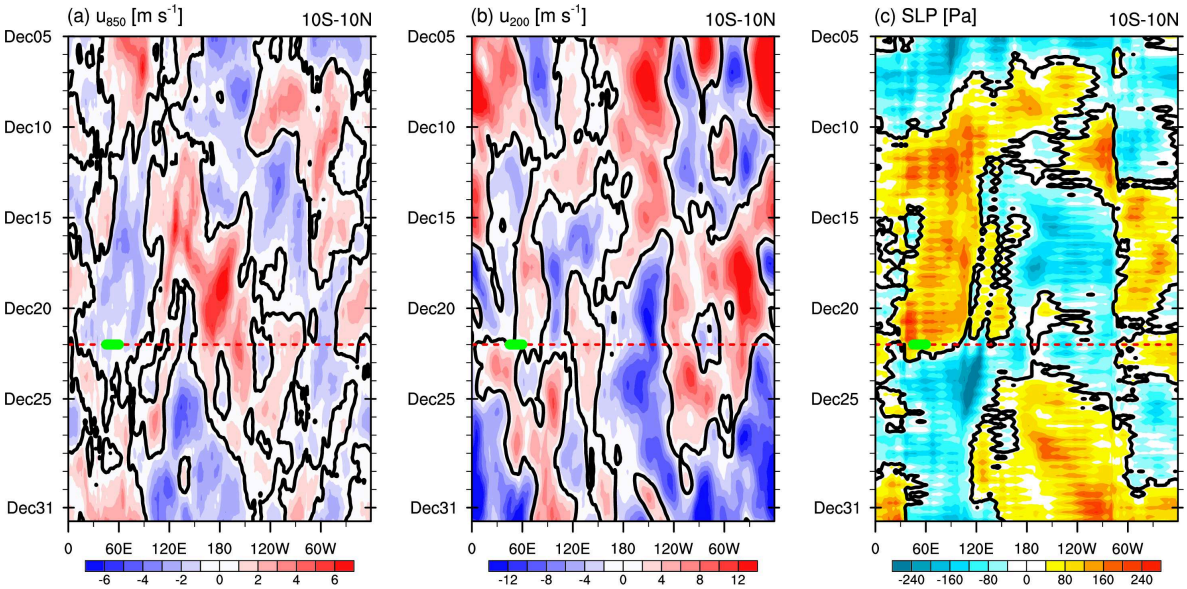

Figure 2.15: Same as Fig. 2.14, but for the YMC-Sumatra 2017 period.

The above MRG-related processes are also confirmed in other two MJO events during DYNAMO campaign (Oct-MJO and Nov-MJO), although I should note that they are not as evident in Oct-MJO as MJO2 and Nov-MJO. In Nov-MJO, quite similar to MJO2, one difference is that MRG propagation and contraction over the IO is evident in the more upper troposphere, which suggests that the altitude where MRG modulation is especially obvious can be arbitrary to some extent in the middle-to-upper troposphere.

For comparison with pre-existing mechanisms of MJO initiation, I especially examine the comparative roles of MRGs and circumnavigating Kelvin waves. While MRGs play a direct role in dynamical triggering of MJO convection, Kelvin waves can contribute to setting appropriate environments for MJO realization, inferred from the fact that Oct-MJO starts eastward propagation as upper-level convergence is gradually relaxed in accordance with Kelvin-wave propagation. As for the propagation, my standpoint is theoretically close to that of Majda and Stechmann (2009b) and, more specifically, to that of Yang and Ingersoll (2011). Although Yang and Ingersoll (2011) concluded that the MRG wave packet does not explain a large fraction of the MJO structure in OLR fields, I still believe it is worth revisiting the MJO–MRG relationship by focusing on dynamical fields, because MRG dynamics is helpful enough to *trigger* MJO convection to the east. In fact, the potential importance of

triggered convection in the MJO is implicated in Yang and Ingersoll (2013, 2014). This does not deny that the organization and maintenance of triggered convection can be affected by large-scale low-frequency physics implemented in a quasi-equilibrium framework such as the moisture-mode theory.

The proposed mechanism covers a classical view that MJO convection comprises westward convective disturbances (Nakazawa, 1988) and insights from the long-term aqua-planet simulation (Takasuka et al., 2018). Thus, in the next chapter, the generality of the dynamical roles of MRGs in MJO realization during boreal winter in 1982–2012 will be discussed.

Chapter 3

Dynamical Roles of Mixed Rossby–Gravity Waves in Driving Convective Initiation and Propagation of the MJO: General Views

本章については 5 年以内に雑誌論文として出版予定のため、非公開（下記参照）

The contents of this chapter were submitted to *Journal of the Atmospheric Sciences* as follows: "Dynamical Roles of Mixed Rossby–Gravity Waves in Driving Convective Initiation and Propagation of the MJO: General Views".

Chapter 4

Diversity of Initiation Regions of the MJO Associated with the Mutual Relationship Between the Intraseasonal and Low-frequency Variability

本章については 5 年以内に雑誌論文として出版予定のため、非公開（下記参照）

The contents of this chapter will be submitted to *Journal of Climate* as follows: "Diversity of Initiation Regions of the MJO Associated with the Mutual Relationship Between the Intraseasonal and Low-frequency Variability".

Chapter 5

General Discussion and Conclusion

In this study, the cross-scale interaction in the realization processes of the Madden–Julian oscillation (MJO) has been explored to provide new views to our major understanding of MJO initiation and propagation which mainly focuses on large-scale intraseasonal variations. In particular, I have examined (i) the robust roles of synoptic-scale equatorial waves in the initiation and the start of eastward propagation of MJO convection in the Indian Ocean (Chapters 2 and 3), and (ii) the mechanism of the modulation of MJO initiation regions and common characteristics of MJO initiation processes which do not depend on where the MJO is initiated in terms of the mutual relationship between the intraseasonal and interannual variability (Chapter 4). This chapter summarizes the main results in Chapters 2, 3 and 4, and discusses relationship among those chapters, implications for the previous studies, and future perspectives.

5.1 Summary

Chapter 2: Observational Evidence of Mixed Rossby–Gravity Waves as a Driving Force for the MJO Convective Initiation and Propagation

I propose a new mechanism for MJO convective initiation and propagation in the Indian Ocean (IO) in which mixed Rossby–gravity waves (MRGs) play a significant role, mainly based on observational data analyses of an MJO event initiated in December 2017 during the field campaign of the Years of the Maritime Continent (YMC) Project. The intensive observation has captured mid-tropospheric wind variations associated with MRGs, and the westward propagation of those signals has been confirmed over the IO in the MJO-suppressed phase. The transition to the MJO-active phase follows (i) tight MRG–convection coupling, which is enhanced when the wavelength becomes shorter due to weak midlevel convergence in the western IO, and (ii) basin-scale anomalous mid-tropospheric moistening due to shallow circulations associated with MRGs. These two processes lead to the lower-tropospheric MRG wave packet formation and successive triggering of MJO convection via MRG dynamics with its eastward group velocity ($\sim 5\ \mathrm{m\ s^{-1}}$), which results in the subsequent convective propagation of the MJO.

To discuss potential for robustness of this MJO–MRG relationship, the two additional MJO cases initiated in October and November 2011 during the dynamics of the MJO (DYNAMO) field campaign are further analyzed. The roles of MRGs in convective triggering for MJO initiation and propagation are especially confirmed in the MJO event in November, although they are weakly recognized in the October event. Notably, an equatorially circumnavigating Kelvin wave appears to contribute to help MJO convection for the October event begin to propagate eastward.

Chapter 3: Dynamical Roles of Mixed Rossby–Gravity Waves in Driving Convective Initiation and Propagation of the MJO: General Views

Using observational daily data of atmospheric and sea surface temperature (SST) fields, I statistically explore how robust and necessary the MJO–MRG relationship proposed in Chapter 2 is. MJO events initiated in the IO during boreal winter (DJFM) in 1982–2012 are objectively identified solely using outgoing longwave radiation data. The lagged-composite analysis of detected MJO events demonstrates that MJO convection is initially generated in the southwestern IO (SWIO), where strong MRG–convection coupling is statistically found. Further classification of MJO cases in terms of intraseasonal convection and MRG activities in the SWIO suggests that 26 of 47 cases are related to more enhanced MRG activities than any other convectively coupled equatorial waves. For those MRG-enhanced MJO events, MJO initiation is characterized as convective triggering by low-level MRG circulations which develop via the enhancement of downward energy dispersion in accordance with upper-tropospheric baroclinic conversion processes. This is supported by the modulation of MRG structure associated with zonal wave contraction due to upper-tropospheric zonal convergence, and plentiful moisture advected into the western IO. Following this MRG-induced convection in the SWIO and mid-tropospheric pre-moistening in the IO caused by MRG shallow circulations as well as intraseasonal winds during the MJO-suppressed phase, low-level MRG winds with eastward group velocity successively trigger convection to the east, which helps MJO convective propagation in the IO.

The comparison between the MRG-enhanced events and all others suggests that intraseasonal cross-equatorial circulations during the MJO-suppressed phase in the IO, which is possibly originated from the equatorial asymmetry of background convective activities, may be the source of MRGs. Whether the MRG-related processes are effective or not may depend on the strength in this asymmetry modulated by the low-frequency variability and seasonal march.

Chapter 4: Diversity of Initiation Regions of the MJO Associated With the Mutual Relationship Between the Intraseasonal and Low-frequency Variability

To advance comprehensive understanding of favorable environments for MJO initiation, the diversity of MJO initiation regions associated with the intraseasonal and interannual variability has been focused. Based on observation, MJO events initiated over the IO (IO-MJO), Maritime Continent (MC-MJO), and western Pacific (WP-MJO) are targeted. Both observational data analyses and a seiries of perpetual-boreal-winter experiments with an atmospheric GCM have revealed that horizontal advective moistening mainly by equatorial intraseasonal circulations is commonly important before MJO initiation in every region, and that the modulation of where this moistening process is more likely to work in accordance with the change in interannually varying SST-forced background circulations is one of reasons for the variety of MJO source regions. For IO-MJO cases as the canonical MJO under the climatological background condition, because background ascending motions in the MC–WP can support intraseasonal convective organization there, resultant convective suppression around the western MC can lead to advective moistening in the IO by inducing intraseasonal low-level easterly anomalies. Meanwhile, the MC-MJO cases are more favored under the eastern-Pacific (EP) El Niño-like condition, because the SST-induced background suppressed convection in the eastern MC can cause the eastward shift (by about 30°) of the intraseasonal circulation and convective pattern seen in IO-MJO cases and result in efficient moistening and subsequent development of convection around the western MC. The favorableness of WP-MJO

cases is supported by the central-Pacific (CP) Niño-like state and the dipole SST structure in the southern IO. This is because the background convective enhancement in the WP–CP and suppression in the southeastern IO and EP can more easily realize selective moistening in the WP associated with westward intrusion of enhanced disturbances (e.g., equatorial Rossby waves). The study in this chapter is the first to clarify the detailed mechanism of MJO initiation outside the IO by noticing the relationship between the intraseasonal and interannual variability.

5.2 Concluding discussion

Relationship among the chapters

This study has emphasized that considering the hierarchical relationship ranging from synoptic-scale variations to interannual variabilities is important to the precise and comprehensive description of MJO realization. Chapter 4 has shown the two points as follows; (i) equatorial background circulations which are modulated by the SST-related interannual variabilities can determine where the establishment of equatorial zonal circulations on the intraseasonal time scale is fundamentally allowed, and (ii) the established intraseasonal zonal circulations directly contribute to making a favorable condition for MJO initiation through moisture accumulation by anomalous horizontal advective moistening. In Chapters 2 and 3, on a premise that this preferred environment for MJO realization is provided in the IO following the processes described in Chapter 4, it has been found that synoptic-scale wave disturbances, specifically MRGs, enhanced within the equatorial intraseasonal zonal circulations play a crucial role in triggering convection responsible for MJO initiation and propagation as well as pre-moistening in the IO. Taken together, potential roles of interannual, intraseasonal, and synoptic-scale variations in the mechanics of the MJO are to affect the existence of equatorial intraseasonal zonal circulations related to the MJO, to provide a necessary environment for MJO realization through allowance of sufficient moistening, and to directly trigger MJO convection and assist moisture transport in a favorable environment for the MJO, respectively.

If the aforementioned position is taken, it is worthwhile to grasp what kinds of synoptic-

scale wave disturbances may cause convective triggering leading to MJO initiation in the MC and WP to connect the perspectives in the three chapters. Although detailed analyses are left for future work, I now discuss this topic based on the presented results and previous studies. In horizontal distributions of intraseasonal convective activities before the MC-MJO initiation (Fig. **??**b), large-scale convective suppression associated with the equatorial zonal circulations found in Fig. **??**c is prominent especially in the Southern Hemisphere. In this context, cross-equatorial southerly anomalies in the lower-troposphere are also recognized around the MC region (90°–150°E). This equatorial asymmetry of convective fields is probably related to the background enhanced precipitation in the southern MC in boreal winter, as discussed in Section **??**. Resultantly, active convection is triggered to the north of the equator around 90°E at day −5 and then organized with expansion to the south. This evolution is reminiscent of the contribution from MRGs to convective triggering because it resembles the MRG-related IO-MJO initiation processes revealed in Chapter 3.

MRG-like disturbances are actually detected over the southern MC–northern Australian region in boreal winter by some previous studies (e.g., Widiyatmi et al., 1999, 2001; Fukutomi, 2019), although they do not point out the relationship with the MJO. Widiyatmi et al. (2001) have reported westward-propagating convective and lower-tropospheric meridional wind signals with a zonal wavelength of about 3500 km and periodicities of 3–6 days around the Indonesian MC area based on the 4-yr in-situ observations. Fukutomi (2019) has also statistically confirmed this characteristics together with eastward group velocity along the westerly Australian summer monsoon using the 37-yr atmospheric data. Notably, a zonal wavelength of those MRG-like disturbances is shorter than typically observed MRGs over the tropical Pacific ocean (e.g., Takayabu and Nitta, 1993; Wheeler and Kiladis, 1999; Kiladis et al., 2009), which is a common characteristics to MRGs identified in the southwestern IO where IO-MJO convection is initially developed (Fig. **??**). These circumstantial evidences suggest that, as with the IO-MJO cases, strong MRG–convection coupling associated with wave contraction might also trigger the MC-MJO convective initiation.

The WP-MJO convective initiation can be interpreted as the result of the interaction be-

tween equatorial Rossby waves (ERs) as synoptic-to-intraseasonal disturbances with plentiful moisture and background low-level zonal convergence (e.g., Figs. **??** and **??**). Interestingly, Masunaga et al. (2006) and Miura et al. (2007) have also pointed out that westward intrusion of ERs into the WP is important to intensified MJO convection there, although their findings have been derived from the analysis of MJO propagation. This suggests that the realization of ERs before MJO convective activation around the WP may be inevitable to some extent. The verification of its detailed mechanism should be revisited in the future.

Implication for the previous studies

This study about cross-scale processes in MJO realization has some implications for the previous studies which have proposed the mechanisms of MJO initiation and propagation in terms of large-scale intraseasonal variations. Now I discuss how the pre-existing MJO mechanisms should be verified or modified based on my results.

Initiation mechanisms

As introduced in Chapter 1, the major candidates for the MJO initiation mechanisms are (i) equatorial circumnavigation of large-scale Kelvin waves, (ii) discharge-recharge hypothesis, and (iii) MJO-scale moisture advection. The results in Chapters 2–4 provide useful information to reconsider all the three candidates.

Chapters 2 and 3 have suggested that MRG dynamics can directly trigger MJO convective initiation in the IO, which means that equatorially circumnavigating Kelvin waves are not always required for triggering MJO convection. This is consistent with several studies which have denied the necessity of Kelvin waves for the existence of the MJO using different GCMs (Zhao et al., 2013; Maloney and Wolding, 2015; Ma and Kuang, 2016; Takasuka et al., 2018), and is indirectly supported by the observational fact that MJO initiation is achieved even outside the IO probably with the aid of another disturbance (cf. Chapter 4 and the related discussion above). Meanwhile, Chapter 2 has also shown that large-scale Kelvin waves can help an MJO event be initiated in October 2011 through the weakening of upper-tropospheric

large-scale convergence. Hence, the role of circumnavigating Kelvin waves in preparing for a suitable environment for MJO initiation rather than triggering convection should not be easily discarded in some observational cases (e.g., Powell and Houze, 2015a). It may be worth examining in more detail under what conditions Kelvin-wave-related processes are especially effective in MJO initiation.

The discharge-recharge hypothesis also appears not to be fully supported in this study. This standpoint is based on the results in Chapters 2 and 3 that the moistening processes before MJO initiation are partly driven by wave dynamics such as MRG-related shallow circulations. This agrees with the previous studies which have claimed that not local development of cumulus congestus but larger-scale dynamical convergence is more responsible for tropospheric moistening (Hohenegger and Stevens, 2013; Masunaga, 2013). However, there are not so many studies which have quantitatively evaluated the contribution of convective eddy moisture fluxes and large-scale dynamics to the moistening in the context of MJO initiation (e.g., Hagos et al., 2014; Janiga and Zhang, 2016), and there are discrepancies between the results. For example, Hagos et al. (2014) have suggested that anomalous large-scale moisture advection is more important to moisture buildup for MJO initiation, whereas Janiga and Zhang (2016) have found the comparable importance of such advection and eddy moisture transport during the developing phase of the MJO. Since these two studies have looked into only limited MJO events during the DYNAMO campaign and used different models with different configurations, it is further required to examine the relative importance of moistening by wave-induced circulations and shallow cloud convection utilizing other high-resolution cloud-resolving simulations for more MJO cases.

Although MJO-scale moisture advection is actually recognized before the IO- and MC-MJO initiation in Chapter 4, the contribution from synoptic-scale waves (i.e., MRGs in Chapters 2 and 3, and ERs for the WP-MJO initiation in Chapter 4) to the pre-moistening implicates a deficiency of the MJO-scale moisture advective process. In addition, an observational evidence that MJO convective initiation itself is triggered by high-frequency dynamical variations under the sufficient moistened environment (Chapters 2 and 3) suggests that mois-

ture variations alone associated with MJO-scale winds may not be able to describe MJO initiation processes precisely. As described later, this idea has something in common with the modification of the moisture-mode theory (e.g., Adames and Kim, 2016).

Propagation mechanisms

As for the propagation, there are the three representative mechanisms: (i) importance of atmosphere–ocean coupled processes, (ii) Kelvin–Rossby wave dynamics with planetary boundary layer (PBL) frictional moisture convergence, and (iii) moisture mode. Since this study does not look into intraseasonal SST variations as reviewed in Demott et al. (2015), it is beyond the scope of this dissertation to discuss the relationship between my results and mechanism (i) in detail. Nevertheless, Chapters 2 and 3 have shown that MJO convective propagation in the IO can be explained only by atmospheric wave dynamics, which implicates that the intraseasonal atmosphere–ocean coupled processes are not always essential for the MJO. Zhu et al. (2017) have reported, however, that SST feedback is key to MJO propagation across the MC using a set of numerical simulations. Since complete MJO propagation is often recognized as the migration of large-scale convective envelopes into the WP, it is valuable to examine at what stage during the propagation the air–sea interaction is important.

A new perspective that MRG dynamics can help MJO convection propagate eastward at least in the IO (Chapters 2 and 3) suggests that mechanisms (ii) and (iii) have room for modification in terms of both scaling of the dynamic equations and the moisture–dynamics interaction. For the former, it may be inappropriate to assume that large-scale Kelvin and Rossby waves or responses alone compose dynamical components which impact on MJO propagation in several linear models (e.g., Wang et al., 2016; Adames and Kim, 2016). Although there is no doubt that MJO structure is regarded as the Kelvin–Rossby couplet pattern on the $O(10^3$ km) spatial and intraseasonal time scale to a first-order approximation (Hendon and Salby, 1994; Kiladis et al., 2005; Adames and Wallace, 2015, Fig. 1.3), this does not necessarily mean that the large-scale dynamical pattern directly drives MJO propagation in the real world as inferred from Chapters 2 and 3. For the other point, as questioned by

Pritchard and Yang (2016), there is a possibility that the moisture-mode theory (mechanism (iii)) may oversimplify propagation processes of the MJO by explicitly considering only the evolution of moisture or MSE (e.g., Sobel and Maloney, 2012, 2013; Adames and Kim, 2016). In fact, the MRG-related propagation mechanism revealed in this study highlights the importance of high-frequency *dynamics* in triggering convection, which is close to thinking in Yang and Ingersoll (2013, 2014). Based on these insights, I believe that one of possible modification directions is that dynamical contributions from synoptic-scale high-frequency waves such as MRGs implemented in the MJO should be explicitly fed back onto the first-order MJO structure through the interaction with convective and moisture fields. To achieve this, it can be helpful to advance the "MJO skeleton" theory (Majda and Stechmann, 2009b, 2011), which considers the collective effect of convective envelopes associated with synoptic-scale disturbances. In that case, a multiple-time approach adopted in the self-consistent multi-scale model (Majda and Klein, 2003), which makes it possible to treat the interaction across multiple spatio-temporal scales by expanding any variables for each different time scale, may be usable.

Although Chapter 4 itself does not focus on any theories of MJO propagation, the time–longitude diagrams of OLR anomalies for IO-, MC-, and WP-MJO cases (Fig. **??**) have an implication for the westward group velocity of eastward-propagating MJO convection predicted by the moisture-mode linear theory in Adames and Kim (2016). For MC-MJO cases, the westward development of eastward propagation of OLR anomalies is recognized before their initiation (Fig. **??**b). In similar to this, the WP-MJO initiation is followed by large-scale convective suppression to the west and subsequent active convection in the IO around day 20 (Fig. **??**c). These convective evolutions under the EP or CP El Niño conditions seem to be related to the westward group velocity of MJO convective envelopes, consistent with a finding in Wei and Ren (2019) that the westward dispersion of the MJO is robust during the El Niño winters. Meanwhile, such a dispersive characteristics is not so evident for IO-MJO cases under the near-climatological background (Fig. **??**a), which corresponds to the near-zero group velocity in a statistical sense as reported by Chen and Wang (2018a). These results

implicate that the observed westward group velocity may not follow the theoretical prediction but may come from the interaction between the intraseasonal and interannual variability. To examine the validity of the 2-D moisture-mode theory, it will be required to understand the consistency in the dispersive feature of the MJO between the theory and observation.

Future perspectives

At the end of this dissertation, some future perspectives related to limitations and applicability of this study are discussed. First, the reason why MRGs are selectively realized before MJO initiation in the IO has not been confidently revealed. The statistical analysis in Chapter 3 has suggested that MRGs can be induced by equatorially anti-symmetric heating associated with the intraseasonal cross-equatorial meridional circulation during the MJO-suppressed phase over the IO. This speculation, however, has the following two unclear points. One is a specific process of trapping of MRGs in the troposphere. This topic may be clarified by the analysis of a transient process in a simple numerical/analytical model (e.g., multi-level shallow water system with simple physics) on which some heating is imposed. The other is how the meridional overturning on the intraseasonal time scale is physically driven under the moisture–convection–radiation interactive processes, although it has been simply interpreted in terms of the relationship between moisture and precipitation variations and background convective activities in Chapter 3. To elucidate its detailed mechanism, it is useful to focus on radiative feedbacks and vertical heating profiles before MJO initiation in the IO utilizing satellite observations and realistic numerical experiments. The detailed clarification of these points will lead to complete understanding of the MRG-related MJO initiation mechanism proposed in this study.

Secondly, it is unclear what determines the spatial scale of intraseasonal zonal circulations. While Chapter 4 has implicitly presumed the spatial extent of influences of zonal circulations associated with a pair of intraseasonal enhanced and suppressed convection especially seen before the IO- and MC-MJO initiation (cf. schematic diagram in Figs. **??**a,b), it still remains elusive why the zonal distance between the core of an ascending and descending

branch is about 90° (Figs. **??**a–d). Answering this question can greatly advance knowledge about the scale selection of tropical convection including the MJO. In fact, it has been vigorously investigated under the radiative-convective equilibrium framework in terms of moisture–convection feedback (e.g., Grabowski and Moncrieff, 2004), cloud-radiation feedback (e.g., Arnold and Randall, 2015; Beucler et al., 2018), remoistening processes in the dry PBL (Wing and Cronin, 2016), and density variations in the PBL (Yang, 2018). A theoretical approach can also be valuable, as Kuang (2008) has examined the scale selection of convectively coupled equatorial waves by constructing a simple model which focuses on a moisture–stratiform instability.

Lastly, the results of this study can provide a guideline for improving the representation of MJO convection in numerical models. Considering that the modulation of MRG vertical structure and resultant dynamics–convection coupling are important to the MJO initiation in the IO, an increase in the number of vertical layers may contribute to precise prediction of the timing and processes of MJO convective onset by leading to better-simulated wave structure and vertical moisture transport. In addition, the impacts of the SST-forced interannual atmospheric variability on MJO initiation have implicated that it is essential for GCMs to simulate realistic background states such as the mean Walker and Hadley circulations in order to get good skill of MJO prediction and reproduction. This view is also motivated by some previous studies which have claimed the importance of well-represented mean westerlies in MJO simulations (e.g., Inness et al., 2003; Ling et al., 2017) and of basic-state tropical circulations in the longevity of the MJO (Suematsu and Miura, 2018; Suematsu, 2018). Since MJO-active regions include the MC where many GCMs tend to suffer from the systematic biases of the mean state (e.g., Toh et al., 2018), it is required to reduce them through the improvement of physics schemes about cumulus convection and PBL processes which are involved in the interaction between land-ocean surfaces and the free troposphere. I believe that such improvements of GCMs are absolutely necessary for more quantitative understanding of MJO dynamics.

References

Adames, Á. F., and D. Kim, 2016: The MJO as a dispersive, convectively coupled moisture wave: Theory and observations. *J. Atmos. Sci.*, **73 (3)**, 913–941, doi: 10.1175/JAS-D-15-0170.1.

Adames, Á. F., and J. M. Wallace, 2015: Three-Dimensional Structure and Evolution of the Moisture Field in the MJO. *J. Atmos. Sci.*, **72 (10)**, 3733–3754, doi: 10.1175/JAS-D-15-0003.1.

Ahn, M. S., D. Kim, K. R. Sperber, I. S. Kang, E. Maloney, D. Waliser, and H. Hendon, 2017: MJO simulation in CMIP5 climate models: MJO skill metrics and process-oriented diagnosis. *Clim. Dyn.*, **49 (11-12)**, 4023–4045, doi:10.1007/s00382-017-3558-4.

Andersen, J. A., and Z. Kuang, 2012: Moist static energy budget of MJO-like disturbances in the atmosphere of a zonally symmetric aquaplanet. *J. Climate*, **25 (8)**, 2782–2804, doi:10.1175/JCLI-D-11-00168.1.

Arnold, N. P., Z. Kuang, and E. Tziperman, 2013: Enhanced MJO-like variability at high SST. *J. Climate*, **26 (3)**, 988–1001, doi:10.1175/JCLI-D-12-00272.1.

Arnold, N. P., and D. A. Randall, 2015: Global-scale convective aggregation: Implications for the Madden-Julian Oscillation. *J. Adv. Model. Earth Syst.*, **7 (4)**, 1499–1518, doi:10.1002/2015MS000498.

Ashok, K., S. K. Behera, S. A. Rao, H. Weng, and T. Yamagata, 2007: El Niño Modoki and its possible teleconnection. *J. Geophys. Res. Oceans*, **112 (11)**, 1–27, doi:10.1029/2006JC003798.

Bechtold, P., M. Köhler, T. Jung, F. Doblas-Reyes, M. Leutbecher, M. J. Rodwell, F. Vitart, and G. Balsamo, 2008: Advances in simulating atmospheric variability with the ECMWF

model: From synoptic to decadal time-scales. *Quart. J. Roy. Meteor. Soc.*, **134 (634)**, 1337–1351, doi:10.1002/qj.289.

Bellenger, H., and J. P. Duvel, 2012: The event-to-event variability of the boreal winter MJO. *Geophys. Res. Lett.*, **39 (8)**, 1–7, doi:10.1029/2012GL051294.

Benedict, J. J., and D. A. Randall, 2007: Observed Characteristics of the MJO Relative to Maximum Rainfall. *J. Atmos. Sci.*, **64 (7)**, 2332–2354, doi:10.1175/JAS3968.1.

Benedict, J. J., and D. A. Randall, 2009: Structure of the Madden–Julian Oscillation in the Superparameterized CAM. *J. Atmos. Sci.*, **66 (11)**, 3277–3296, doi:10.1175/2009JAS3030.1.

Benedict, J. J., and D. A. Randall, 2011: Impacts of Idealized Air–Sea Coupling on Madden–Julian Oscillation Structure in the Superparameterized CAM. *J. Atmos. Sci.*, **68 (9)**, 1990–2008, doi:10.1175/JAS-D-11-04.1.

Beucler, T., T. Cronin, and K. Emanuel, 2018: A Linear Response Framework for Radiative-Convective Instability. *J. Adv. Model. Earth Syst.*, **10 (8)**, 1924–1951, doi:10.1029/2018MS001280.

Biello, J. A., and A. J. Majda, 2005: A New Multiscale Model for the Madden–Julian Oscillation. *J. Atmos. Sci.*, **62 (6)**, 1694–1721, doi:10.1175/JAS3455.1.

Bladé, I., and D. L. Hartmann, 1993: Tropical Intraseasonal Oscillations in a Simple Nonlinear Model. *J. Atmos. Sci.*, **50 (17)**, 2922–2939, doi:10.1175/1520-0469(1993)050<2922:TIOIAS>2.0.CO;2.

Bony, S., and K. A. Emanuel, 2005: On the role of moist processes in tropical intraseasonal variability: Cloud-radiation and moisture-convection feedbacks. *J. Atmos. Sci.*, **62 (8)**, 2770–2789, doi:10.1175/JAS3506.1.

Bretherton, C. S., M. E. Peters, and L. E. Back, 2004: Relationships between Water Vapor Path and Precipitation over the Tropical Oceans. *J. Climate*, **17 (7)**, 1517–1528, doi:10.1175/1520-0442(2004)017<1517:RBWVPA>2.0.CO;2.

Chen, G., and B. Wang, 2018a: Does the MJO have a westward group velocity? *J. Climate*, **31 (6)**, 2435–2443, doi:10.1175/JCLI-D-17-0446.1.

Chen, G., and B. Wang, 2018b: Effects of enhanced front Walker cell on the eastward propagation of the MJO. *J. Climate*, **31 (10)**, 7719–7738, doi:10.1175/JCLI-D-17-0383.1.

Chen, S., and Coauthors, 2015: A Study of CINDY/DYNAMO MJO Suppressed Phase. *J. Atmos. Sci.*, **72 (10)**, 3755–3779, doi:10.1175/JAS-D-13-0348.1.

Chen, S. S., R. A. Houze, and B. E. Mapes, 1996: Multiscale Variability of Deep Convection In Realation to Large-Scale Circulation in TOGA COARE. *J. Atmos. Sci.*, **53 (10)**, 1380–1409, doi:10.1175/1520-0469(1996)053<1380:MVODCI>2.0.CO;2.

Chen, X., J. Ling, and C. Li, 2016: Evolution of the Madden-Julian oscillation in two types of El Niño. *J. Climate*, **29 (5)**, 1919–1934, doi:10.1175/JCLI-D-15-0486.1.

Chen, X., and F. Zhang, 2019: Relative Roles of Preconditioning Moistening and Global Circumnavigating Mode on the MJO Convective Initiation During DYNAMO. *Geophys. Res. Lett.*, **46 (2)**, 1079–1087, doi:10.1029/2018GL080987.

Crueger, T., and B. Stevens, 2015: The effect of atmospheric radiative heating by clouds on the Madden-Julian Oscillation. *J. Adv. Model. Earth Syst.*, **7 (2)**, 854–864, doi:10.1002/2015MS000434.

Dee, D. P., and Coauthors, 2011: The ERA-Interim reanalysis: Configuration and performance of the data assimilation system. *Quart. J. Roy. Meteor. Soc.*, **137 (656)**, 553–597, doi:10.1002/qj.828.

Del Genio, A. D., Y. Chen, D. Kim, and M.-S. Yao, 2012: The MJO Transition from Shallow to Deep Convection in CloudSat /CALIPSO Data and GISS GCM Simulations. *J. Climate*, **25 (11)**, 3755–3770, doi:10.1175/JCLI-D-11-00384.1.

Demott, C. A., N. P. Klingaman, and S. J. Woolnough, 2015: Atmosphere-ocean coupled processes in the Madden-Julian oscillation. *Rev. Geophys.*, **53**, doi:10.1002/2014RG000478.

DeMott, C. A., C. Stan, D. A. Randall, and M. D. Branson, 2014: Intraseasonal variability in coupled GCMs: The roles of ocean feedbacks and model physics. *J. Climate*, **27 (13)**, 4970–4995, doi:10.1175/JCLI-D-13-00760.1.

Dias, J., S. Leroux, S. N. Tulich, and G. N. Kiladis, 2013: How systematic is organized

tropical convection within the MJO? *Geophys. Res. Lett.*, **40 (7)**, 1420–1425, doi:10.1002/grl.50308.

Dias, J., N. Sakaeda, G. N. Kiladis, and K. Kikuchi, 2017: Influences of the MJO on the space-time organization of tropical convection. *J. Geophys. Res. Atmos.*, **122 (15)**, 8012–8032, doi:10.1002/2017JD026526.

Duchon, C. E., 1979: Lanczos Filtering in One and Two Dimensions. *J. Appl. Meteorol.*, **18 (8)**, 1016–1022, doi:10.1175/1520-0450(1979)018<1016:LFIOAT>2.0.CO;2.

Dunkerton, T. J., and M. P. Baldwin, 1995: Observation of 3–6-Day Meridional Wind Oscillations over the Tropical Pacific, 1973–1992: Horizontal Structure and Propagation. *J. Atmos. Sci.*, **52 (10)**, 1585–1601, doi:10.1175/1520-0469(1995)052<1585:OODMWO>2.0.CO;2.

Dunkerton, T. J., and F. X. Crum, 1995: Eastward propagating ∼2- to 15-day equatorial convection and its relation to the tropical intraseasonal oscillation. *J. Geophys. Res. Atmos.*, **100 (D12)**, doi:10.1029/95jd02678.

Emanuel, K. A., 1987: An Air-Sea Interaction Model of Intraseasonal Oscillations in the Tropics. *J. Atmos. Sci.*, **44 (16)**, 2324–2340, doi:10.1175/1520-0469(1987)044<2324:AASIMO>2.0.CO;2.

Feng, J., P. Liu, W. Chen, and X. Wang, 2015: Contrasting Madden–Julian oscillation activity during various stages of EP and CP El Niños. *Atmos. Sci. Lett.*, **16 (1)**, 32–37, doi:10.1002/asl2.516.

Fink, A., and P. Speth, 1997: Some potential forcing mechanisms of the year-to-year variability of the tropical convection and its intraseasonal (25–70-day) variability. *Int. J. Clim.*, **17 (14)**, 1513–1534, doi:10.1002/(SICI)1097-0088(19971130)17:14<1513::AID-JOC210>3.0.CO;2-U.

Flatau, M., P. J. Flatau, P. Phoebus, and P. P. Niiler, 1997: The Feedback between Equatorial Convection and Local Radiative and Evaporative Processes: The Implications for Intraseasonal Oscillations. *J. Atmos. Sci.*, **54 (19)**, 2373–2386, doi:10.1175/1520-0469(1997)054<2373:TFBECA>2.0.CO;2.

Frank, W. M., and P. E. Roundy, 2006: The Role of Tropical Waves in Tropical Cyclogenesis. *Mon. Wea. Rev.*, **134 (9)**, 2397–2417, doi:10.1175/MWR3204.1.

Fu, X., W. Wang, J.-Y. Lee, B. Wang, K. Kikuchi, J. Xu, J. Li, and S. Weaver, 2015: Distinctive Roles of Air–Sea Coupling on Different MJO Events: A New Perspective Revealed from the DYNAMO/CINDY Field Campaign. *Mon. Wea. Rev.*, **143 (3)**, 794–812, doi:10.1175/MWR-D-14-00221.1.

Fukutomi, Y., 2019: Tropical Synoptic-Scale Waves Propagating Across the Maritime Continent and Northern Australia. *J. Geophys. Res. Atmos.*, **124 (14)**, 7665–7682, doi:10.1029/2018JD029795.

Gill, A. E., 1980: Some simple solutions for heat induced tropical circulation. *Quart. J. Roy. Meteor. Soc.*, **106 (449)**, 447–462, doi:10.1002/qj.49710644905.

Grabowski, W. W., and M. W. Moncrieff, 2004: Moisture–convection feedback in the tropics. *Quart. J. Roy. Meteor. Soc.*, **130 C (604)**, 3081–3104, doi:10.1256/qj.03.135.

Guo, Y., D. E. Waliser, and X. Jiang, 2015: A Systematic relationship between the representations of convectively coupled equatorial wave activity and the Madden-Julian oscillation in climate model simulations. *J. Climate*, **28 (5)**, 1881–1904, doi:10.1175/JCLI-D-14-00485.1.

Haertel, P., K. Straub, and A. Budsock, 2015: Transforming circumnavigating Kelvin waves that initiate and dissipate the Madden-Julian Oscillation. *Quart. J. Roy. Meteor. Soc.*, **141 (690)**, 1586–1602, doi:10.1002/qj.2461.

Hagos, S., Z. Feng, K. Landu, and C. N. Long, 2014: Advection, moistening, and shallow-to-deep convection transitions during the initiation and propagation of Madden-Julian Oscillation. *J. Adv. Model. Earth Syst.*, **6 (3)**, 938–949, doi:10.1002/2014MS000335.

Hannah, W. M., and E. D. Maloney, 2011: The role of moisture-convection feedbacks in simulating the Madden-Julian oscillation. *J. Climate*, **24 (11)**, 2754–2770, doi:10.1175/2011JCLI3803.1.

Hendon, H. H., and B. Liebmann, 1990: The Intraseasonal (30–50 day) Oscillation of the Australian Summer Monsoon. *J. Atmos. Sci.*, **47 (24)**, 2909–2924, doi:10.1175/

1520-0469(1990)047<2909:TIDOOT>2.0.CO;2.

Hendon, H. H., and B. Liebmann, 1994: Organization of convection within the Madden-Julian oscillation. *J. Geophys. Res. Atmos.*, **99 (D4)**, 8073–8083, doi:10.1029/94JD00045.

Hendon, H. H., and M. L. Salby, 1994: The Life Cycle of the Madden–Julian Oscillation. *J. Atmos. Sci.*, **51 (15)**, 2225–2237, doi:10.1175/1520-0469(1994)051<2225:TLCOTM>2.0.CO;2.

Hendon, H. H., M. C. Wheeler, and C. Zhang, 2007: Seasonal Dependence of the MJO–ENSO Relationship. *J. Climate*, **20 (3)**, 531–543, doi:10.1175/JCLI4003.1.

Hendon, H. H., C. Zhang, and J. D. Glick, 1999: Interannual variation of the Madden-Julian oscillation during austral summer. *J. Climate*, **12 (8)**, 2538–2550, doi:10.1175/1520-0442(1999)012<2538:ivotmj>2.0.co;2.

Hirata, F. E., P. J. Webster, and V. E. Toma, 2013: Distinct manifestations of austral summer tropical intraseasonal oscillations. *Geophys. Res. Lett.*, **40 (12)**, 3337–3341, doi:10.1002/grl.50632.

Hohenegger, C., and B. Stevens, 2013: Preconditioning deep convection with cumulus congestus. *J. Atmos. Sci.*, **70 (2)**, 448–464, doi:10.1175/JAS-D-12-089.1.

Holloway, C. E., and D. J. Neelin, 2009: Moisture vertical structure, column water vapor, and tropical deep convection. *J. Atmos. Sci.*, **66 (6)**, 1665–1683, doi:10.1175/2008JAS2806.1.

Hsu, P. C., and T. Li, 2012: Role of the boundary layer moisture asymmetry in causing the eastward propagation of the Madden-Julian oscillation. *J. Climate*, **25 (14)**, 4914–4931, doi:10.1175/JCLI-D-11-00310.1.

Hung, C.-S., and C.-H. Sui, 2018: A Diagnostic Study of the Evolution of the MJO from Indian Ocean to Maritime Continent: Wave Dynamics versus Advective Moistening Processes. *J. Climate*, **31 (10)**, 4095–4115, doi:10.1175/JCLI-D-17-0139.1.

Hung, M. P., J. L. Lin, W. Wang, D. Kim, T. Shinoda, and S. J. Weaver, 2013: MJO and convectively coupled equatorial waves simulated by CMIP5 climate models. *J. Climate*, **26 (17)**, 6185–6214, doi:10.1175/JCLI-D-12-00541.1.

Ichikawa, H., and T. Yasunari, 2007: Propagating diurnal disturbances embedded in

the Madden-Julian Oscillation. *Geophys. Res. Lett.*, **34 (18)**, L18 811, doi:10.1029/2007GL030480.

Inness, P. M., and J. M. Slingo, 2003: Simulation of the Madden–Julian Oscillation in a Coupled General Circulation Model. Part I: Comparison with Observations and an Atmosphere-Only GCM. *J. Climate*, **16 (3)**, 345–364, doi:10.1175/1520-0442(2003)016<0345:SOTMJO>2.0.CO;2.

Inness, P. M., J. M. Slingo, E. Guilyardi, and J. Cole, 2003: Simulation of the Madden-Julian oscillation in a coupled general circulation model. Part II: The role of the basic state. *J. Climate*, **16 (3)**, 365–382, doi:10.1175/1520-0442(2003)016<0365:SOTMJO>2.0.CO;2.

Janiga, M. A., and C. Zhang, 2016: MJO moisture budget during DYNAMO in a cloud-resolving model. *J. Atmos. Sci.*, **73 (6)**, 2257–2278, doi:10.1175/JAS-D-14-0379.1.

Jiang, X., 2017: Key processes for the eastward propagation of the Madden-Julian Oscillation based on multimodel simulations. *J. Geophys. Res. Atmos.*, **122 (2)**, 755–770, doi:10.1002/2016JD025955.

Jiang, X., á. F. Adames, M. Zhao, D. Waliser, and E. Maloney, 2018: A unified moisture mode framework for seasonality of the Madden-Julian oscillation. *J. Climate*, **31 (11)**, 4215–4224, doi:10.1175/JCLI-D-17-0671.1.

Jiang, X., and Coauthors, 2015: Vertical structure and physical processes of the Madden-Julian oscillation: Exploring key model physics in climate simulations. *J. Geophys. Res. Atmos.*, **120 (10)**, 4718–4748, doi:10.1002/2014JD022375.

Kang, I.-S., F. Liu, M.-S. Ahn, Y.-M. Yang, and B. Wang, 2013: The Role of SST Structure in Convectively Coupled Kelvin–Rossby Waves and Its Implications for MJO Formation. *J. Climate*, **26 (16)**, 5915–5930, doi:10.1175/JCLI-D-12-00303.1.

Kao, H.-Y., and J.-Y. Yu, 2009: Contrasting Eastern-Pacific and Central-Pacific Types of ENSO. *J. Climate*, **22 (3)**, 615–632, doi:10.1175/2008JCLI2309.1.

Kemball-Cook, S., B. Wang, and X. Fu, 2002: Simulation of the Intraseasonal Oscillation in the ECHAM-4 Model: The Impact of Coupling with an Ocean Model. *J. Atmos. Sci.*,

59 (9), 1433–1453, doi:10.1175/1520-0469(2002)059<1433:SOTIOI>2.0.CO;2.

Kemball-Cook, S. R., and B. C. Weare, 2001: The onset of convection in the Madden-Julian oscillation. *J. Climate*, **14 (5)**, 780–793, doi:10.1175/1520-0442(2001)014<0780:TOOCIT>2.0.CO;2.

Kerns, B. W., and S. S. Chen, 2014: Equatorial Dry Air Intrusion and Related Synoptic Variability in MJO Initiation during DYNAMO. *Mon. Wea. Rev.*, **142 (3)**, 1326–1343, doi:10.1175/MWR-D-13-00159.1.

Kessler, W. S., 2001: EOF representations of the Madden-Julian and its connection with ENSO. *J. Climate*, **14 (13)**, 3055–3061, doi:10.1175/1520-0442(2001)014<3055:EROTMJ>2.0.CO;2.

Khairoutdinov, M. F., and K. Emanuel, 2018: Intraseasonal variability in a cloud-permitting near-global equatorial aquaplanet model. *J. Atmos. Sci.*, **75 (12)**, 4337–4355, doi:10.1175/JAS-D-18-0152.1.

Kikuchi, K., G. N. Kiladis, J. Dias, and T. Nasuno, 2018: Convectively coupled equatorial waves within the MJO during CINDY/DYNAMO: slow Kelvin waves as building blocks. *Clim. Dyn.*, **50 (11-12)**, 4211–4230, doi:10.1007/s00382-017-3869-5.

Kikuchi, K., and Y. N. Takayabu, 2003: Equatorial Circumnavigation of Moisture Signal Associated with the Madden-Julian Oscillation (MJO) during Boreal Winter. *J. Meteor. Soc. Japan*, **81 (4)**, 851–869, doi:10.2151/jmsj.81.851.

Kikuchi, K., and B. Wang, 2010: Spatiotemporal wavelet transform and the multiscale behavior of the Madden-Julian oscillation. *J. Climate*, **23 (14)**, 3814–3834, doi:10.1175/2010JCLI2693.1.

Kikuchi, K., B. Wang, and Y. Kajikawa, 2012: Bimodal representation of the tropical intraseasonal oscillation. *Clim. Dyn.*, **38 (9-10)**, 1989–2000, doi:10.1007/s00382-011-1159-1.

Kiladis, G. N., K. H. Straub, and P. T. Haertel, 2005: Zonal and Vertical Structure of the Madden–Julian Oscillation. *J. Atmos. Sci.*, **62 (8)**, 2790–2809, doi:10.1175/JAS3520.1.

Kiladis, G. N., M. C. Wheeler, P. T. Haertel, K. H. Straub, and P. E. Roundy, 2009: Convectively coupled equatorial waves. *Rev. Geophys.*, **47 (2)**, RG2003, doi:10.1029/

2008RG000266.

Kim, D., H. Kim, and M. I. Lee, 2017: Why does the MJO detour the Maritime Continent during austral summer? *Geophys. Res. Lett.*, **44 (5)**, 2579–2587, doi: 10.1002/2017GL072643.

Kiranmayi, L., and E. D. Maloney, 2011: Intraseasonal moist static energy budget in reanalysis data. *J. Geophys. Res. Atmos.*, **116 (21)**, 1–12, doi:10.1029/2011JD016031.

Klingaman, N. P., and S. J. Woolnough, 2014: The role of air-sea coupling in the simulation of the Madden-Julian oscillation in the Hadley Centre model. *Quart. J. Roy. Meteor. Soc.*, **140 (684)**, 2272–2286, doi:10.1002/qj.2295.

Knapp, K. R., and Coauthors, 2011: Globally Gridded Satellite Observations for Climate Studies. *Bull. Amer. Meteor. Soc.*, **92 (7)**, 893–907, doi:10.1175/2011BAMS3039.1.

Knutson, T. R., and K. M. Weickmann, 1987: 30–60 Day Atmospheric Oscillations: Composite Life Cycles of Convection and Circulation Anomalies. *Mon. Wea. Rev.*, **115 (7)**, 1407–1436, doi:10.1175/1520-0493(1987)115<1407:DAOCLC>2.0.CO;2.

Kuang, Z., 2008: A Moisture-Stratiform Instability for Convectively Coupled Waves. *J. Atmos. Sci.*, **65 (3)**, 834–854, doi:10.1175/2007JAS2444.1.

Kubota, H., K. Yoneyama, J.-I. Hamada, P. Wu, A. Sudaraynto, and I. B. Wahyono, 2015: Role of Maritime Continent Convection during the Preconditioning Stage of the Madden-Julian Oscillation Observed in CINDY2011/DYNAMO. *J. Meteor. Soc. Japan. Ser. II*, **93A (0)**, 101–114, doi:10.2151/jmsj.2015-050.

Lau, K. K.-M., and L. Peng, 1987: Origin of Low-Frequency (Intraseasonal) Oscillations in the Tropical Atmosphere. Part I: Basic Theory. *J. Atmos. Sci.*, **44 (6)**, 950–972, doi:10.1175/1520-0469(1987)044<0950:OOLFOI>2.0.CO;2.

Lau, W. K.-M., and D. E. Waliser, 2012: *Intraseasonal Variability in the Atmosphere-Ocean Climate System*. 2nd ed., Springer-Verlag, 614 pp.

Li, T., C. Zhao, P. C. Hsu, and T. Nasuno, 2015: MJO initiation processes over the tropical Indian ocean during DYNAMO/CINDY2011. *J. Climate*, **28 (6)**, 2121–2135, doi:10.1175/JCLI-D-14-00328.1.

Liebmann, B., and H. H. Hendon, 1990: Synoptic-Scale Disturbances near the Equator. **47 (12)**, 1463–1479, doi:10.1175/1520-0469(1990)047<1463:SSDNTE>2.0.CO;2.

Lighthill, J., 1978: *Waves in fluids*. 1st ed., Cambridge University Press., 504 pp.

Ling, J., C. Zhang, S. Wang, and C. Li, 2017: A new interpretation of the ability of global models to simulate the MJO. *Geophys. Res. Lett.*, **44 (11)**, 5798–5806, doi:10.1002/2017GL073891.

Ling, J., Y. Zhao, and G. Chen, 2019: Barrier effect on MJO propagation by the Maritime Continent in the MJO Task Force/GeWEX atmospheric system study models. *J. Climate*, **32 (17)**, 5529–5547, doi:10.1175/JCLI-D-18-0870.1.

Liu, F., and B. Wang, 2013: An Air–Sea Coupled Skeleton Model for the Madden–Julian Oscillation. *J. Atmos. Sci.*, **70 (10)**, 3147–3156, doi:10.1175/JAS-D-12-0348.1.

Ma, D., and Z. Kuang, 2016: A mechanism-denial study on the Madden-Julian Oscillation. *Geophys. Res. Lett.*, **43**, 2989–2997, doi:10.1002/2016GL067702.

Madden, R. A., and P. R. Julian, 1971: Detection of a 40–50 Day Oscillation in the Zonal Wind in the Tropical Pacific. *J. Atmos. Sci.*, **28 (5)**, 702–708, doi:10.1175/1520-0469(1971)028<0702:DOADOI>2.0.CO;2.

Madden, R. A., and P. R. Julian, 1972: Description of Global-Scale Circulation Cells in the Tropics with a 40–50 Day Period. *J. Atmos. Sci.*, **29 (6)**, 1109–1123, doi:10.1175/1520-0469(1972)029<1109:DOGSCC>2.0.CO;2.

Majda, A. J., and J. A. Biello, 2004: A multiscale model for tropical intraseasonal oscillations. *Proc. Natl. Acad. Sci. (USA)*, **101 (14)**, 4736–4741, doi:10.1073/pnas.0401034101.

Majda, A. J., and R. Klein, 2003: Systematic multiscale models for the tropics. *J. Atmos. Sci.*, **60 (2)**, 393–408, doi:10.1175/1520-0469(2003)060<0393:SMMFTT>2.0.CO;2.

Majda, A. J., and S. N. Stechmann, 2009a: A Simple Dynamical Model with Features of Convective Momentum Transport. *J. Atmos. Sci.*, **66 (2)**, 373–392, doi:10.1175/2008JAS2805.1.

Majda, A. J., and S. N. Stechmann, 2009b: The skeleton of tropical intraseasonal oscillations. *Proc. Natl. Acad. Sci. (USA)*, **106 (21)**, 8417–8422, doi:10.1073/pnas.0903367106.

Majda, A. J., and S. N. Stechmann, 2011: Nonlinear Dynamics and Regional Variations in the MJO Skeleton. *J. Atmos. Sci.*, **68 (12)**, 3053–3071, doi:10.1175/JAS-D-11-053.1.

Maloney, E. D., 2009: The moist static energy budget of a composite tropical intraseasonal oscillation in a climate model. *J. Climate*, **22 (3)**, 711–729, doi:10.1175/2008JCLI2542.1.

Maloney, E. D., and D. L. Hartmann, 1998: Frictional Moisture Convergence in a Composite Life Cycle of the Madden–Julian Oscillation. *J. Climate*, **11 (9)**, 2387–2403, doi:10.1175/1520-0442(1998)011<2387:FMCIAC>2.0.CO;2.

Maloney, E. D., and D. L. Hartmann, 2000: Modulation of Eastern North Pacific Hurricanes by the Madden–Julian Oscillation. *J. Climate*, **13 (9)**, 1451–1460, doi:10.1175/1520-0442(2000)013<1451:MOENPH>2.0.CO;2.

Maloney, E. D., and A. H. Sobel, 2004: Surface fluxes and ocean coupling in the tropical intraseasonal oscillation. *J. Climate*, **17 (22)**, 4368–4386, doi:10.1175/JCLI-3212.1.

Maloney, E. D., and B. O. Wolding, 2015: Initiation of an intraseasonal oscillation in an aquaplanet general circulation model. *J. Adv. Model. Earth Syst.*, **7 (4)**, 1956–1976, doi:10.1002/2015MS000495.

Masunaga, H., 2013: A satellite study of tropical moist convection and environmental variability: A moisture and thermal budget analysis. *J. Atmos. Sci.*, **70 (8)**, 2443–2466, doi:10.1175/JAS-D-12-0273.1.

Masunaga, H., T. S. L'Ecuyer, and C. D. Kummerow, 2006: The Madden–Julian Oscillation Recorded in Early Observations from the Tropical Rainfall Measuring Mission (TRMM). *J. Atmos. Sci.*, **63 (11)**, 2777–2794, doi:10.1175/JAS3783.1.

Matsuno, T., 1966: Quasi-geostrophic motions in the equatorial area. *J. Meteor. Soc. Japan*, **44 (2)**, 25–43, doi:10.1002/qj.49710644905.

Matthews, A. J., 2000: Propagation mechanisms for the Madden-Julian Oscillation. *Quart. J. Roy. Meteor. Soc.*, **126 (569)**, 2637–2651, doi:10.1256/smsqj.56901.

Matthews, A. J., 2008: Primary and successive events in the Madden–Julian Oscillation. *Quart. J. Roy. Meteor. Soc.*, **134 (631)**, 439–453, doi:10.1002/qj.224.

Matthews, A. J., B. J. Hoskins, and M. Masutani, 2004: The global response to tropical heating in the Madden–Julian oscillation during the northern winter. *Quart. J. Roy. Meteor. Soc.*, **130 (601)**, 1991–2011, doi:10.1256/qj.02.123.

McPhaden, M. J., 1999: Genesis and Evolution of the 1997-98 El Niño. *Science*, **283 (5404)**, 950–954, doi:10.1126/science.283.5404.950.

Miura, H., M. Satoh, and M. Katsumata, 2009: Spontaneous onset of a Madden-Julian oscillation event in a cloud-system-resolving simulation. *Geophys. Res. Lett.*, **36 (13)**, 2–6, doi:10.1029/2009GL039056.

Miura, H., M. Satoh, T. Nasuno, A. T. Noda, and K. Oouchi, 2007: A Madden-Julian Oscillation Event Realistically Simulated by a Global Cloud-Resolving Model. *Science*, **318 (5857)**, 1763–1765, doi:10.1126/science.1148443.

Miyakawa, T., H. Yashiro, T. Suzuki, H. Tatebe, and M. Satoh, 2017: A Madden-Julian Oscillation event remotely accelerates ocean upwelling to abruptly terminate the 1997/1998 super El Niño. *Geophys. Res. Lett.*, **44 (18)**, 9489–9495, doi:10.1002/2017GL074683.

Miyakawa, T., and Coauthors, 2014: Madden–Julian Oscillation prediction skill of a new-generation global model demonstrated using a supercomputer. *Nature Communications*, **5 (5)**, 1–6, doi:10.1038/ncomms4769.

Muraleedharan, P. M., S. Prasanna Kumar, K. Mohana kumar, S. Sijikumar, K. U. Sivakumar, and T. Mathew, 2015: Observational evidence of Mixed Rossby Gravity waves at the central equatorial Indian Ocean. *Meteor. Atmos. Phys.*, **127 (4)**, 407–417, doi:10.1007/s00703-015-0376-2.

Nakazawa, N., 1988: Tropical Super Clusters within Intraseasonal Variations over the Western Pacific. *J. Meteor. Soc. Japan*, **66 (6)**, 823–839, doi:10.2151/jmsj1965.66.6_823.

Nasuno, T., T. Li, and K. Kikuchi, 2015: Moistening Processes before the Convective Initiation of Madden–Julian Oscillation Events during the CINDY2011/DYNAMO Period. *Mon. Wea. Rev.*, **143 (2)**, 622–643, doi:10.1175/MWR-D-14-00132.1.

Nasuno, T., H. Miura, M. Satoh, A. T. Noda, and K. Oouchi, 2009: Multi-scale Organization of Convection in a Global Numerical Simulation of the December 2006 MJO Event

Using Explicit Moist Processes. *J. Meteor. Soc. Japan*, **87 (2)**, 335–345, doi:10.2151/jmsj.87.335.

Neelin, J. D., I. M. Held, and K. H. Cook, 1987: Evaporation-Wind Feedback and Low-Frequency Variability in the Tropical Atmosphere. *J. Atmos. Sci.*, **44 (16)**, 2341–2348, doi:10.1175/1520-0469(1987)044<2341:EWFALF>2.0.CO;2.

Neelin, J. D., and J.-Y. Yu, 1994: Modes of Tropical Variability under Convective Adjustment and the Madden–Julian Oscillation. Part I: Analytical Theory. *J. Atmos. Sci.*, **51 (13)**, 1876–1894, doi:10.1175/1520-0469(1994)051<1876:MOTVUC>2.0.CO;2.

Nitta, T., 1970: Statistical Study of Tropospheric Wave Disturbances in the Tropical Pacific Region. *J. Meteor. Soc. Japan*, **48 (1)**, 1876–1894, doi:10.2151/jmsj1965.48.1_47.

Okamoto, K., T. Ushio, T. Iguchi, N. Takahashi, and K. Iwanami, 2005: The Global Satellite Mapping of Precipitation (GSMaP) project. *International Geoscience and Remote Sensing Symposium (IGARSS)*, **5 (3)**, 3414–3416, doi:10.1109/IGARSS.2005.1526575.

Peatman, S. C., A. J. Matthews, and D. P. Stevens, 2014: Propagation of the Madden-Julian Oscillation through the Maritime Continent and scale interaction with the diurnal cycle of precipitation. *Quart. J. Roy. Meteor. Soc.*, **140 (680)**, 814–825, doi:10.1002/qj.2161.

Powell, S. W., and R. A. Houze, 2013: The cloud population and onset of the Madden-Julian Oscillation over the Indian Ocean during DYNAMO-AMIE. *J. Geophys. Res. Atmos.*, **118 (21)**, 11 979–11 995, doi:10.1002/2013JD020421.

Powell, S. W., and R. A. Houze, 2015a: Effect of dry large-scale vertical motions on initial MJO convective onset. *J. Geophys. Res. Atmos.*, **120 (10)**, 4783–4805, doi:10.1002/2014JD022961.

Powell, S. W., and R. A. Houze, 2015b: Evolution of precipitation and convective echo top heights observed by TRMM radar over the Indian Ocean during DYNAMO. *J. Geophys. Res. Atmos.*, **120 (9)**, 3906–3919, doi:10.1002/2014JD022934.

Pritchard, M. S., and C. S. Bretherton, 2014: Causal Evidence that Rotational Moisture Advection is Critical to the Superparameterized Madden–Julian Oscillation. *J. Atmos. Sci.*, **71 (2)**, 800–815, doi:10.1175/JAS-D-13-0119.1.

Pritchard, M. S., and D. Yang, 2016: Response of the superparameterized Madden-Julian oscillation to extreme climate and basic-state variation challenges a moisture mode view. *J. Climate*, **29 (13)**, 4995–5008, doi:10.1175/JCLI-D-15-0790.1.

Raymond, D. J., 2001: A New Model of the Madden–Julian Oscillation. *J. Atmos. Sci.*, **58 (18)**, 2807–2819, doi:10.1175/1520-0469(2001)058<2807:ANMOTM>2.0.CO;2.

Raymond, D. J., and Ž. Fuchs, 2007: Convectively coupled gravity and moisture modes in a simple atmospheric model. *Tellus*, **59 (5)**, 627–640, doi:10.1111/j.1600-0870.2007.00268.x.

Raymond, D. J., and Ž. Fuchs, 2009: Moisture modes and the Madden-Julian oscillation. *J. Climate*, **22 (11)**, 3031–3046, doi:10.1175/2008JCLI2739.1.

Riley, E. M., B. E. Mapes, and S. N. Tulich, 2011: Clouds Associated with the Madden–Julian Oscillation: A New Perspective from CloudSat. *J. Atmos. Sci.*, **68 (12)**, 3032–3051, doi:10.1175/JAS-D-11-030.1.

Seiki, A., and Y. N. Takayabu, 2007: Westerly Wind Bursts and Their Relationship with Intraseasonal Variations and ENSO. Part II: Energetics over the Western and Central Pacific. *Mon. Wea. Rev.*, **135 (10)**, 3346–3361, doi:10.1175/MWR3503.1.

Seo, K.-H., and K.-Y. Kim, 2003: Propagation and initiation mechanisms of the Madden-Julian oscillation. *J. Geophys. Res. Atmos.*, **108 (D13)**, 4384, doi:10.1029/2002JD002876.

Seo, K.-H., and S.-W. Son, 2012: The Global Atmospheric Circulation Response to Tropical Diabatic Heating Associated with the Madden–Julian Oscillation during Northern Winter. *J. Atmos. Sci.*, **69 (1)**, 79–96, doi:10.1175/2011JAS3686.1.

Shi, X., D. Kim, Á. F. Adames, and J. Sukhatme, 2018: WISHE-moisture mode in an aquaplanet simulation. *J. Adv. Model. Earth Syst.*, **10 (10)**, 2393–2407, doi:10.1029/2018MS001441.

Shinoda, T., H. H. Hendon, and J. Glick, 1998: Intraseasonal Variability of Surface Fluxes and Sea Surface Temperature in the Tropical Western Pacific and Indian Oceans. *J. Climate*, **11 (7)**, 1685–1702, doi:10.1175/1520-0442(1998)011<1685:IVOSFA>2.0.CO;2.

Sobel, A., and E. Maloney, 2012: An Idealized Semi-Empirical Framework for Model-

ing the Madden–Julian Oscillation. *J. Atmos. Sci.*, **69 (5)**, 1691–1705, doi:10.1175/JAS-D-11-0118.1.

Sobel, A., and E. Maloney, 2013: Moisture Modes and the Eastward Propagation of the MJO. *J. Atmos. Sci.*, **70 (1)**, 187–192, doi:10.1175/JAS-D-12-0189.1.

Sobel, A. H., and C. S. Bretherton, 1999: Development of Synoptic-Scale Disturbances over the Summertime Tropical Northwest Pacific. *J. Atmos. Sci.*, **56 (17)**, 3106–3127, doi:10.1175/1520-0469(1999)056<3106:DOSSDO>2.0.CO;2.

Sobel, A. H., E. D. Maloney, G. Bellon, and D. M. Frierson, 2008: The role of surface heat fluxes in tropical intraseasonal oscillations. *Nature Geoscience*, **1 (10)**, 653–657, doi:10.1038/ngeo312.

Sobel, A. H., E. D. Maloney, G. Bellon, and D. M. Frierson, 2010: Surface fluxes and tropical intraseasonal variability: A reassessment. *J. Adv. Model. Earth Syst.*, **2**, 1–27, doi:10.3894/JAMES.2010.2.2.

Sobel, A. H., J. Nilsson, and L. M. Polvani, 2001: The Weak Temperature Gradient Approximation and Balanced Tropical Moisture Waves. *J. Atmos. Sci.*, **58 (23)**, 3650–3665, doi:10.1175/1520-0469(2001)058<3650:TWTGAA>2.0.CO;2.

Sperber, K. R., 2003: Propagation and the Vertical Structure of the Madden–Julian Oscillation. *Mon. Wea. Rev.*, **131 (12)**, 3018–3037, doi:10.1175/1520-0493(2003)131<3018:PATVSO>2.0.CO;2.

Straub, K. H., and G. N. Kiladis, 2003: Interactions between the Boreal Summer Intraseasonal Oscillation and Higher-Frequency Tropical Wave Activity. *Mon. Wea. Rev.*, **131 (5)**, 945–960, doi:10.1175/1520-0493(2003)131<0945:IBTBSI>2.0.co;2.

Suematsu, T., 2018: *A study on the background sea surface temperature field and moist processes contributing to the realization of the Madden-Julian Oscillation (Doctoral Dissertation)*. The University of Tokyo.

Suematsu, T., and H. Miura, 2018: Zonal SST difference as a potential environmental factor supporting the longevity of the Madden-Julian oscillation. *J. Climate*, **31 (18)**, 7549–7564, doi:10.1175/JCLI-D-17-0822.1.

Sugiyama, M., 2009: The Moisture Mode in the Quasi-Equilibrium Tropical Circulation Model. Part I: Analysis Based on the Weak Temperature Gradient Approximation. *J. Atmos. Sci.*, **66 (6)**, 1507–1523, doi:10.1080/07349165.1996.9725892.

Takasuka, D., M. Satoh, T. Miyakawa, and H. Miura, 2018: Initiation Processes of the Tropical Intraseasonal Variability Simulated in an Aqua-Planet Experiment: What is the Intrinsic Mechanism for MJO Onset? *J. Adv. Model. Earth Syst.*, **10 (4)**, 1047–1073, doi:10.1002/2017MS001243.

Takayabu, Y. N., 1994: Large-Scale Cloud Disturbances Features Associated of the with Cloud Equatorial Disturbances Waves. Part I: Spectral Features of the Cloud Disturbances. *J. Meteor. Soc. Japan*, **72 (3)**, 433–449.

Takayabu, Y. N., T. Iguchi, M. Kachi, A. Shibata, and H. Kanzawa, 1999: Abrupt termination of the 1997–98 El Niño in response to a Madden–Julian oscillation. *Nature*, **402 (6759)**, 279–282, doi:10.1038/46254.

Takayabu, Y. N., K.-M. Lau, and C.-H. Sui, 1996: Observation of a Quasi-2-Day Wave during TOGA COARE. *Mon. Wea. Rev.*, **124 (9)**, 1892–1913.

Takayabu, Y. N., and T. Nitta, 1993: 3–5 Day-Period Disturbances Coupled with Convection over the Tropical Pacific Ocean. *J. Meteor. Soc. Japan. Ser. II*, **71 (2)**, 221–246, doi: 10.2151/jmsj1965.71.2_221.

Tam, C. Y., and N. C. Lau, 2005: Modulation of the Madden-Julian Oscillation by ENSO: Inferences from observations and GCM simulations. *J. Meteor. Soc. Japan*, **83 (5)**, 727–743, doi:10.2151/jmsj.83.727.

Toh, Y. Y., A. G. Turner, S. J. Johnson, and C. E. Holloway, 2018: Maritime Continent seasonal climate biases in AMIP experiments of the CMIP5 multimodel ensemble. *Clim. Dyn.*, **50 (3-4)**, 777–800, doi:10.1007/s00382-017-3641-x.

Tseng, W.-L., B.-J. Tsuang, N. S. Keenlyside, H.-H. Hsu, and C.-Y. Tu, 2015: Resolving the upper-ocean warm layer improves the simulation of the Madden–Julian oscillation. *Clim. Dyn.*, **44 (5-6)**, 1487–1503, doi:10.1007/s00382-014-2315-1.

Vincent, D. G., A. Fink, J. M. Schrage, and P. Speth, 1998: High- and Low-Frequency

Intraseasonal Variance of OLR on Annual and ENSO Timescales. *J. Climate*, **11 (5)**, 968–986, doi:10.1175/1520-0442(1998)011<0968:HALFIV>2.0.CO;2.

Vitart, F., and A. W. Robertson, 2018: The sub-seasonal to seasonal prediction project (S2S) and the prediction of extreme events. *npj Climate and Atmospheric Science*, **1 (1)**, 1–7, doi:10.1038/s41612-018-0013-0.

Wallace, J. M., 1971: Spectral studies of tropospheric wave disturbances in the tropical western Pacific. *Rev. Geophys.*, **9 (3)**, 557–612, doi:10.1029/RG009i003p00557.

Wang, B., and G. Chen, 2017: A general theoretical framework for understanding essential dynamics of Madden–Julian oscillation. *Clim. Dyn.*, **49 (7-8)**, 2309–2328, doi:10.1007/s00382-016-3448-1.

Wang, B., and T. Li, 1994: Convective Interaction with Boundary-Layer Dynamics in the Development of a Tropical Intraseasonal System. *J. Atmos. Sci.*, **51 (11)**, 1386–1400, doi:10.1175/1520-0469(1994)051<1386:ciwbld>2.0.co;2.

Wang, B., and F. Liu, 2011: A model for scale interaction in the Madden-Julian oscillation. *J. Atmos. Sci.*, **68 (11)**, 2524–2536, doi:10.1175/2011JAS3660.1.

Wang, B., F. Liu, and G. Chen, 2016: A trio-interaction theory for Madden–Julian oscillation. *Geosci. Lett.*, **3 (1)**, doi:10.1186/s40562-016-0066-z.

Wang, B., and H. Rui, 1990: Dynamics of the Coupled Moist Kelvin–Rossby Wave on an Equatorial β-Plane. *J. Atmos. Sci.*, **47 (4)**, 397–413, doi:10.1175/1520-0469(1990)047<0397:DOTCMK>2.0.CO;2.

Wang, B., and X. Xie, 1998: Coupled modes of the warm pool climate system. Part I: The role of air-sea interaction in maintaining Madden-Julian oscillation. *J. Climate*, **11 (8)**, 2116–2135, doi:10.1175/1520-0442-11.8.2116.

Wang, B., and Coauthors, 2018a: Dynamics-oriented diagnostics for the Madden-Julian oscillation. *J. Climate*, **31 (8)**, 3117–3135, doi:10.1175/JCLI-D-17-0332.1.

Wang, L., T. Li, L. Chen, S. K. Behera, and T. Nasuno, 2018b: Modulation of the MJO intensity over the equatorial western Pacific by two types of El Niño. *Clim. Dyn.*, **51 (1-2)**, 687–700, doi:10.1007/s00382-017-3949-6.

Wei, Y., and H.-L. Ren, 2019: Modulation of ENSO on Fast and Slow MJO Modes during Boreal Winter. *J. Climate*, **32 (21)**, 7483–7506, doi:10.1175/JCLI-D-19-0013.1.

Wheeler, M., and G. N. Kiladis, 1999: Convectively Coupled Equatorial Waves: Analysis of Clouds and Temperature in the Wavenumber–Frequency Domain. *J. Atmos. Sci.*, **56 (3)**, 374–399, doi:10.1175/1520-0469(1999)056<0374:CCEWAO>2.0.CO;2.

Wheeler, M. C., and H. H. Hendon, 2004: An All-Season Real-Time Multivariate MJO Index: Development of an Index for Monitoring and Prediction. *Mon. Wea. Rev.*, **132 (8)**, 1917–1932, doi:10.1175/1520-0493(2004)132<1917:AARMMI>2.0.CO;2.

Widiyatmi, I., M. D. Yamanaka, H. Hashiguchi, S. Fukao, T. Tsuda, S. Y. Ogino, S. W. B. Harijono, and H. Wiryosumarto, 1999: Quasi 4 day mode observed by a boundary layer radar at Serpong (6°S, 107°E), Indonesia. *J. Meteor. Soc. Japan*, **77 (6)**, 1177–1184, doi:10.2151/jmsj1965.77.6_1177.

Widiyatmi, I., and Coauthors, 2001: Examination of 3-6 day disturbances over quatorial Indonesia based on boundary layer radar observations during 1996-1999 at Bukittinggi, Serpong and Biak. *J. Meteor. Soc. Japan*, **79 (1 SPEC. ISSUE)**, 317–331, doi:10.2151/jmsj.79.317.

Wing, A. A., and T. W. Cronin, 2016: Self-aggregation of convection in long channel geometry. *Quart. J. Roy. Meteor. Soc.*, **142 (694)**, 1–15, doi:10.1002/qj.2628.

Xu, W., and S. A. Rutledge, 2016: Time scales of shallow-to-deep convective transition associated with the onset of Madden-Julian Oscillations. *Geophys. Res. Lett.*, **43 (6)**, 2880–2888, doi:10.1002/2016GL068269.

Yanai, M., and Y. Hayashi, 1969: Large-Scale Equatorial Waves Penetrating from the Upper Troposphere into the. Lower Stratosphere. *J. Meteor. Soc. Japan*, **47 (3)**, 167–182, doi:10.2151/jmsj1965.47.3_167.

Yanai, M., and T. Maruyama, 1966: Stratospheric Wave Disturbances Propagating over the Equatorial Pacific. *J. Meteor. Soc. Japan*, **44 (5)**, 291–294, doi:10.2151/jmsj1965.44.5_291.

Yanai, M., T. Maruyama, T. Nitta, and Y. Hayashi, 1968: Power Spectra of Large-Scale

Disturbances over the Tropical Pacific. *J. Meteor. Soc. Japan*, **46 (4)**, 308–323, doi: 10.2151/jmsj1965.46.4_308.

Yanai, M., and M. Murakami, 1970: Spectrum Analysis of Symmetric and Antisymmetric Equatorial Waves. *J. Meteor. Soc. Japan*, **48 (4)**, 331–347.

Yang, D., 2018: Boundary-layer diabatic processes, the virtual effect, and convective self-aggregation. *J. Adv. Model. Earth Syst.*, doi:10.1029/2017MS001261.

Yang, D., and A. P. Ingersoll, 2011: Testing the Hypothesis that the MJO is a Mixed Rossby–Gravity Wave Packet. *J. Atmos. Sci.*, **68 (2)**, 226–239, doi:10.1175/2010JAS3563.1.

Yang, D., and A. P. Ingersoll, 2013: Triggered Convection, Gravity Waves, and the MJO: A Shallow-Water Model. *J. Atmos. Sci.*, **70 (8)**, 2476–2486, doi:10.1175/JAS-D-12-0255.1.

Yang, D., and A. P. Ingersoll, 2014: A theory of the MJO horizontal scale. *Geophys. Res. Lett.*, **41 (3)**, 1059–1064, doi:10.1002/2013GL058542.

Yasunaga, K., 2011: Seasonality and Regionality of the Madden-Julian Oscillation and Convectively Coupled Equatorial Waves. *SOLA*, **7**, 153–156, doi:10.2151/sola.2011-039.

Yasunaga, K., K. Yoneyama, Q. Moteki, M. Fujita, Y. N. Takayabu, J. Suzuki, T. Ushiyama, and B. Mapes, 2010: Characteristics of 3–4- and 6–8-Day Period Disturbances Observed over the Tropical Indian Ocean. *Mon. Wea. Rev.*, **138 (11)**, 4158–4174, doi:10.1175/2010MWR3469.1.

Yasunari, T., 1979: Cloudiness Fluctuations Associated with the Northern Hemisphere Summer Monsoon. *J. Meteor. Soc. Japan. Ser. II*, **57 (3)**, 227–242, doi:10.2151/jmsj1965.57.3_227.

Yokoi, S., and A. H. Sobel, 2015: Intraseasonal Variability and Seasonal March of the Moist Static Energy Budget over the Eastern Maritime Continent during CINDY2011 / DYNAMO. *J. Meteor. Soc. Japan*, **93A**, 81–100, doi:10.2151/jmsj.2015-041.

Yoneyama, K., C. Zhang, and C. N. Long, 2013: Tracking pulses of the Madden-Julian oscillation. *Bull. Amer. Meteor. Soc.*, **94 (12)**, 1871–1891, doi:10.1175/BAMS-D-12-00157.1.

Yoneyama, K., and Coauthors, 2008: MISMO Field Experiment in the Equatorial Indian Ocean. *Bull. Amer. Meteor. Soc.*, **89 (12)**, 1889–1904, doi:10.1175/2008BAMS2519.1.

Zhang, B., R. J. Kramer, and B. J. Soden, 2019: Radiative Feedbacks Associated with the Madden–Julian Oscillation. *J. Climate*, **32 (20)**, 7055–7065, doi:10.1175/JCLI-D-19-0144.1.

Zhang, C., 2005: Madden-Julian Oscillation. *Rev. Geophys.*, **43 (2)**, RG2003, doi:10.1029/2004RG000158.

Zhang, C., 2013: Madden-Julian oscillation: Bridging weather and climate. *Bull. Amer. Meteor. Soc.*, **94 (12)**, 1849–1870, doi:10.1175/BAMS-D-12-00026.1.

Zhang, F., S. Taraphdar, and S. Wang, 2017: The role of global circumnavigating mode in the MJO initiation and propagation. *J. Geophys. Res. Atmos.*, **122 (20)**, 5837–5856, doi:10.1002/2016JD025665.

Zhao, C., T. Li, and T. Zhou, 2013: Precursor signals and processes associated with MJO initiation over the tropical indian ocean. *J. Climate*, **26 (1)**, 291–307, doi:10.1175/JCLI-D-12-00113.1.

Zhou, X., and B. Wang, 2007: Transition from an eastern Pacific upper-level mixed Rossby-gravity wave to a western Pacific tropical cyclone. *Geophys. Res. Lett.*, **34 (24)**, 2–6, doi:10.1029/2007GL031831.

Zhu, J., W. Wang, and A. Kumar, 2017: Simulations of MJO Propagation across the Maritime Continent: Impacts of SST Feedback. *J. Climate*, **30 (5)**, 1689–1704, doi:10.1175/JCLI-D-16-0367.1.